

A Parametric Framework for Modelling of Bioelectrical Signals

YAR MUHAMMAD
(YAR M. MUGHAL)

TALLINN UNIVERSITY OF TECHNOLOGY
Faculty of Information Technology
Thomas Johann Seebeck Department of Electronics

This dissertation was accepted for defence of the degree of Doctor of Philosophy in Engineering on April 09, 2015.

Supervisor:

Prof. Toomas Rang

Thomas Johann Seebeck Department of Electronics, Faculty of Information Technology,
Tallinn University of Technology

Co-supervisors:

Dr. Paul Annus

Thomas Johann Seebeck Department of Electronics, Faculty of Information Technology,
Tallinn University of Technology

Dr. Yannick Le Moullec

Thomas Johann Seebeck Department of Electronics, Faculty of Information Technology,
Tallinn University of Technology

Opponents:

Dr. Serge Dos Santos

INSA Centre Nobel de Loire, Blois, France

Dr. Jüri Vedru

University of Tartu, Institute of Physics BME group, Estonia

Defence of the thesis: June 05, 2015

Declaration:

I hereby declare that this doctoral thesis, my original investigation and achievement, submitted for the doctoral degree at Tallinn University of Technology has not previously been submitted for any academic degree.

/Yar Muhammad/



European Union
European Social Fund



Investing in your future

Copyright: Yar Muhammad, 2015

ISSN 1406-4731

ISBN 978-9949-23-763-0 (publication)

ISBN 978-9949-23-764-7 (PDF)

Parameetriline raamistik bioelektriliste signaalide modelleerimiseks

YAR MUHAMMAD
(YAR M. MUGHAL)

ABSTRACT

Extraction of useful information from cardiac signals for the diagnosis of diseases and judgment of heart function is of special interest to medical personnel. Thus, the development of effective, robust, and efficient diagnostic tools for heart diseases is required. The aim when developing new techniques and tools is to minimize the required cost and long hospitalization time, and increase the patient's ease and safety. In accordance with this statement, in this PhD thesis, non-invasive electrical-based methods are of special interest. However, extracting useful information from measured biomedical data is not always trivial. The research community, including our previous contributions, has developed many algorithms for separating the signals of different origins, e.g., cardiac, respiratory, and muscular activities, etc. Nevertheless, none of the existing methods provides any mechanism to evaluate the performance of the developed algorithms. Thus, there exist uncertainties regarding the properties of the signals, such as its amplitude, waveform, components, and the origin of the signal waveform, which, in turn, limits the quality of the diagnostics of diseases and conditions.

In this PhD thesis, it is argued that modelling the measured signals offers several advantages to help dealing with the above problems, as compared to relying on measured data only. By using a formalized representation, the parameters of the signal model can be easily manipulated and/or modified, thus providing mechanisms that allow researchers to reproduce and control such signals.

In turn, having such a formalized signal model makes it possible to develop computer tools that can be used for manipulating and understanding how the signal changes depend on various heart conditions, as well as for generating input signals for experimenting with and evaluating the performance of, e.g. useful signal extraction methods.

In this work, the focus is on bioelectrical information, mainly electrical bio-impedance (EBI). Once the EBI is measured, it is necessary to model the corresponding signals for analysis. In this case, the so-called advanced user should have to follow a structured approach to move from real measured data to the model of the corresponding signals. For this, a generic framework is proposed in the PhD work. It has been used to guide the modelling of the impedance cardiography (ICG) and impedance respirography (IRG) signals. Here, based on statistical parameters and visual fit, a Fourier series is selected to model the ICG and IRG signals.

The proposed framework has been used to guide the development of the corresponding bio-impedance signal simulator (BISS). The internal details of the simulator are presented, including the various model parameters and the mechanisms for adding modulation, noise, and motion artefacts. As a result, the implemented BISS generates simulated EBI signals and BISS gives freedom to the end-user to control the essential properties of the generated EBI signals depending on his/her needs. Predefined human conditions/activities states are also included for ease of use.

ANNOTATSIOON

Erinevate mõõteseadmete loomisel on kasuliku informatsiooni eraldamine mõõtesignaalist üks olulisemaid ja samas ka keerukamaid ülesandeid. Näiteks on meedikutele oluline omada head ülevaadet südame tööst ja selle võimalikest häiretest. Bioimpedantssignaalis on vajalik informatsioon olemas, kuid lisaks sellele on seal ka palju häirivaid ja segavaid komponente. Kuigi kasulike komponentide eraldamisega on tegeletud pikka aega, puudub seni universaalne meetod, mis töötaks kõikides mõõtesituatsioonides ühtviisi usaldusväärselt. Saadud mõõtesignaali kvaliteet on tihedas sõltuvuses mõõdetava olekust. Kui eraldusalgoritmid töötavad reeglina hästi tervete ja puhkeolekus inimeste puhul, siis haigete südametegevus ja hingamine võivad olla sellisel määral häiritud, et nende äratundmine ja eraldamine ei õnnestu. Liikuva inimese puhul lisanduvad häired, mis on seotud lihaskonna tegevuse ja mõõteelektroodide liikumisega. Sellised häired on tüüpiliselt suurusjärgude võrra suuremad kui kasulik signaal ja võivad viimase täielikult maskeerida. Mõõte ja signaalieristusemeetodite arendamist ja evalueerimist raskendab paraku võrdlusbaasi puudumine või puudumine.

Käesolev dissertatsioon pakubki lahendusi eespool käsitletud probleemile. Välja on arendatud raamistik, mis võimaldab, lähtudes kasulike signaalide mudelist, genereerida reaalsele sarnanevaid mõõtesignaale. Kasulike signaalide mudelid põhinevad üldistatud mõõtmistulemustel. Nende abil genereeritud südame ja hingamissignaale lisatakse vajadusel müra ja häireid, neid moduleeritakse, moonutatakse vastavalt haigusele jne.

Mõõtesignaali modelleerimine annab hea võimaluse erinevate eraldusalgoritmide täpseks numbriliseks võrdlemiseks erinevates reaalsetes esineda võivates mõõtesituatsioonides. Kasutades formaliseeritud esitusviisi, on võimalik mudeli signaalide parameetreid kergesti manipuleerida ja modifitseerida. Lisaks pakub selline formaliseeritud lähenemine võimaluse välja töötada programmvaralisi vahendeid, ennustamaks signaalide muutustest tegelikke südame olukordade muutusi.

Käesolevas uuringus on põhifookus asetatud bioimpedantsi mõõtmistest (EBI) pärinevate signaalide töötlemisele, aga tulemused on rakendatavad ka laiemalt. Dissertatsioonis esitatakse üldine mudel-raamistik tööks impedants-kardiograafia (ICG) ja impedants-respirograafia (IRG) signaalidega ning näidatakse võimalust bioimpedantsi signaalisimulaatori (BISS) loomiseks. Uuritakse mudel-raamistiku erinevate parameetrite mõju mudeli väljundile, arvestatakse modulatsiooni, müra ja liikumise artefaktidega, mille tulemusena BISS genereerib parima sobivusega EBI signaali. Sellega antakse lõpptarbijale võimalus lihtsalt ning korratavalt kontrollida signaali töötlemise ja lahutamise algoritmide käitumist erinevates inimese tegutsemisest ja tervisest sõltuvates tingimustes tegelikku katset läbi viimata.

ACKNOWLEDGEMENT

This work would not have been possible without the valuable advice of my colleagues and friends from Thomas Johann Seebeck Department of Electronics at Tallinn University of Technology, or without the support of the Foundation Archimedes ESF DoRa programme. I particularly wish to thank the Estonian Research Council for supporting this research under research Project IUT19-11, and the Foundation Archimedes through the Centre of Excellence CEBE (TK05U01) for supporting the technology-oriented scientific projects in Estonia.

I appreciate the fruitful and valuable advice, support, and discussions with Prof. Mart Min, Dr. Olev Märtens, Dr. Raul Land, Dr. Jaan Ojarand, Dr. Rauno Gordon, Dr. Muhammad Naveed, Mrs. Galina Rang, Ms. Anu Johannes, and Ms. Riina Vilgats. Thank you very much all of you for your kind help and cooperation.

I highly appreciate the valuable suggestions and comments from Prof. Emeritus Enn Velmre, who helped me to enhance the dissertation and make it more readable.

My special thanks go to Dr. Toomas Parve. He was always ready to help whenever I had a question.

I would like to thank Dr. Andrei Krivoshei for his great experience that guided me throughout the entire study.

I am highly thankful to my second co-supervisor, Dr. Yannick Le Moullec, for his great help and support. He was always ready to help me and gave me valuable suggestions and feedback.

I am also especially highly thankful to my first co-supervisor, Dr. Paul Annus, for his excellent supervision and advice. He continuously gave me new ideas and challenges to carry out my research work. I also thank him for his encouragement throughout my research work.

My heartiest thanks go to my supervisor, Prof. Toomas Rang, for his excellent supervision, and for giving me the opportunity to work with enthusiastic colleagues. He is the person who gave me a research direction and kept me on track.

Finally, I would like to thank my family for the support and understanding that helped me through the exciting but difficult task of writing this PhD thesis.

CONTENTS

| | |
|--|-----------|
| LIST OF PUBLICATIONS..... | 11 |
| ABBREVIATIONS | 13 |
| LIST OF SYMBOLS | 13 |
| SHORT DEFINITIONS OF TERMS..... | 14 |
| 1. INTRODUCTION AND MOTIVATION | 15 |
| 1.1 Problems and Statements of Data Acquisition | 16 |
| 1.1.1 Issues with Extraction of a Useful Signal: the Example of Separation of Cardiac and Respiratory Signals during Non-invasive Procedures..... | 16 |
| 1.2 Need for Modelling the Cardiac and Respiratory Signals and Development of the Corresponding Signal Simulator | 18 |
| 1.3 Framework for Biomedical Applications for Modelling and Simulating Bioelectrical Signals | 19 |
| 1.4 Research Questions | 19 |
| 1.5 Main Contributions of the Thesis | 19 |
| 1.6 Structure of the Thesis | 20 |
| 2. STATE OF THE ART OF MODELLING AND SIMULATION OF THE PHYSIOLOGICAL SYSTEMS | 21 |
| 2.1 Cardiovascular System | 21 |
| 2.1.1 Structure and Functioning of the Cardiovascular System..... | 21 |
| 2.1.2 The Respiratory Centre | 24 |
| 2.2 Model of the Cardiovascular System | 25 |
| 2.2.1 From Physiology to Mathematical Representation of the CVS..... | 25 |
| 2.2.2 Structure of the Cardiovascular Model | 26 |
| 2.3 Overview of the Existing CVS Simulator and Software Tools for EBI | 28 |
| 2.3.1 Cardiovascular Simulator (CVSim) | 28 |
| 2.3.2 Software Tool for Analysis of Breathing-Related Errors in Trans- thoracic Electrical Bio-Impedance Spectroscopy Measurements (EBSM) | 30 |
| 2.3.3 Simulation of Lung Edema in Impedance Cardiography | 31 |
| 2.4 Acquiring Physiological Information from the Cardiovascular System..... | 31 |
| 2.4.1 Need for Non-invasive Methods | 32 |
| 2.4.2 Analysis of Impedance Models | 37 |
| 2.4.3 The Issue Regarding the Origin of the ICG Signal..... | 39 |
| 2.4.4 Existing Configurations of Electrodes | 41 |
| 2.5 Analysis of Existing Approaches for Modelling the Bio-Impedance Signal..... | 42 |
| 2.6 Summary of the Chapter | 43 |

| | |
|---|------------|
| 3. PROPOSED NOVEL GENERIC FRAMEWORK FOR MODELLING THE BIOELECTRICAL INFORMATION..... | 45 |
| 3.1 Novel Generic Framework | 47 |
| 3.2 Detailed Explanation of Each Step of the Novel Generic Framework | 48 |
| 3.2.1 Description of the Biological System/Object (Step 1)..... | 48 |
| 3.2.2 Selection of the Data Source of the Interest (Step 2)..... | 54 |
| 3.2.3 Measurement of the Parameters of Interest (Step 3)..... | 55 |
| 3.2.4 Data Cleaning (Step 4) | 56 |
| 3.2.5 Modelling of the ICG and IRG Signals and Building a Corresponding Simulator (Step 5) | 57 |
| 3.2.6 Applications (Step 6)..... | 58 |
| 3.3 Summary of the Chapter | 59 |
| 4. IMPLEMENTATION OF THE FRAMEWORK AND THE EXPERIMENTAL RESULTS | 61 |
| 4.1 Measurement of the EBI Signals | 61 |
| 4.1.1 Measurement Setup | 61 |
| 4.1.2 Waveforms and Spectra of the EBI Signals..... | 63 |
| 4.2 Method for Modelling of Bio-Impedance Signal..... | 67 |
| 4.2.1 Curve-Fitting Method..... | 67 |
| 4.2.2 Results of Modelling and Comparison of the Models of Curve Fitting | 69 |
| 4.3 Proposed Bio-Impedance Signal Simulator | 75 |
| 4.3.1 Development of the Simulator | 75 |
| 4.4 Generic Framework for Modelling the Bio-Impedance Information | 79 |
| 4.4.1 Implementation of the Proposed Novel Generic Framework for the Development of the EBI Signal Simulator..... | 80 |
| 4.5 Summary of the Chapter | 86 |
| 5. CONCLUSIONS | 87 |
| REFERENCES..... | 91 |
| APPENDIX..... | 99 |
| Paper I | 101 |
| Paper II..... | 107 |
| Paper III | 115 |
| Paper IV | 121 |
| Paper V..... | 127 |
| <i>Curriculum Vitae</i> (in English)..... | 133 |
| <i>Curriculum Vitae</i> (in Estonian)..... | 135 |

LIST OF PUBLICATIONS

Here is the list of the main publications upon which this work is based, according to Tallinn University of Technology's classification scheme. Copies of the publications can be found in Appendix (Papers I–IV)

I. Yar M. Mughal, Yannick Le Moullec, Paul Annus, Mart Min

“Development of a Bio-Impedance Signal Simulator on the basis of the Regression based Model of the Cardiac and Respiratory Impedance Signals”

in *IFMBE Proceedings, Volume 48*, 16th Nordic-Baltic Conference on Biomedical Engineering, 16. NBC & 10. MTD 2014 Joint Conferences, Gothenburg, Sweden, October 14–16, 2014, pages 92–95.

Conference participants numbered 430. For this paper, I was awarded the Young Investigator Award (YIA) at the conference. The award was given by Springer and IFMBE.

II. Yar M. Mughal, Paul Annus, Mart Min, Rauno Gordon

“An Overview of the Impedance Models of the Thorax and the Origin of the Impedance Cardiography Signal and Modeling of the Impedance Signals”,

in *Proceeding of 2014 IEEE Conference on Biomedical Engineering and Sciences (IECBES 2014)*, Miri, Malaysia, December 8–10, 2014.

III. Yar M. Mughal

“Decomposing of cardiac and respiratory signals from electrical bio-impedance data using filtering method”,

in the *IFMBE Proceedings, Volume 42*, International Conference on Health Informatics (ICHI'13), Vilamoura, Portugal. November 07–09, 2013, pages 252–255.

IV. Yar M. Mughal, A. Krivoshei, P. Annus

“Separation of cardiac and respiratory components from the electrical bio-impedance signal using PCA and fast ICA”,

in the *Proceedings of the International Conference on Control, Engineering & Information Technology (CEIT'13)*, Sousse, Tunisia, June 04–07, 2013.

The following paper is also published in the same field, but does not form a main part of this thesis. A copy of the publication can be found in the Appendix (Paper V).

V. P Annus, R Land, M Reidla, J Ojarand, **Y Mughal**, M Min

“Simplified signal processing for impedance spectroscopy with spectrally sparse sequences”,

- *Journal of Physics: Conference Series*, Volume 434, Conference 1,

Proceedings of the XV International Conference on Electrical Bio-Impedance (ICEBI) and XIV Conference on Electrical Impedance Tomography (EIT), Heilbad Heiligenstadt, Germany, April 22–25, 2013.

Author's Contribution to the Publications

Here is a list of the author's contributions to the papers listed on the previous page.

Paper I

The author of this thesis is the main contributor of this paper. The author has built the Impedance Cardiography (ICG) and Impedance Respirography (IRG) signals model by means of a Fourier series curve-fitting method. The author has also compared three mathematic models on different EBI datasets. The author has analysed the best-fit model of ICG and IRG signals based on statistical parameters and visual fit. Finally, the author has developed and implemented the corresponding simulator, namely the Bio-impedance Signal Simulator (BISS), which imitates the real phenomena of the signals. The author of this thesis has performed a significant part of the writing of the paper.

Paper II

The author of this thesis is the main contributor of this paper. The author has conducted the literature survey for a realistic thorax impedance model for modelling ICG and IRG signals. The author has studied five different impedance models of the thorax to evaluate their suitability with respect to development of the ICG signal model. The author has reviewed generation of the (bio-)impedance signal in order to understand the origin of the ICG waveform. Finally, the author drew the conclusion of the study. The author of this thesis wrote major parts of the paper.

Paper III

The author of this thesis was involved in preparation of the setup to measure EBI datasets. The author developed an algorithm to attempt to decompose cardiac and respiratory signals from EBI datasets. Moreover, the author drew the conclusion of the study. This paper was written by the author of this thesis.

Paper IV

The author of this thesis developed an algorithm for attempting to separate cardiac and respiratory signals from the EBI dataset. The author applied Principal Component Analysis (PCA) and Independent Component Analysis (ICA) to solve the separation problem. Finally, the author drew the conclusion of the study. The author of this paper wrote substantial parts of the paper.

Paper V

The author of this thesis was involved in the experimental phase of the study.

ABBREVIATIONS

The following frequent abbreviations are used in the thesis.

| | |
|------|--------------------------------------|
| BISS | Bio-Impedance Signal Simulator |
| CO | Cardiac Output |
| CT | Computed Tomography |
| CVS | Cardiovascular System |
| EBI | Electrical Bio-Impedance |
| ECG | Electrocardiogram |
| EIT | Electrical Impedance Tomography |
| EWI | Electro-mechanical Wave Imaging |
| FCG | Foucault Cardiography |
| HR | Heart Rate |
| ICG | Impedance Cardiography |
| ICT | Information Communication Technology |
| IRG | Impedance Respirography |
| MRI | Magnetic Resonance Imaging |
| OEP | Opto-Electronic Plethysmography |
| RR | Respiration Rate |
| RV | Respiration Volume |
| SV | Stroke Volume |
| TEB | Thoracic Electrical Bio-Impedance |
| TPR | Total Peripheral Resistance |
| TV | Tidal Volume |

LIST OF SYMBOLS

The following symbols are used in the thesis.

| | |
|-----------|-----------------------------------|
| \dot{Z} | impedance [Ω] |
| V | Voltage [V] |
| I | Current [A] |
| R | Resistance [Ω] |
| f | Frequency [cycles per second, Hz] |
| t | Time [s] [1 min = 60 s] |
| S | Signal (in general) |

SHORT DEFINITIONS OF TERMS

Signal:

A signal is a function in time that conveys information about the behaviour or attributes of some phenomenon. In this work, examples of signals include impedance cardiography (ICG) and impedance respirography (IRG) signals.

Signal Modelling:

The idea of signal modelling is to represent the signal via (some) model parameters. For example, in this work, the ICG and IRG signals are modelled by means of Fourier series.

Signal simulator:

A signal simulator is a system designed to provide a realistic imitation of a signal with the possibility to control its operation. A Bio-Impedance Signal Simulator (BISS) is developed in this work.

Simulation:

Simulation is the imitation of the operation of a real-world process or system over time. The act of simulating such a process or system first requires that a model be developed.

This model represents the key characteristics or behaviours/functions of the selected physical or abstract process or system.

In this work, Bio-Impedance Signal Simulator (BISS) is used to simulate the Electrical Bio-Impedance (EBI) signals based on the ICG and IRG signal models.

Framework:

A framework is a conceptual structure intended to serve as a support or guide for building an application. In this work, a framework for developing bioelectrical applications is proposed. Furthermore, its usage is exemplified for the EBI case.

1. INTRODUCTION AND MOTIVATION

Healthcare is becoming an important challenge around the world. Many developed countries are facing socio-economic problems such as increasing healthcare costs. For example, in 2010, the USA alone spent about US \$2.5 trillion (17% of its GDP) on healthcare, and this number is expected to grow in the future due to emerging new requirements in healthcare. In response to these growing concerns, developed countries such as the USA, EU, and Japan are advancing a new healthcare model called “Personalized Healthcare” to control the healthcare costs while improving the medical quality by use of Information Communication Technology (ICT) (Wu 2011).

These concerns result from phenomena such as a) increasing average life expectancy and the ageing of baby boomers, as well as b) the growth of chronic diseases (e.g. cardiovascular diseases) related to, e.g. dietary and lifestyle factors.

Regarding a), the increased size of the elderly population (65+) is becoming a worldwide demographic phenomenon. It is approximated that in 2050 people aged 65 or more will be found as follows: in Europe ~40%, in Japan 36%, in China the figure will increase from 10% in 2006 to 28% in 2040, and in the USA it will reach 19.6% in 2030 (Wu 2011).

Regarding b), cardiovascular diseases are very common. For example, in the USA cardiovascular diseases caused 788,000 deaths in 2010, which was 32% of all deaths. The cardiovascular disease-related number of deaths increased considerably from 1900 to 1970 and remains high. Heart disease is the top cause of death; the primary case, coronary heart disease, caused 380,000 deaths (NIH 2010).

In Europe, cardiovascular diseases cause over 4 million deaths every year, including more than 1.9 million deaths in the European Union (EU). Cardiovascular diseases cause 47% of all deaths in Europe and 40% in the EU. Cardiovascular disease is the primary cause of death in women in all European countries and is the primary cause of death in men in all but 6 European countries (EHN 2012).

To deal with issues related to a) and b), there is an increasing need and requirements for monitoring and analysing human cardiovascular functions, especially for enhancing continuously for non-invasively and non-obtrusively underneath clinical and ambulatory conditions.

In particular, how to extract useful information from cardiac signals for the diagnosis of diseases and judgment of heart function is of special interest. Thus, the development of effective, robust, and efficient diagnostic tools for heart disease symptoms such as cardiac rhythm disorder and arrhythmia is required to help medical personnel to investigate and analyse the cardiac signals in detail (Kersulyte et al. 2009; Gargasas et al. 2004).

In this context, electrocardiogram (ECG) analysis is mostly used in clinic practice, but usually only in a visual way (Gargasas et al. 2004; Kersulyte et al. 2009).

Generally speaking, the aim when developing new techniques and tools is to minimize the required cost, long hospitalizations and increase patient’s ease and safety

(Solà et al. 2011). Thus, in this PhD project, non-invasive electrical-based methods are of special interest; such non-invasive electrical signal-based procedures are now very common (further discussed in detail in Section 2.4.1 of Chapter 2). The main advantage of this type of procedures is that they do not need to break the skin and are not only used for making a diagnosis but are also usable for treating patients (e.g. electrotherapy, radiotherapy, as discussed in Section 2.4 of Chapter 2).

Nevertheless, non-invasive procedures are not without their own practical problems. In what follows, examples of such problems are discussed.

1.1 Problems and Statements of Data Acquisition

Non-invasive data acquisition suffers from various problems; some of them are discussed below.

- a) The human body is inhomogeneous; this makes it difficult to measure accurate and valuable information from the body, such as when measuring cardiac and respiratory information.
- b) The body evaluation model is a combination of three different sublevel models, i.e. electrical, mechanical (hydraulic and pneumatic), and geometrical models of the body (Malmivuo & Plonsey 1995).
- c) It is important to place the measuring sensors according to the body's model. The optimal positioning of the measuring sensors increases the measurement accuracy and influences the reliability of data, as well as repeatability and accuracy of the evaluated haemodynamic parameters.
- d) The measured data is a combination of various signals (e.g. cardiac (S_{Cardiac}), respiratory ($S_{\text{Respiratory}}$), motion artefacts (S_{Artefact}), noise (S_{Noise}), etc.). As an example, the measured data are useful only if one can separate cardiac and respiratory signals and simultaneously suppress the unwanted artefacts such as motion artefacts, noise, and stochastic disturbance.
- e) The quality of instruments and sensors should assure the quality of the measurement.

1.1.1 Issues with Extraction of a Useful Signal: the Example of Separation of Cardiac and Respiratory Signals during Non-invasive Procedures

Separating cardiac and respiratory signals are useful to cardiologists (medical personnel) for diagnosing and monitoring purposes. By means of measurements, one can assess physiological activities and the structural configuration of a tissue, as well as offer the possibility to analyse dynamic processes in organs such as the heart and lungs. Thus, a method needs to be developed that is capable of separating the useful signals, mainly cardiac and respiratory ones, and to suppress the unwanted artefacts, such as noise and motion artefacts, from the measured signal. The method should work robustly and efficiently in a real-time environment.

The research community has developed many algorithms to solve the separation problem (Krivoshei et al. 2008; Krivoshei 2006; Krivoshei et al. 2006), including our previous studies (Mughal et al. 2013; Mughal 2014), where algorithms are developed to solve the separation problem of the cardiac and respiratory signals from measured data. However, none of these methods provides any mechanism to evaluate the performance of the developed algorithms.

Because of the measurement and useful signal extraction problem, there exist uncertainties regarding a) the properties of the signals such as amplitude, waveform, components (e.g. cardiac vs. respiration), and b) the origin of the signal waveform (e.g. is it due to configuration/positioning of electrodes/sensors or the condition of the patient). This, in turn, limits the quality of the diagnostics for diseases and conditions.

To help in dealing with the measurement and useful signal extraction problems discussed above, it is argued that modelling the measured signals offers several advantages as compared to relying on measured data only:

- a) By using a formalized representation (e.g. mathematical), the parameters of the signal model can be easily manipulated and/or modified, thus providing mechanisms that allow researchers to reproduce and control such signals.
- b) In turn, having such a formalized signal model makes it possible to develop tools (e.g. simulators) that can be used for manipulating and understanding how the signal changes depending on various conditions, as well as for generating input signals for experimenting with and evaluating the performance of, e.g. useful signal extraction methods such as separation algorithms.

Once the (bio-electrical) data is measured, it is necessary to model the corresponding signals for analysis. In this case, the so-called advanced user¹ should have to follow a structured approach to move from real measured data to model the corresponding signals. Therefore, in this PhD work it is proposed to:

- a) devise a generic framework that could be used to guide both the modelling of the signals of interest and the development of an application for bioelectrical information for further processing; and
- b) implement the framework as a specific example for the EBI case.

¹ An advanced user is a person who makes the decisions in each step and analyses the results in order to develop an application.

1.2 Need for Modelling the Cardiac and Respiratory Signals and Development of the Corresponding Signal Simulator

The modelling of the heart and lung signals allows the advancement of knowledge regarding the interplay of anatomical structures and physical phenomena, which contribute to cardiac and respiratory physiological and pathophysiological behaviours. Applications of this knowledge are found in biomedical research, education and training. An important application of modelling in biomedical research is to evaluate the performance of, e.g. separation algorithms. The models provide a somewhat simplified description of the heart and lungs and can exist in physical and mathematical representations. Mathematical models are commonly computer-based and applied in numerical simulations.

Because of the aforementioned problems, signals need to be modelled and a corresponding simulator must be developed. The end-user² can use the simulator to model the signals as per his/her needs.

Our study results (Mughal 2014; Mughal et al. 2013) provide the motivation to develop a signal model which imitates the real phenomena of cardiac and respiratory signals. In addition, the end-user has the freedom to generate the required simulated signal(s) based on his/her needs and mix artefacts and noise artificially. This idea led to developing a framework for biological information. In this study, the focus was narrowed down to develop a generic framework for modelling the bioelectrical information, and this framework is implemented, as an example, for EBI signals.

For the example at hand, the separation problem was initially addressed and an electrical bio-impedance signal model and corresponding simulator were developed. The latter could be used to evaluate the performance of separation algorithms because it is very difficult to evaluate the performance of separation algorithms based on the measured dataset only. For this purpose, a signal model is required to simulate artificial signals, which imitate the real cardiac and respiratory phenomena in order to evaluate the performance of algorithms before applying the developed separation algorithm on real measured data.

The developed simulator, namely the Bio-Impedance Signal Simulator (BISS), could also be used in teaching and training of physiological courses for engineering and health science students. It would give a “hand-on means” to the students to understand the complicated physiological phenomena.

² The end-user is a non-technical person who uses BISS to simulate the signals as per need/requirement/wish.

1.3 Framework for Biomedical Applications for Modelling and Simulating Bioelectrical Signals

The basic principle of a framework is “Not having to reinvent the wheel” (Hunter & Tan 2006) each time new bioelectrical applications must be developed.

Thus, in this work, a framework is a conceptual structure intended to serve as a support or guide for building bioelectrical applications. It provides a basis on which developers can develop applications for the specific tasks. It includes several phases, which point to the kind of steps that can or should be followed, and how these steps would interrelate.

1.4 Research Questions

To deal with the issues discussed above, several research questions can be posed. The following questions will be investigated in this thesis:

- a) Is it possible to develop a generic framework for modelling the measurable bioelectrical signals? In particular, what are the main steps and parameters that must be taken into account?
- b) Is it possible to develop a sufficiently accurate signal model of the bioelectrical signals that:
 - i) imitates the real physiological phenomena in the form of corresponding cardiac and respiratory signals and
 - ii) simulates the parameters such as heart rate (HR), respiration rate (RR), artefacts, and noise? This would illustrate how the generic framework can be applied.
- c) How to implement a simulator (tool) that incorporates the above signal model and lets the end-user simulate the signal as per his/her need?
The end-user should be able to control parameters such as HR, RR, timeframe, amplitude (amplitude of heart rate, respiration rate, artefacts, and noise) and load/save different human states/conditions that reflect these parameters.

1.5 Main Contributions of the Thesis

The main contributions of this thesis are:

- a) A novel generic framework for modelling the bioelectrical information is proposed. To the best of my knowledge, this is a unique approach to proposal of such a framework and the first effort that provides support and guidance for building bioelectrical applications, namely the steps that range from measuring the bioelectrical data from the subject, the cleaning process for the measured bioelectrical data, and developing the corresponding simulator. Thus, the framework provides a pathway between biological systems and bioelectrical applications (see Chapter 3).

- b) A bio-impedance signal model is developed by means of a regression-based curve-fitting method to imitate the real ICG and IRG phenomena; the proposed approach is more realistic than existing approaches (see Section 2.5 in Chapter 2 and Section 4.2 in Chapter 4).
- c) Three regression models for modelling the ICG and IRG signals are tested and compared for six datasets. For modelling the ICG and IRG signals, a Fourier series is found to be better than the polynomials and the sum of sines. This is because the resulting modelled signals have the lowest error compared to the real signals and a high correlation with these signals (i.e. between the modelled and template signals; see Section 4.2 in Chapter 4) and visually a Fourier series model is also the best fit with the template signals.
- d) Based on the developed bio-impedance signal model, the corresponding novel BISS is developed. To the best of my knowledge, BISS is the first EBI signal simulator that both imitates the real ICG and IRG signals phenomena and gives the freedom to the end-user to simulate EBI signals as per his/her needs (see Section 4.3 in Chapter 4).

1.6 Structure of the Thesis

The rest of the thesis is structured as follows:

Chapter 2 describes the state of the art related to the physiology of cardiovascular systems, the cardiovascular model, acquiring physiological information from the cardiovascular system, CVSim (a cardiovascular simulator developed at MIT), and the analysis of existing approaches for modelling the bio-impedance signal. This chapter is mostly based on Paper II and also partially based on Papers I, III and IV.

Chapter 3 focuses on the proposed novel generic framework for modelling the bioelectrical information, including a detailed description of the various steps involved. At the time of writing, the contributions of this chapter are being included in a paper that will possibly be submitted for a journal publication.

Chapter 4 describes an implementation example of the proposed framework and the experimental results of the modelling and simulations. The measurement method and proposed method for modelling the bio-impedance signal and corresponding BISS are discussed. The EBI method is used as an example to implement the proposed novel generic framework for modelling the EBI data. This chapter is mostly based on Paper I and also partially based on Paper II.

Chapter 5 concludes the research findings and presents further research directions.

The remainder of the thesis consists of one appendix. It presents the four main publications (Papers I to IV) from the full list of five, which are shown on page 11, and the author's CV (English and Estonian).

2. STATE OF THE ART OF MODELLING AND SIMULATION OF THE PHYSIOLOGICAL SYSTEMS

This chapter reviews the physiology of the cardiovascular system in order to understand its main mechanisms and parameters, which are of interest in this PhD work. This chapter also describes other researchers' approaches to developing cardiovascular system models as well as three simulation examples, namely a) a cardiovascular simulator ("CVSim"), b) a software tool for analysing breathing-related errors in transthoracic electrical bio-impedance spectroscopy measurements, and c) simulation of lung edema in impedance cardiography.

However, a detailed study of the physiology of the cardiovascular system is not performed since this is beyond the scope of this thesis work.

Based on the understanding gained in the review, a generic framework is devised to guide the development of bioelectrical information signal models; this framework is discussed later in Chapter 3. Subsequently, ICG and IRG signal models and a corresponding simulator are developed, which are discussed in Chapter 4.

2.1 Cardiovascular System

Before looking at the existing models of the cardiovascular system (CVS) in Section 2.2, this section gives a short background to the actual human CVS in order to aid the reader understanding the basis on which these models were developed.

2.1.1 Structure and Functioning of the Cardiovascular System

The CVS is the central transport system in the human body. The transport of substances which must be distributed to different parts of the body is carried out through blood flow by the vessels of the two circuits of the CVS, i.e. the systemic circuit and the pulmonary circuit (Timischl 1998; Kappel & Peer 1993).

Blood is the transport medium inside the CVS wherein the substances which have to be transported are either dissolved in plasma (for example, the main part of carbon dioxide (CO_2)), or bound to carrier molecules (for example, oxygen (O_2), which is bound to the haemoglobin of the red blood cells).

The essential blood flow is created by the heart, which can be considered as a serial arrangement of two pulsatile pumps (left and right ventricles); this is depicted in Figure 2.1. The systemic circuit is the part of the CVS that actually distributes the substances in the body, although the pulmonary circuit, along with the lungs, is primarily responsible for the exchange of the oxygen blood gases (O_2 and CO_2) (Kappel 2012).

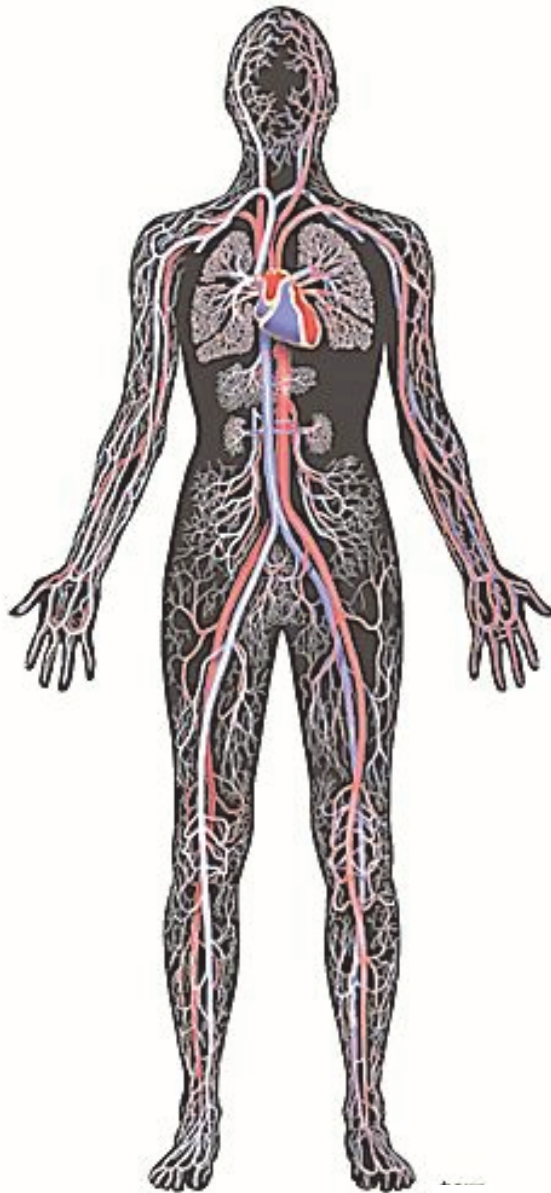


Figure 2.1 The simplified human circulatory system (Harrub 2005).
Oxygenated blood (red) and deoxygenated blood (blue).

The heart is the primary organ in the human body; we cannot live without the heart. Although the heart is “just” a pump that makes the blood circulate in the body, the heart is nevertheless a complex and important organ. Like all other pumps, it can become clogged, break down, and require repair. This is why understanding how the heart works is critical. The anatomy of the heart is depicted in Figure 2.2; with some knowledge

about one's heart and what is good or bad for it, one can significantly reduce his/her risk for heart disease (Bianco 2014).

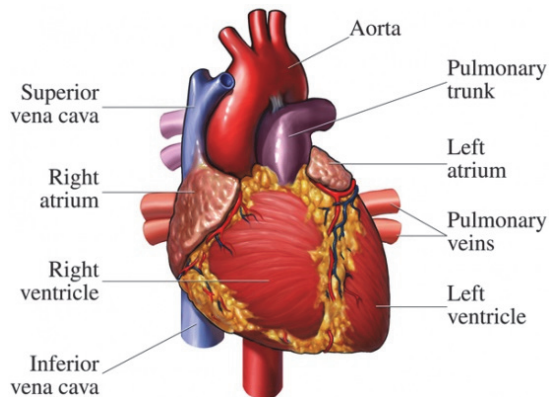


Figure 2.2 Anatomy of the heart (Bianco 2014).

Heart disease is the leading cause of death in the United States. Almost 2,000 Americans die of heart disease each day. This means that every 44 seconds someone dies of a heart-related issue in the USA. On the other hand, the good news is that the heart disease death rate has been steadily falling. Unfortunately, heart diseases are still a reason for sudden death and many people die before even reaching the hospital (Bianco 2014).

The Baroreceptor Reflex

The baroreceptor reflex is the most powerful mechanism in the control of systemic arterial pressure. The baroreceptors are spray-type nerve finishes in the walls of the carotid sinus and the aortic arch. The impulse rate of the baroreceptors is an exact image of the transmural pressure. The transmural pressure is the difference in pressure between two sides of a wall or an equivalent separator.

The firing rate increases during systole and decreases during diastole; therefore, the mean firing rate increases with mean arterial pressure. Moreover, the faster the pressure changes, the greater the response of the baroreceptors. In the absence of arterial baroreceptors, the mean arterial pressure would be higher and there would be large variations around the mean value (Timischl 1998).

Control of Local Blood Flow

The control of local blood flow is an important mechanism of the circulatory system. Each tissue has the capability to control its own local blood flow according to its demand. Certain vessels, especially arteries in the brain and kidneys, can adjust their resistance so that the blood flow stays almost constant if the blood pressure changes. This mechanism is called the Bayliss effect or myogenic auto-regulation.

Another important mechanism of blood flow control is metabolic auto-regulation, which exists in the small arterioles. If the metabolic rate increases or if less oxygen exists, different chemical substances (a “metabolic cocktail”) are released which cause vasodilation of the small arterioles. Thus, the blood flow is increased and consequently, on the one hand, more nutrients per time are carried to the tissues, and, on the other hand, more unnecessary waste products are removed from the tissues (Timischl 1998).

Frank-Starling Mechanism and the Bowditch Effect

The pumping capability of the heart depends upon contractility, pre-load and heart rate (HR). The entire heart can increase its contractility with the help of three mechanisms: the Frank-Starling mechanism, the Bowditch effect, and sympathetic activation.

- a) The Frank-Starling mechanism refers to the intrinsic capability of the heart to adjust to changing loads of inflowing blood. The heart pumps all the blood that comes into the aorta. For instance if pre-load and force are increased, so in this way increased stroke volume (SV) and pumped against the unchanged aortic pressure. One of the most important effects of the Frank-Starling mechanism is that changes in the arterial pressure against which the heart pumps (=afterload) have almost no effect on SV. If everything else remains constant, SV increases with increased afterload and vice versa. Afterload influences SV by affecting the velocity of contraction (“force-velocity relationship”) (Timischl 1998; Patterson et al. 1914).
- b) The Bowditch effect is reported as the sensitivity of the cardiac muscle to the interval between contractions. The vigour of the contractions increases if the heart rate increases. The reason is that the interval between heartbeats influences the quantity of calcium available to the force-velocity relationship (Timischl 1998; Patterson et al. 1914; Franz et al. 1983).
- c) The sympathetic nervous system increases the heart rate (HR) and contractility.

2.1.2 The Respiratory Centre

Strictly speaking, the respiratory centre is not part of the CVS, but it plays an important role closely related to that of the CVS.

The respiratory centre is situated in the medulla oblongata³ and pons; it contains various broadly dispersed groups of neurons. The so-called vagal and glossopharyngeal nerves transmit sensory signals into the respiratory centre from the peripheral chemoreceptors, the baroreceptors, and from different types of receptors in the lungs.

³ The medulla oblongata is the lower half of the brainstem, which is continuous with the spinal cord, the upper half being the pons. It is mostly related to the medulla. The medulla covers the cardiac, respiratory, vomiting, and vasomotor centre, and hence deals with the autonomic (involuntary) functions of heart rate, breathing, and blood pressure.

The respiratory centre is also closely related to the vasomotor activity⁴. Nearly any cause that increases the degree of vasomotor activity also increases, at least moderately, respiration. The neurons in the respiratory centre make the rhythm of respiration and transmit nervous signals to the inspiratory muscles (Timischl 1998).

The overall level of respiratory centre activity is controlled based on the ventilation (i.e. breathing) needs of the body. It is the ultimate goal of respiration to uphold proper concentrations of carbon dioxide, hydrogen ions and oxygen in the body fluids. This is achieved, on the one hand, via feedback that makes the respiratory centre react to changes in the chemical composition of the blood, and, on the other hand, by excitatory signals from other parts of the nervous system that control the respiratory activity (Timischl 1998).

2.2 Models of the Cardiovascular System

Given the complexity of the cardiovascular system (CVS), it would be beneficial to model it for simulation purposes, for example. Thus, developing computational models of the CVS has caught the interest of many researchers over the past decades. What follows summarizes the main developments undertaken since the 50s to model the CVS.

2.2.1 From Physiology to Mathematical Representation of the CVS

The past has witnessed concentrated re-examination of the concepts related to cardiac output regulation (Stead and Warren, 1947; Hamilton, 1953, 1955; Katz, 1955; Sarnoff, 1955; Guyton, 1955; Gregg, Sabiston, and Theilin, 1955; Rushmer, 1955, 1956; Gauer, 1955; Richards, 1955) (Grodins 1959).

Controversies have arisen, some real and some only apparent. These controversies served to focus and emphasize the requirement for a basic integration of cardiovascular dynamics.

In 1959, Grodins (Grodins 1959) developed a CVS model based on electrical circuit components. He started with the ventricles, later added a pulmonary circuit, and lastly added a systemic circuit to achieve a closed-loop model with fourteen parameters.

Later in 1963, Defares, Osborne, and Hara (Defares et al. 1963) developed a simple circulation model with six compartments. Each compartment was modelled as a capacitor connected to a ground and to the two end-to-end nodes by impedances; current (flow) through the ventricular compartments was regulated by diodes representing valves. Furthermore, Defares and his colleagues applied their model using discrete analogue components to develop an electrical circuit analogue computer for

⁴ The vasomotor centre (VMC) is a part of the *medulla oblongata*, which regulates the blood pressure and other homeostatic processes.

simulating haemodynamics with real-time behaviour grossly similar to that observed in vivo in humans.

In 1978, Katz and colleagues (Katz et al. 1978) were able to create a real-time digital simulator that was very simple. The co-called Windkessel model was programmed in the FORTRAN program language; it was run on a PDP-12 with output via D/A converters to a polygraph recorder. Thanks to the superior flexibility afforded by digital computer programs over analogue circuit models, it allowed students to vary parameters such as heart rate (HR), stroke volume (SV), total peripheral resistance (TPR), compliance, and valve competence numerically.

In 1982, Campbell and colleagues (Campbell et al. 1982) implemented a CVS model of canine haemodynamics with a five-compartment closed; they used a Hewlett-Packard 1000 computer equipped with an XY plotter. This model was similar to that of Defares; then in the model they incorporated time-varying capacitances, which had already been performed by Suga and Sagawa (Sunagawa & Sagawa 1982); the model ran noticeably slower than real time on the available hardware, because of the complexity of the model.

2.2.2 Structure of the Cardiovascular Model

In the study by Timischl (Timischl 1998), the developed part of the cardiovascular model contains two circuits (systemic and pulmonary). Both circuits are placed in series and include two pumps (left and right ventricles); this configuration is depicted in Figure 2.3.

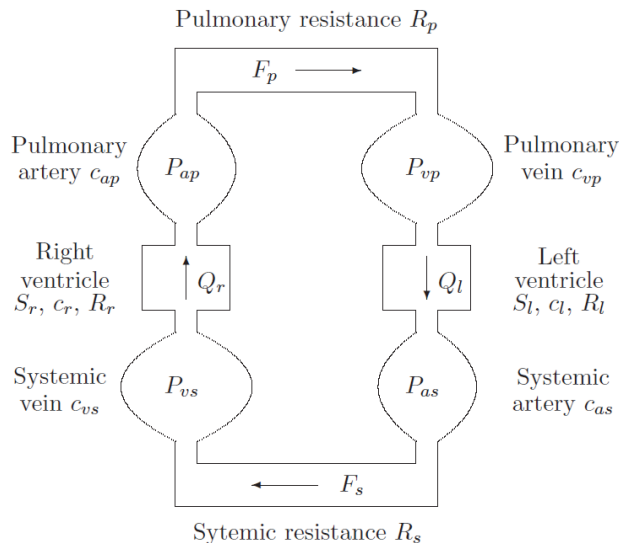


Figure 2.3 The cardiovascular part of the cardiovascular model (Timischl 1998).

A fixed blood volume V_0 is circulated between the systemic and pulmonary arteries and the systemic and pulmonary veins. The pumps and the resistance vessels are expected to represent an unimportantly small volume.

In (Timischl 1998), the cardiac circle event is ignored and it is assumed one-way and non-pulsatile blood flow by the left and right ventricles. Therefore, during a steady state, the left and right cardiac outputs Q_l and Q_r , respectively, along with the blood pressures P_{as} (systemic arterial), P_{vs} (systemic venous), P_{ap} (pulmonary arterial), and P_{vp} (pulmonary venous) in different part of the circuits are fixed. Their values represent the respective mean values over the length of a pulse (Timischl 1998; Kappel & Peer 1993).

The Mass Balance Equations

In her study (Timischl 1998), Timischl derived a continuity equation for each of the four compartments, which are the systemic artery, the systemic vein, the pulmonary artery, and the pulmonary vein. The variation of blood volume controls the systemic artery, which is the deviation between inflow (Q_l) and outflow from systemic flow (F_s). This phenomenon is depicted in Figure 2.3.

The Dependence of Ventricle Output on the Blood Pressures

During the time of steady state, the left cardiac output (Q_l) is fixed and it is determined as the mean blood flow over the length of a pulse.

The arterial and venous blood pressures depend upon the cardiac outputs. In turn, the cardiac outputs depend upon the blood pressures. To develop these relationships, the venous filling pressure, the arterial load pressure (pressure opposing ejection of the blood) and the heart rate are considered constant inputs, which can be set arbitrarily. In this way, the impact of each of them on the cardiac output and ventricular volumes can be analysed ("isolated heart").

In the study by Timischl (Timischl 1998), the objective was to derive the dependence of the stroke volume (V_{str}) on the venous (filling) pressure and the arterial (load) pressure.

Hagen-Poiseuille's Law

It is presumed that blood is a homogeneous fluid; its flow depends on the forcing pressure difference and on the opposing viscous resistance via Hagen-Poiseuilles' law (Timischl 1998). For a model considering the dependence of resistance on blood pressure, metabolic auto-regulation is taken into account when modelling exercise. Up to now, by regarding R_s and R_p as parameters, the resistance vessels are modelled as unbending tubes (Timischl 1998).

2.3 Overview of the Existing CVS Simulator and Software Tools for EBI

Many researchers are working on modelling and simulation in the area of biomedical engineering. Three relevant examples for my work are discussed below. These selected simulator and software tools are focused on cardiovascular simulation (this provides a general basis on how to structure and implement such a simulator) and on thoracic electrical bio-impedance (these provide valuable insight related to the effects of artefacts and estimation errors in EBI measurement and simulation).

2.3.1 Cardiovascular Simulator (CVSim) (Developed at MIT)

CVSim (Heldt et al. 2010) was initially aimed at teaching purposes, but it has subsequently also been used for research purposes.

In this PhD work, inspiration was gained from CVSim to develop a novel simulator (tool) for the EBI signal that could be used as a research tool to model and simulate bio-impedance signals, mainly cardiac and respiratory signals, to subsequently evaluate the performance of signal processing algorithms. It could also be used for teaching and training purposes for engineering and medicine students. More details about the simulator developed in this PhD work are discussed in Section 4.3, Chapter 4.

The first version of the cardiovascular simulator (CVSim) was developed in 1983 by Robert Sah based on Defares' model, and is similar to that of Campbell. Both models are discussed above in Section 2.2 of this chapter. Figure 2.4 depicts the six-compartment circuit model, which is introduced by CVSim.

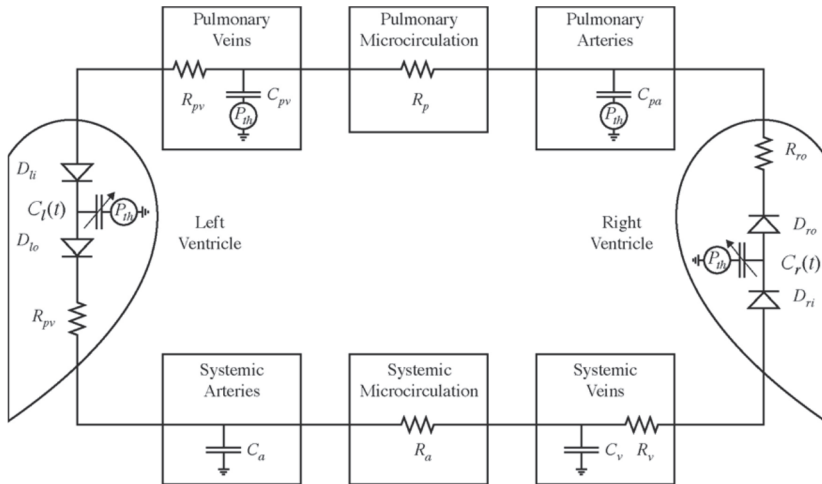


Figure 2.4 Six-compartment circuit model (Heldt et al. 2010). Counter-clockwise blood flow (electrical current) is driven by contraction of the ventricles (time-varying capacitors).

The two compartments represent the left and right ventricles utilizing time-varying capacitors joined via diodes representing heart valves. The other four compartments relate to the systemic and pulmonary arteries and veins, modelled utilizing linear capacitors and resistors representing the compliance and resistance of the vasculature fragments (Heldt et al. 2010).

In the beginning, CVSim was considered only for teaching and training purposes. Beginning in the late 1990s, Thomas Heldt and Eun Bo Shim – and, individually, Ramakrishna Mukkamala – adapted CVSim for research uses. It is a lumped-parameter model of the human CVS that has been built and applied for research purposes, as well as for teaching quantitative physiology courses at MIT and Harvard Medical School since 1984 (Heldt et al. 2010).

The CVS model is established on realistic parameter values indicating normal human physiology and contains the main arterial baroreflex system for blood pressure homeostasis. The graphical user interface (GUI) allows easy and intuitive interaction with the model. It is capable of simulating pulsatile blood pressures, volumes, and flow rates whose mean, systolic, and diastolic values are within the normal ranges of an adult human (Heldt et al. 2010).

Application

Teaching: CVSim has been employed since 1984 for teaching and training the lumped-parameter cardiovascular model to engineering students at MIT and medical students.

Research: In research, CVSim has been extended in various ways. These may be categorized as either the development and assessment of novel algorithms, or the study of cardiovascular responses to physiologic perturbations.

The Research CardioVascular SIMulator (RCVSIM) has been effectively used to build and assess system identification algorithms for evaluating transfer functions and parameters that describe the main cardiovascular regulatory mechanisms (e.g. baroreflex (BRR), control of heart rate (HR) and total peripheral resistance (TPR)), and haemodynamic parameters (maximal ventricular elastance changes) from non-invasive measurements of beat-to-beat cardio-respiratory variability (Chen et al. 2008; Lu & Mukkamala 2004; Lu & Mukkamala 2005; Mukkamala & Cohen 2001; Mukkamala et al. 2003).

The benefit of applying a cardiovascular simulator for this aim is that the real reference values of the quantities required for assessment are precisely known. Independent reference measurements in an experimental model may be difficult or even impossible in the case of a transfer function (Heldt et al. 2010).

2.3.2 Software Tool for Analysis of Breathing-Related Errors in Transthoracic Electrical Bio-Impedance Spectroscopy Measurements (EBSM) (Developed at KTH, UB and KI, Sweden and Philips, Netherlands)

In this study (Abtahi et al. 2012), the authors focused on developing a software tool (Figure 2.5) that can be employed to simulate the influence of respiration activity in frequency-sweep EBSM of the human thorax to examine the effects of the different sources of error. The helpfulness of the software tool is showcased by an example of deviations and errors gained in estimation of Cole parameters. The impedance of respiration is only modelled as a sinusoid with its amplitude controlled by an end-user to simulate spectrum measurements which are not synchronized with respiration cycle.

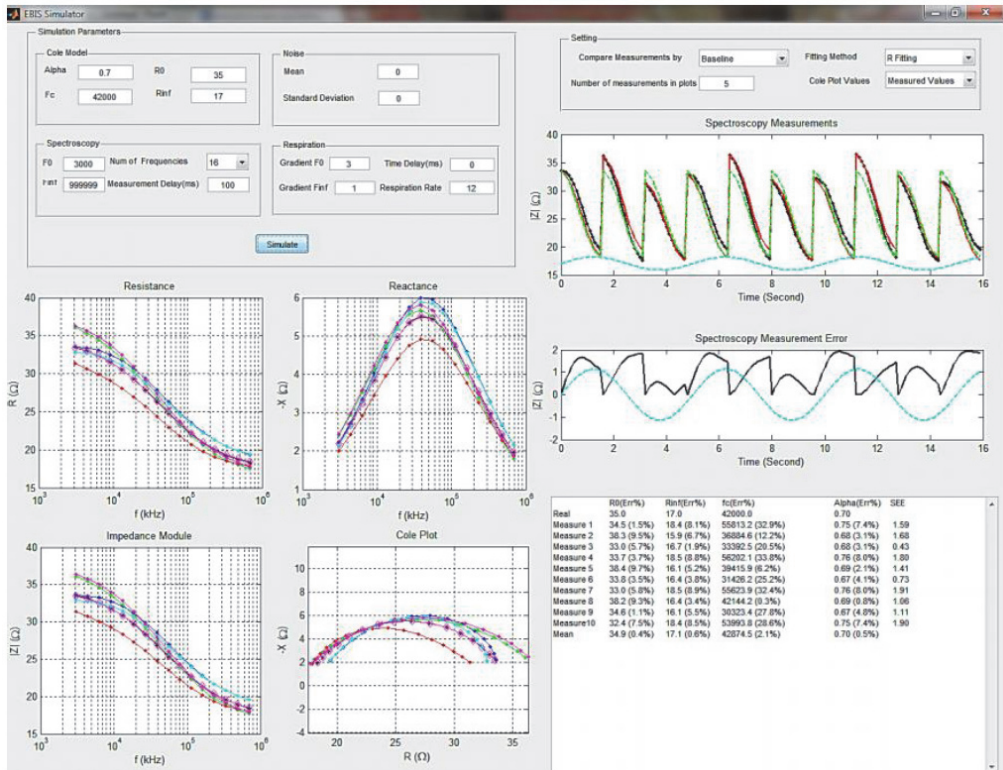


Figure 2.5 GUI of the developed software tool for Electrical Bio-impedance Spectroscopy Measurements (EBSM) (Abtahi et al. 2012).

The application of the tool has helped the authors to affirm their hypothesis that the measurement time delay caused by sweeping between frequencies on the acquisition of EBIS measurements influences the measured spectrum, generating a measurement artefact, and accordingly taints any subsequent data analysis using Cole parameter classifications.

2.3.3 Simulation of Lung Edema in Impedance Cardiography

(Developed at Philips, Germany and Netherlands)

In (Ulbrich et al. 2012), the aim was to recognize the causes for inaccuracy of the ICG in assessing the SV for heart failure patients. Thus, simulations using a finite element model (FEM) examined the effect of lung edema on the ICG.

The simulation model is based on human MRI data, along with volumetric variations of the heartbeat and aortic expansion, as well as variations during lung perfusion and erythrocyte orientation.

2.4 Acquiring Physiological Information from the Cardiovascular System

In medicine, an extensive variety of procedures, tests, and tools are already available for diagnosing and treating cardiovascular disease. Some of these procedures are very simple to use on patients, some of them are very difficult, whilst others are not only difficult but also very risky for the patients.

In a very wide and general sense, such procedures can be divided into invasive procedures and non-invasive procedures.

Invasive procedures are medical procedures that break or penetrate the skin, via catheterization or other ways of entering a body cavity. This is a large category and contains just about all major surgeries and many diagnostic tests. If it leaves a mark, it is most probably an invasive procedure.

Non-invasive procedures are also medical procedures that are very common. These procedures do not need to break the skin. Simple examples include inspecting the inside of the nose and performing a check-up of the eardrum. However, more advanced or complicated procedures can also be performed non-invasively.

Non-invasive procedures comprise a large category including methods such as imaging studies, together with x-rays, ultrasound, MRI, and CT scans. ECGs also fall under the non-invasive category. Some of these procedures are not only for making a good diagnosis; they are also used for treatment of patients. For instance, radiotherapy is used to treat cancer patients. In this procedure, a simple radiation is applied to the particular area of the patient's body in order to kill a cancerous tumour. In this procedure, it is not required to break the patient's skin, as the radiation beam can be applied from the outside (Rosenberger 2009). The literature reports on the various studies that took place to compare invasive and non-invasive methods; more details can be found in e.g. Jurjević et al. 2009 and Soudon et al. 2008.

2.4.1 Need for Non-invasive Methods

The aim of non-invasive methods is to minimize the required cost and hospitalization time, as well as to increase patient ease and safety (Solà et al. 2011). The ECGs, intermittent blood pressure (BP) monitors, and pulse oximeters have been successfully released into the market, paving the way towards the monitoring of cardiac and vascular parameters in hospitals and out-patients (Parati et al. 2008).

The non-invasive electrical-based methods are of special interest because these are mostly simple, safe, and inexpensive means of assessing haemodynamic parameters. The following lists the most relevant ones and their respective use related to cardiac diseases.

- a) **Electrocardiogram (ECG)** is a record of the electrical activity of the heart. The sensors detect electrical impulses coming from the heart, where the heart muscle contracts. ECG is normally used to detect abnormal heart rhythms and to inquire as to the cause of chest pains (Kenny & Tidy 2012).
- b) **Opto-Electronic Plethysmography (OEP)** is a relatively novel technique to assess the ventilation pattern by an external measurement of the chest wall surface motion. The OEP system measures variations in the complex shape of the chest wall while breathing by modelling the thoracoabdominal surface with a large number of points belonging to chosen anatomical reference sites of the rib cage and abdomen (Santos et al. 2013).
- c) **Electrical Impedance Tomography (EIT)** is monitoring technology based on the analysis of multiple bio-impedance signals. From an electrical perspective, the thoracic cavity is composed of distributed impedance volumes. While the lungs are filled with air, they form high impedance volumes, whereas the heart and blood vessels, filled with blood, form volumes with lower impedance (Solà et al. 2011).
- d) **Impedance Cardiography (ICG)** measurement has been offered as a cost-effective non-invasive method for monitoring haemodynamic parameters. The time-variant part of the bio-impedance (BI) phasor reflects processes in the patient's physiological state, since some changes in BI can be caused by normal activity or pathological reasons (Grimnes & Martinsen 2014; Mughal 2014). Extracting information from impedance signals for diagnosing diseases and assessing heart function is essential for exploiting this method (Mughal et al. 2015).
- e) **Foucault Cardiography (FCG)** is a method for monitoring the cardio-haemodynamic cases of the cardiac region of the thorax with the eddy currents induced in it using radio-frequency magnetic field. The measurable signal is acquired because of the variation in the power absorbed by the tissues, along with the variation of their electrical impedance (Trolla & Vedru 2001).
- f) **Electro-mechanical Wave Imaging (EWI)** is an entirely non-invasive, non-ionizing, ultrasound-based imaging method. It is based on mapping the electro-mechanical activation sequence of the myocardium along various echocardiographic planes. EWI is capable of detecting and mapping the electromechanical contraction wave (Kohl, Peter Sachs, Frederick Franz 2011).

From the measured data (obtained by means of one or several of the above procedures), one can assess physiological activities and structural configurations of a tissue, as well as analyse dynamic processes in organs such as the heart and lungs.

Data measurement plays a key role in measurement of the stroke volume (SV) of the heart, cardiovascular system, and many other parameters, as described by Cotter et al. 2006.

The six non-invasive bioelectrical methods listed above have their own merits and limitations. Still, one key problem shared by all of them is that of the measurement and useful signal extraction. In particular, there exist uncertainties regarding the properties of the signals, such as amplitude, waveform, components (e.g. cardiac vs. respiration), and the origin of the signal waveform (e.g. is it due to configuration/positioning of electrodes/sensors or the condition of the patient). This, in turn, limits the quality of the diagnostics for diseases and conditions.

Therefore, being able to model the signals obtained by the above methods is highly desirable for analysis and comparison purposes. In order to create models and simulators for bioelectrical signals, a generic framework has been devised in this PhD work. This framework can be used to guide the development of such signal models and simulators for the six methods above by means of a structured flow that includes the measured object, measurement and pre-processing, modelling and simulation, and the final application. This framework is described later on in Chapter 3.

In this PhD work, the measured EBI data is used to model the ICG and IRG signals and to build the corresponding simulator (BISS). The ICG does not separate different objects during the measurement. Electrode positioning can help (at least somewhat). If the electrodes are placed properly, relative to what is required to be measured, such as HR, SV, cardiac output (CO), respiration rate (RR), muscular movement, etc., then in this case ICG is one of the very prospective method among the above/mentioned non-invasive methods. The ICG is a verified method. The determination of the cardiac stroke volume is an area in which accurate, easily applied methods are desirable (Malmivuo & Plonsey 1995).

The remaining above-mentioned methods also have some limitations; for example, ECG does not reflect the actual blood flow and cardiac output, and it does not tell much about the real pumping effectiveness of the heart. The OEP is multipoint; it cannot be simple. The EIT is a complicated multi-electrode system for which intensive computing is needed; this is the reason for which the EIT is a complex and expensive method. The FCG has quite unsuitable dependence on sensitivity from the size of the coil and from the distance/depth of the organ of interest. The EWI results in images (like MRI); the question is what to do with them and how to analyse them.

Given the above discussion and the fact that the EBI method is at the centre of various on-going research efforts in the department (giving, among others, access to EBI measurement datasets), the EBI method (including ICG and IRG) has been selected as the case study in this PhD work.

The next sections introduce the ICG and IRG methods, their parameters, and respective problems.

Impedance Cardiography

Impedance cardiography (ICG) is also known as impedance plethysmography or thoracic electrical bio-impedance (TEB). TEB is a method that converts variations in thoracic impedance to changes in volume over time. These measurements, which are gathered non-invasively and continuously, have become more sophisticated and more accurate with the development of data signal processing and improved mathematical algorithms (Deborah & Alvater 2002). The time-variant part of the EBI is caused by the physiological activity of the heart. The cardiac activity is the basis of the ICG in the raw EBI data.

This method is a safe and non-invasive, and can be used to estimate the haemodynamic status of a patient (Cotter et al. 2006). This technique was first introduced by NASA in the 1960s. The first correlation between the measured EBI variations and the cardiac activity was published by Atzler and Lehmann in 1932 and Nyboer et al. in the 1940s. Nowadays, this non-invasive technique is used for estimating the cardiac output (CO) on a large scale in clinics (Deborah & Alvater 2002).

How the technique works

Through electrodes, an electrical current is supplied and then the voltage drop is measured, or the other way around, i.e. a voltage is applied and the current is measured. A low amplitude electrical current passes through the chest to excite the thoracic fluid. In each cardiac cycle the fluid volume varies, thus affecting the impedance measured by the electrodes (Deborah & Alvater 2002).

When AC current is supplied through the thorax:

- a) The supplied current first passes through the path which has low resistance, i.e. the blood-filled aorta (blood has a resistance around 1.6 Ωm compared to other tissues).
- b) With every heartbeat, the blood volume and velocity change in the aorta.
- c) ICG reflects the variation of impedance, which can correspond to the process. From ICG, the haemodynamic parameters can be derived if the transfer function is known.

Applications of ICG

The clinical applications of impedance cardiography are discussed below (Deborah & Alvater 2002).

Application in critical care:

- a) Trend and detect haemodynamic variations for earlier intervention.
- b) Provide a non-invasive bridge.
- c) Enable earlier removal of invasive lines.
- d) Quickly assess baseline haemodynamic status with any patient.
- e) Assist in invasive line management and determine need.
- f) Monitor drug titration and fluid management and optimize treatment.

ICG Parameters

This paragraph discusses an evaluation of haemodynamics. Haemodynamics refers to the blood flow or circulation in the body. The blood has high conductance and low

resistance compared to other tissues which are located near the heart and blood vessels. For instance, the blood has a resistance of around $1.6 \Omega\text{m}$, the lungs have a resistance of around $20 \Omega\text{m}$, but the bones have very high resistance, around $170 \Omega\text{m}$ (Malmivuo & Plonsey 1995). If one uses proper configuration of electrodes to measure the EBI raw data combined with a proper algorithm, it would be possible to separate tissue responses accurately (Deborah & Alvater 2002).

The ICG parameters are very important for cardiologists because they relate to stroke volume (SV) and cardiac output (CO). Some parameters will be discussed in Chapter 3, such as stroke volume (SV), heart rate (HR), cardiac output (CO), blood volume (BV), blood pressure (BP), venous return (VR), total peripheral resistance (TPR), respiration rate (RR), respiration volume (RV), etc.

Problems in ICG parameters

The major problem that influences the accuracy of haemodynamic estimation is the Sigman effect. The core of this effect is that the admittance of the blood is flow-dependant. This was reported by Sigman et al. for the first time in 1937. Because blood flow variations are not plethysmographic, this kind of variation gives errors in the measurement of blood volume.

Another issue is that of the accuracy of the SV and estimation of other haemodynamic parameters. In particular, using oversimplified models of the torso and cardiovascular systems can negatively influence the accuracy of the estimation. This oversimplification is often due to ignoring the structure of the tissue and assuming that the haemodynamic parameters are homogenous and isotropic (Krivošei 2009).

The modern cardiac pacemakers are often equipped with EBI measurement tools for calculating the SV values from intra-cardiac impedance data (Krivošei 2009).

These problems are very complicated due to the following reasons:

- a) The cardiac and respiratory components are correlated due to their nature (Sörnmo & Laguna 2005). However, it can be assumed that they could be viewed as uncorrelated under the assumption that this correlation is relatively too weak to cause sufficient errors (Mughal 2012) (Mughal et al. 2013). Both components have different sources, because cardiac signals are generated by the heart and respiratory signals are generated by the lungs.
- b) The spectra of both components partially overlap each other because the respiration rate is around four times lower than the cardiac heart rate; several higher harmonics of the respiratory signal exist in the frequency range of the cardiac signal. This is depicted in Figure 2.6.
The heart rate (HR) is autonomous, in contrast to the respiration rate (RR), which varies by a wide range and has rapid increase and decrease that make the separation problem more complicated, as well as the fact that the cardiac and respiratory signals have low amplitude, which also makes problem challenging.
- c) The EBI components are somewhat stochastic due to variations of HR and RR, stochastic disturbance, and motion artefacts.

EBI measurement problems

- The measurement of EBI relies on the quality of the instruments, such as current source, voltage measurement unit, modulators, analogue to digital convertor (ADC), digital to analogue convertor (DAC), and the quality of the electrodes (sensors). Hence, many factors (e.g. temperature, clock drift, calibration) can influence the quality of the measurements.
- The human body is not homogenous, thus the body evaluation model is a combination of three sublevel models, i.e. electrical, mechanical (hydraulic and pneumatic), and geometrical. Therefore, obtaining accurate and valuable impedance information from the body, mainly the cardiac and respiratory components, is difficult because of the varying properties of the tissues.

It is also important to place the measuring electrodes on the body according to the regions of interest. The optimal position of the measuring electrode increases the measurement accuracy and it influences the reliability of data, repeatability, and accuracy of the evaluated haemodynamic parameters.

In 2009, Andrei Krivoshei (Krivošei 2009) assumed the EBI to be the sum of five components:

$$S(t) = S_0 + S_C(t) + S_R(t) + n_S(t) + n_M(t), \quad (2.1)$$

where the basal S_0 , cardiac $S_C(t)$, and respiratory $S_R(t)$ components are combined with unwanted artefacts, such as stochastic disturbance $n_S(t)$ and motion artefacts $n_M(t)$.

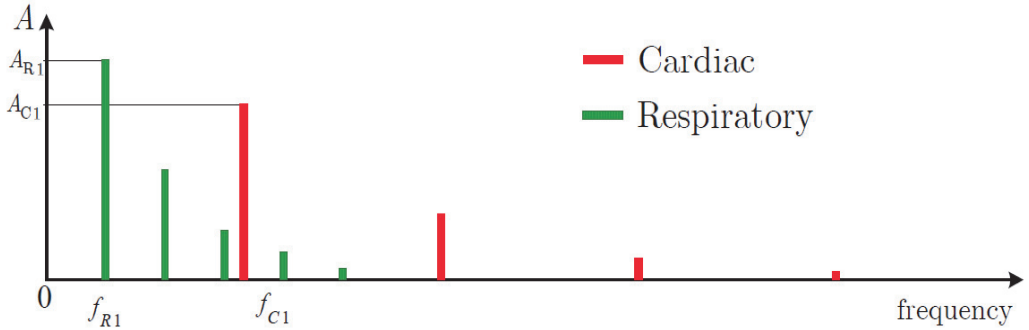


Figure 2.6 Sketch of the possible frequency domain harmonic spectrum of the EBI signal, which consists of the cardiac and respiratory components (Krivošei 2009)).

Vertical axis A is the amplitude of harmonic(s), and the horizontal axis is the frequency in Hertz (Hz).

Impedance Respirography

IRG in EBI is a basic technique for measuring the mechanics of respiration. It measures the time variation of EBI caused by respiration.

It reflects the physiological activities, state of lungs, and respiration. The estimation of pneumodynamic parameters such as minute ventilation (MV) is very important. It is close to metabolic demand during rest at 6 [l/min] and during exercise at 60 [l/min].

The MV is linearly related with the cardiac output (CO) and heart rate. This property is used in pacemakers, where the pneudynamic parameters are used to measure the human workload by metabolic demand which is reflected in ICG (Krivošei 2009).

Parameters of IRG

The important parameters of IRG are the respiration volume (RV) and the tidal volume (TV).

The TV is the volume of gas inhaled and exhaled during one respiratory cycle. In a healthy adult, the TV is approx. 500 ml per inspiration. It is measured in litres and ventilation volumes are estimated based on a patient's ideal body weight. IRG can be smoothed and rectified by using a low-pass filter (LPF)

The RV is the main parameter in respiration; it is actually a flow, which represents a volume variation over time. The RV is the amount of air a person breathes in a minute. The RV [l/min] is the average volume of air inspired into the lungs; it can be evaluated by using values of TV and respiration rate (RR [l/min]) (Krivošei 2009):

$$RV = TV \times RR \quad (2.2)$$

Problems in IRG parameters

The HR is autonomous. If compared to RR, which varies by a wide range, it is hard to estimate it. The RR can be changed by a human person consciously and, for limited amounts of time, even stopped.

2.4.2 Analysis of Impedance Models

The existing physiological impedance information models vary from the simplest ones (e.g. two or more compartments) to the 3D model of the thorax. In this PhD work, these were studied to evaluate their suitability for developing a realistic ICG signal model that is as accurate as possible, i.e. whether or not such thorax models could provide an ICG signal model.

Simplified Model of the Thorax

This is a very simplified thorax model in which the thorax is considered to be divisible into two parts: tissue (A_t) and fluids (A_b). The parts are characterized by area A of the cross-section of each of them. This model was developed to find the relationship between change in blood volume (ΔBV) and impedance change (ΔZ) (Malmivuo & Plonsey 1995; Mughal et al. 2014).

Ideal Cylindrical Models

The cylindrical models can have one or two compartments. The cross-sectional area of the ideal cylinder models may be elliptical, circular, or have any other suitable shape.

In the simple cylindrical model, the thorax is divided into either one or two compartments with the same resistivity.

In the two-compartment model, the two cylinders are physically in parallel and the conductance model is preferred, where $\Delta_v + v_A$ is the volume of the inner cylinder, and v_t is the volume of the outer cylinder; the sensitivity decreases with a larger surrounding volume (v_t) (Grimnes & Martinsen 2014; Mughal et al. 2014).

Kinnen's Thorax Model

Kinnen et al. developed their model based on a cylindrical thorax model. The purpose of this model is to examine the generation of the impedance signal. The thorax model is divided into two cylindrical parts. The inner part of the model characterizes the BV of the heart and primary arteriovenous system of the thorax. The lungs are characterized by the medium outside the inner part. The resistance for the inner part of the model was taken equal to 495 Ω , and 32 Ω for the other part (Mughal et al. 2014; Malmivuo & Plonsey 1995).

Sakamoto's Thorax Model

Sakamoto et al. developed a model that is anatomically more realistic. This model consists of the heart, aorta, lungs, vena cava, and torso shape. The model allows investigation of the effect of conductivity variations of the tissues on the measured impedance. These results showed that information connected to blood circulation in the human thorax could be measured by potential distribution changes on the body surface.

The impedance waveform is affected not only by the CO or the ΔBV in the aorta, but also by the ΔBV in the heart and lungs (Sakamoto et al. 1979; Mughal et al. 2014).

3D Thorax Model

The 3D thorax model is composed of the lungs, muscle, heart and spinal column, as depicted in Figure 2.7.

The potential distribution can reflect different effects when inhaling and exhaling; the lungs become smaller when exhaling and larger when inhaling. The potential distribution fluctuates with the change in resistivity caused by the activities in the thorax, such as inspiration and expiration. Thus, the model is helpful in judging whether there are more or less physiological activities or pathologic variations in the studied subject (Wu et al. 2008; Mughal et al. 2014).

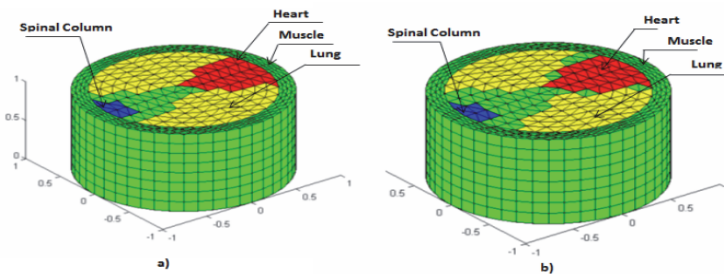


Figure 2.7 3D thorax model at the end of phase: a) inhaling b) exhaling (Wu et al. 2008).

These five models mentioned above are included in the more detailed comparison presented in our contribution (Mughal et al. 2014).

2.4.3 The Issue Regarding the Origin of the ICG Signal

This section reviews the history of the ICG signal origin generation; its understanding and related waveform markers are discussed. In particular, it is found that although a consensus exists within the scientist community, doubts and critical analyses regarding the origin of the ICG signal have been expressed.

Analysis of the Original ICG Signal Waveform

A typical impedance signal (dZ) and its first derivative (dZ/dt) can give detailed information about the physiological activities of the thorax. Figure 2.8 (Woltjer et al. 1997) depicts the different marks on the waveform, which indicate the important points. The corresponding ECG is also depicted in Figure 2.8. Research efforts have focused on discovering the physiological correlation with the ICG signal and its origin. It has been studied together with its first derivative (Woltjer et al. 1997; Xu et al. 2011).

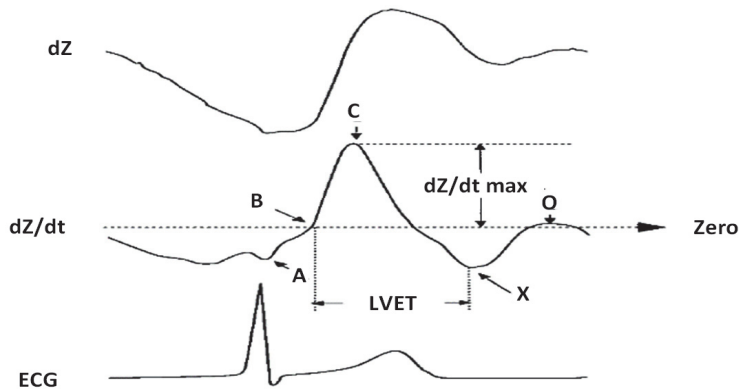


Figure 2.8 Characteristic impedance (dZ) signal [Ohms], first derivative (dZ/dt) of impedance signal [Ohms/sec], and ECG signal [Volts] (Woltjer et al. 1997).

“Zero” is a zero baseline value and x-axis is Time [sec].

In 1970, Karnegis and Kubicek first indicated that the A-wave of the dZ/dt is associated with the P-wave of the ECG and that the C-wave of dZ/dt is associated with ventricular contractions (Karnegis & Kubicek 1970). During diastole, another upward deflection of the O-wave in the dZ/dt signal was noticed. During the study, Karnegis and Kubicek found that the B-point of dZ/dt corresponded to the aortic valve opening and the X-point to the aortic valve closure. Several researchers make use of echocardiography and aortic pressure recordings and have confirmed these observations.

Furthermore, studies are required to confirm the exact physiological and anatomical origin of the impedance cardiography signal. Several investigators have dealt with this topic in the past, including a modelling and study performed on animals (Sakamoto et

al. 1979; Woltjer et al. 1997) (Wittoo & Kottke 1967; Baker et al. 1974; Kubicek et al. 1974; Thompson & Joeke 1981; Wang et al. 1991; Patterson 1985; Sakamoto & Kania 1979; Lamberts et al. 1984; Mohapatra 1981; Penny 1986; Mohapatra 1988; Wang & Patterson 1995; Patterson et al. 1993; Patterson 2010).

In order to unravel a more elaborate explanation of the origin of the C-wave marker, researchers have attempted to imitate impedance cardiographic variations in a model. Still, these are far from reliable evidence, and most fail to give details of the relationship between $(dZ/dt)_{max}$ and other physiological variables as aortic peak flow velocity. More study is required on the contributors to $(dZ/dt)_{max}$ as predicted by a model (Woltjer et al. 1997).

Based on the literature survey and analysis of the existing thorax impedance models and origin of the ICG signal, it can be concluded that none of these models are accurate enough to imitate the real phenomena in the ICG signal. A summary and the limitations of each model are discussed in Table 2.1, reproduced from our contribution (Mughal et al. 2014).

Table 2.1. Summary and Limitations of Existing Models

| Model | Summary and Limitations |
|---------------------------------------|--|
| Simplified Model of the Thorax | This thorax model is highly simplified, since the division into only two uniform tissues is used and geometrically it is not realistic. On the contrary, the real structure of the human thorax is very complicated. |
| Ideal Cylindrical Model of the Thorax | This model is also very simple, because a cylinder is used to represent the thorax structure. In particular, the cross-sectional point of view is not taken into account. |
| Kinnen's Thorax Model | Kinnen's model is simple; it indicates only two conductivity zones (blood volume of the heart and primary arteriovenous system, and the lungs). Most of the current flow would pass by the lungs. In this case, the generation of the impedance signal waveforms is primarily based on the right ventricular (RV), which is not true if we consider the real thorax physiology. |
| Sakamoto's Thorax Model | This is not an accurate enough thorax impedance model, because the blood pumps more toward the left leg side. |
| 3D Thorax Model | The model is not accurate enough because it uses a cylinder as the structure of the thorax. Furthermore, it does not take the variation of heart size during inhaling and exhaling into account. |

Given these limitations, it is thus deemed preferable to build a new signal model from measured data instead of the above models. For this purpose, it is decided to use a 16-electrode configuration belt in order to measure the EBI signal. This type of electrode setup is presumed to allow raising of strong enough amplitude variations of the ICG and IRG signals in order to record the cardiac and respiration activities caused by the heart and lungs. Further details about the EBI measurement setup used in this work can be found in our contribution (Mughal 2014). The next section discusses the existing configuration of electrodes from the literature.

2.4.4 Existing Configurations of Electrodes

The measurement of thoracic EBI has been in practice since the 1930s. Kubicek and colleagues introduced the first practical method for determination of cardiac function in a clinical setting in the 1960s. It is difficult to extract impedance response from the actual mechanical activity of the heart. The blood's volume changes occur during the cardiovascular impedance measurement. Several electrode configurations exist and many suggestions for alternative electrode arrangements are reported in the literature (Kauppinen et al. 1998).

Reliable information should be obtained when using an electrode configuration that covers the region of interest with the proper sensitivity (Kauppinen et al. 1999).

In this study, the following electrode configurations were considered:

- a) *Four circumferential band electrodes*, which were originally introduced by Kubicek et al. and are widely used in ICG applications. Circumferential band electrodes were attached around the end of the thorax. Electrical current is supplied through the outer electrode and the inner electrodes measure the voltage drop. These voltage electrodes were positioned at the lower stomach and upper neck. The distance between current electrodes on the neck and stomach was 3.2 and 6.4 cm, respectively (Kauppinen et al. 1998).
- b) *The four spot electrodes configuration* was used by Penney. The two electrodes were attached to the base of the neck, centred at about a 6-cm distance crosswise from each other. Other two electrodes were attached below the heart on the left anterolateral chest surface, one electrode was attached at the end of the ninth intercostal space, and another electrode attached at an 8-cm distance from first tenth intercostal space. The dropped voltage was measured between the remaining pair (Kauppinen et al. 1998).
- c) *Hands-to-feet spot electrodes* were used by Andrei Krivošei as input data in his research work for which data was collected at JR Medical Ltd, Estonia (Krivošei 2009).
- d) *16-electrodes in a band* are tested at the Thomas Johan Seebeck Department of Electronics, Tallinn University of Technology. A 16-electrode belt was manufactured with each electrode at a 6-cm distance from each other. This belt was worn around a person's thorax. This method was selected to acquire the datasets and is used in this study; more details can be found in Section 4.1, Chapter 4, and in our contribution (Mughal 2014).

2.5 Analysis of Existing Approaches for Modelling the Bio-impedance Signal

In this section, well-known methods that have been applied by several researchers for modelling the bio-impedance signal are discussed.

A simple bio-impedance signal synthesizer (BISS⁵) was proposed by Krivoshei (Krivoshei 2006) to generate cardiac and respiratory signals. The author used a piece-wise linear triangular function to model the cardiac signal, and a trapezium to model the respiratory signal.

The model, however, is too simple to imitate the cardiac and respiratory signals fully, and thus does not allow testing of, e.g. separation algorithms.

A cardio model based on the sum of exponential functions was proposed by Kersulyte et al. (Kersulyte et al. 2009). The purpose of their work was to find a model for cardio signals as precise as possible and compare complexity parameters of the real signals and that of the model for both healthy and sick persons. They compared two function types – polynomial and sum of exponentials.

Their results indicate that both methods lead to similar results in terms of fidelity; however, the authors also indicate that the polynomial equation depends on the signal length and number of intervals, which could lead to too many coefficients and increased computational requirements for complex signals.

A cardiac signal model based on a series of real signals was proposed by Matušek et al. (Matušek et al. 2012). By filtering and averaging the series of real signals, they estimated one average ICG signal cycle and simply replicated this cycle over time to get the final signal model.

One limitation of this approach is that it lacks a mathematical model and thus the user cannot easily reproduce the model and change its parameters.

More details about the three above models are discussed in my contributed paper (Mughal et al. 2015) and in Section 4.2, Chapter 4.

⁵ The BISS acronym is also used by Andrei Krivoshei (a researcher at Tallinn University of Technology, Estonia) in his published paper, “A Bio-Impedance Signal Synthesiser (BISS) for Testing of an Adaptive Filtering System” (Krivoshei 2006)). In his work, BISS stands for Bio-Impedance Signal Synthesizer. In my PhD work, BISS stands for Bio-Impedance Signal Simulator.

2.6 Summary of the Chapter

In this chapter, the state of the art regarding the modelling and simulation of the physiological systems has been discussed based on a survey of the scientific literature in order to understand the physiology of the human body, blood circulation, and structure of the cardiovascular system.

Many of the cardiovascular system (CVS) models are based on electrical circuit components; over time, more advanced CVS models and corresponding simulators have been developed.

However, enhancing the CVS model, the signal model, and the corresponding simulators are still an active specific area of interest.

In relation to this, impedance cardiography (ICG) is a safe and non-invasive method to assess haemodynamic parameters related to the CVS.

An analysis has been performed on the existing impedance thorax models and the origin of the ICG signal in order to evaluate the possible use of one of the models to generate the required bio-impedance signals for further experiments. It has been concluded that none of these models provide electrical bio-impedance data as per the requirement of this PhD work.

Then, a review of how other researchers approach the problem and why these methods are not suitable to solve our problem has been conducted. These methods are not suitable, mostly because other researchers used either a method that was too simple, i.e. which does not model the signal realistically, a method lacking a mathematical signal model, or a method which is computationally expensive.

For this study, it is concluded to be desirable to model the cardiac (ICG) and respiratory (IRG) signals based on measured EBI dataset.

The developed models based on measured clean ICG and IRG signals are better than the models of the ICG and IRG signals based on existing thorax models.

These literature surveys led to development of a framework for modelling the bioelectrical information and use EBI as an example to implement the framework.

In Chapter 3, the proposed framework is discussed. In Chapter 4 the proposed framework is implemented for the EBI case. The cardiac and respiratory signals are modelled and the corresponding simulator is developed in Chapter 4.

3. PROPOSED NOVEL GENERIC FRAMEWORK FOR MODELLING THE BIOELECTRICAL INFORMATION

In this chapter, a generic framework is proposed to guide the modelling of signals and to develop a simulator for the bioelectrical information. The framework is a pathway to develop bioelectrical applications; first, the bioelectrical information must be modelled based on template signals and then a corresponding simulator must be developed.

The modelling of the signals allows the advancement of knowledge regarding the interplay of anatomical structures and physical phenomena, which contribute to pathophysiological behaviours. Applications of this knowledge are found in research and education.

An important application of modelling in biomedical research is to evaluate the performance of algorithms, e.g. separation algorithms. The models provide a simplified description of the physical and mathematical representation. Mathematical models are commonly computer-based and applied in numerical simulations.

Before describing the proposed framework, the generic block diagram is illustrated for modelling of the template signals and for developing a corresponding simulator for bioelectrical information, from which the need for the framework arises.

As depicted in Figure 3.1, the template signals could be modelled with help of methods such as curve fitting, e.g. polynomial, sum of sines, Fourier series, and so on (with the help of tools such as Matlab Curve Fitting toolbox, EzyFit, TableCurve 2D, PeakFit), and waveform generation (e.g. Matlab Waveform Generator), etc.

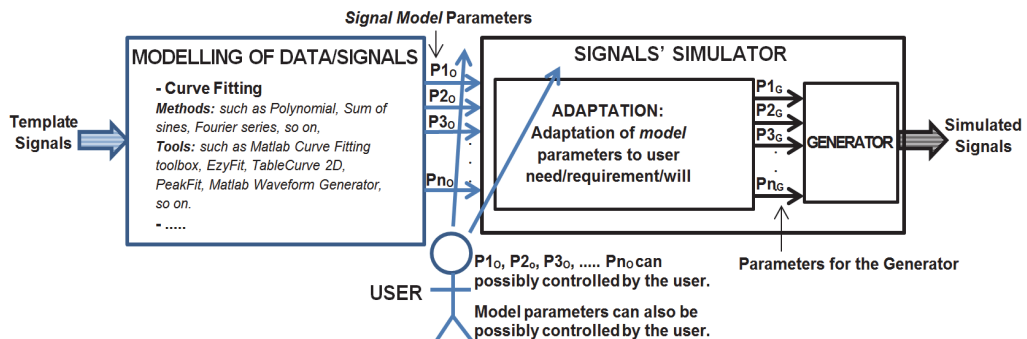


Figure 3.1 Block diagram of generic system for modelling of the template signals and for developing of a corresponding simulator.

Ideally, the developed signal model should be validated against template signals⁶. This validation could be performed based on, for example, statistical parameters such as sum of square error (SSE), correlation between modelled signal and template signal, execution time, and so on. The best-fit modelling method can then be chosen. Alternatively, a visual inspection could be performed to evaluate the fit of the model against the template signal. However, if a very accurate model is required, then both approaches should be performed.

Once the developed signal model has been validated against template signals, and thus can imitate the real phenomena, it means that the original values of the signal model parameters ($P1_O$, $P2_O$, $P3_O$, ... Pn_O) are set. These values will only be modified in the simulator by the end-user.

Now, it is required to build a corresponding simulator where the predefined signal model parameters ($P1_O$, $P2_O$, $P3_O$, ... Pn_O) are also possibly controlled (i.e. overwritten) by the end-user. Moreover, other parameters (internal to the adaptation process) could also be introduced in the simulator by the end-user; these can also be controlled by the end-user. These other parameters are used inside the adaptation process to tune the signal model parameters in order to reflect the actual phenomena that take place in the biological system/object of interest.

The core mechanisms of the simulator include adaptation. Either the adaptation of the signal model is done according to the end user's need/requirement or his/her will to simulate the signals. The generator generates the simulated signals as per end-user's prescribed parameters ($P1_G$, $P2_G$, $P3_G$, ... Pn_G), so that the end-user is able to control the signal model parameters and generate the simulated signals as desired.

The simulated signals could be used for further analysis or evaluation of the performance of algorithms, e.g. separation algorithms.

The above block diagram of a generic system (Figure 3.1) and a generic framework (Figure 3.2) for modelling bioelectrical information that can guide the model and development process has been devised. The framework serves to measure the parameters of interest for the biological system/object and the process to clean the measured data in order to achieve the ideal (template) of signals.

The flow diagram of the processes according to the proposed framework is depicted in Figure 3.2. This flow chart guides the advanced user step by step with the help of the predefined blocks.

Each diagram has specific criteria which must be kept in mind and guidelines that must be followed.

The details of this generic framework are discussed in what follows.

⁶ A template signal is an ideal signal, which has been measured and cleaned.

3.1 Novel Generic Framework

Below, in Figure 3.2, a flow diagram of data acquisition, processing, and modelling and simulation of the bioelectrical information is given.

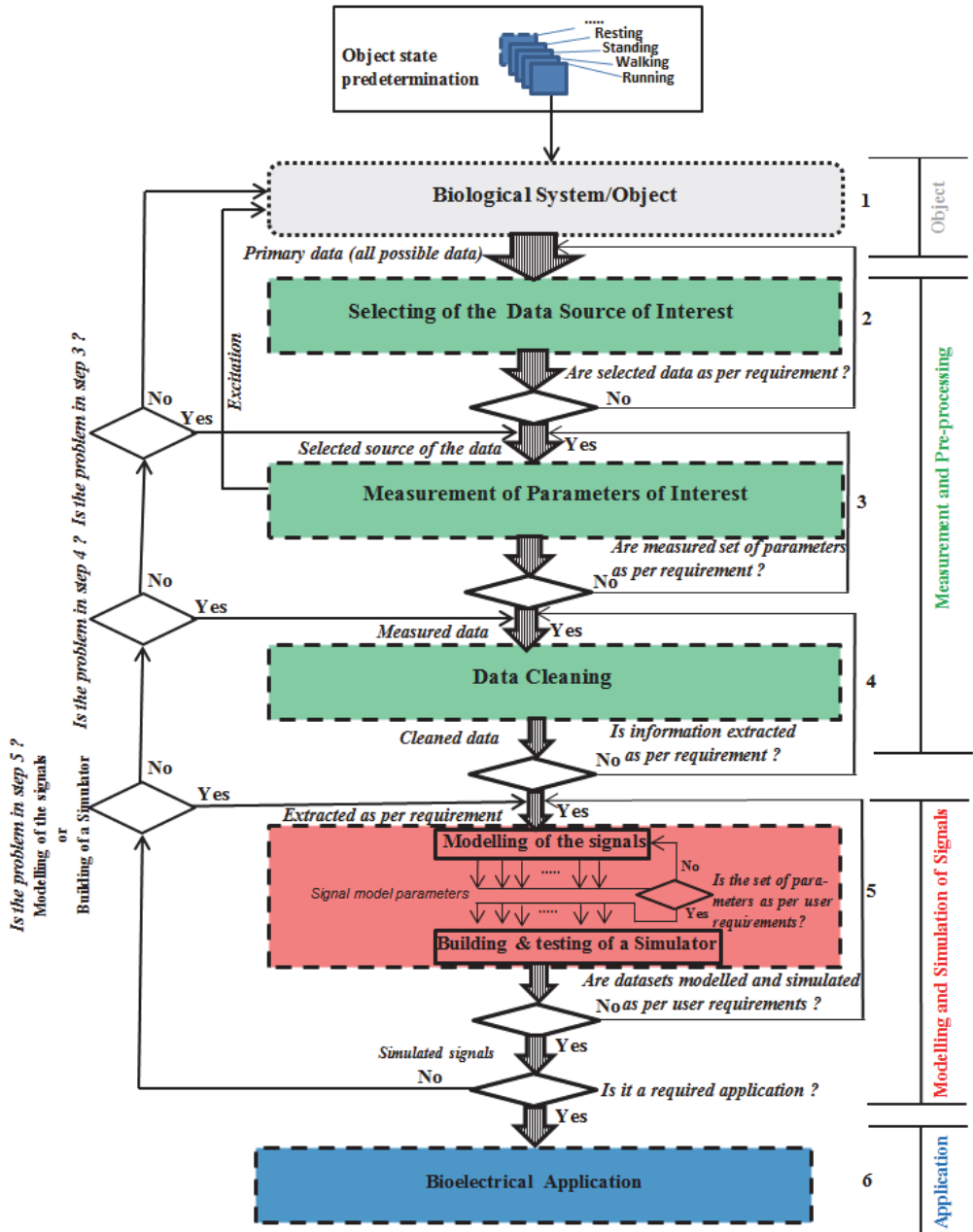


Figure 3.2 Flow diagram of the proposed novel generic framework for modelling and simulation the bioelectrical information.

This flow diagram is the pathway to application in order to model the signals. In the next chapter (see Section 4.4.1 in Chapter 4), this flow diagram is implemented for the specific case of EBI based on the IRG and ICG signals.

In the first step (Step 1 in Figure 3.2), a biological system or an object is selected; in the second step (Step 2), the data source of interest is selected; in the third step (Step 3), the parameters in which the advanced user (e.g. technical measurement personnel) is interested are measured (i.e. those which are directly measurable). After measuring the parameters of interest, data cleaning techniques are applied in the fourth step (Step 4). Then, after cleaning the data, the signals are modelled and a corresponding simulator is built in the fifth step (Step 5). In the sixth and final step (Step 6), the application of interest is developed as per the end user's needs.

3.2 Detailed Explanation of Each Step of the Novel Generic Framework

In this section each step is discussed in detail, from the first step (Step 1, selection of biological system/object) to the last step (Step 6, bioelectrical application of the novel generic framework).

3.2.1 Description of the Biological System/Object (Step 1)

This diagram (Figure 3.3) contains three systems, namely the cardiovascular system, the respiratory system, and the muscular system; each of these is illustrated by a sub-diagram. Each system contains parameters (which are the most interesting in this work), and these parameters are connected with each other within the same system. Some of these parameters are also connected with parameters which are contained in one or both of the two other systems.

Connection/relationship/dependency between the parameters inside the system or outside the system are shown with different arrows as explained below.

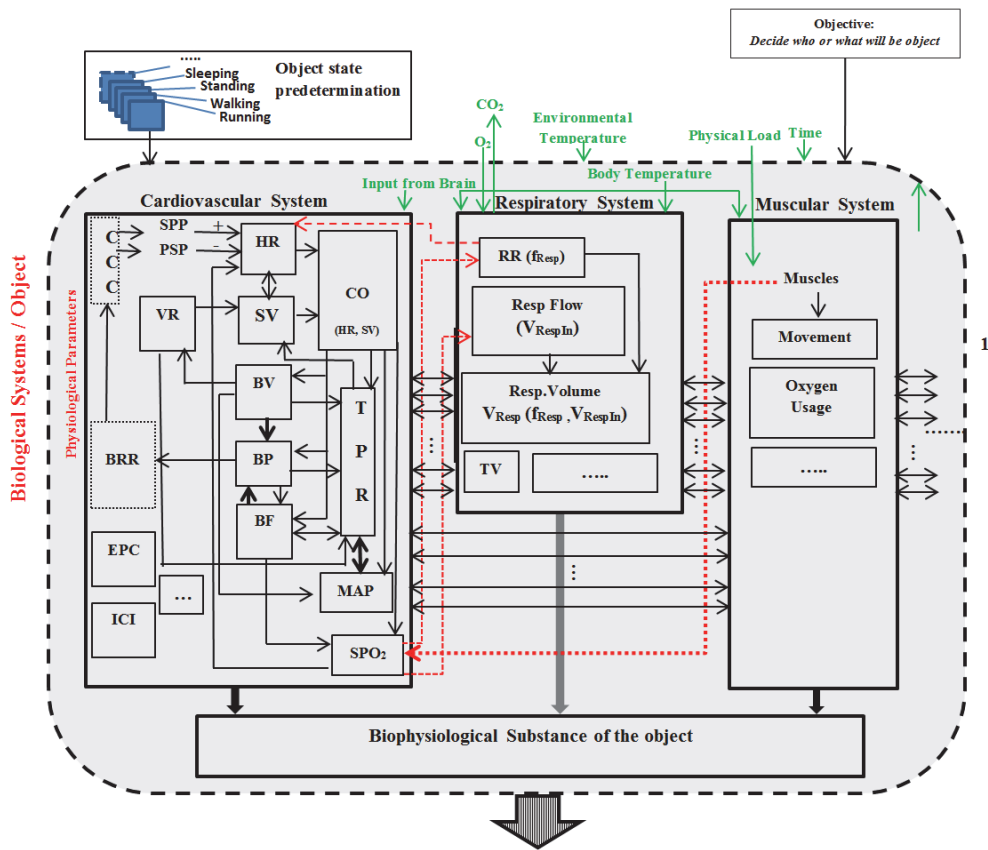


Figure 3.3 Block diagram of the relationship of parameters of three main systems (cardiovascular, respiratory, and muscular).

It shows the connection/relationship/dependency between the parameters inside each system or between the systems.

Thin arrows (solid line): show the dependency to some extent on the other parameter(s) inside the same system.

Thick arrows (solid line): show the direct relation, strong dependency on the other parameter(s) inside the same system.

Thin arrows (dotted line): show the dependency to some extents on the other parameter(s) within another system.

Thick arrows (dotted line): show the direct relation, strong dependency on the parameter(s) within another system.

Thick arrows (both site direction): show the direct proportional to each other with the same system.

The following description starts from the BRR and follows the natural flow of the three systems.

Parameters of the Cardiovascular System

BRR (Baroreceptor Reflexes): Blood pressure (BP) is controlled on a minute-to-minute basis by BRR. Changes in BP affect the frequency of action potentials sent to the Cardiovascular Control Centre (CCC) from the BRR. BRR is discussed previously in Chapter 2 in Section 2.1 and in Timischl 1998.

CCC (Cardiovascular Control Centre): Heart Rate (HR) is controlled by both sympathetic (SPP) and parasympathetic (PSP). SPP (Sympathetic) increase the HR. PSP (Parasympathetic) decrease the HR.

HR (Heart Rate): HR corresponds to the frequency of heartbeat, i.e. the number of heartbeats per minute or reciprocal of the duration of heart cycle $Y_c = 1/T_c$ [beats/minute].

VR (Venous Return): VR is the amount of blood that returns to the heart (VR dependent on BV (Blood Volume)) expressed in time units [l/minute].

SV (Stroke Volume): SV is the volume of blood which is pumped out by the heart with a single beat (SV is dependent on VR and Total Peripheral Resistance (TPR)). The HR and SV are proportional to each other [l/minute].

CO (Cardiac Output): CO is the volume of blood which is pumped out by the heart per minute. It is a function of HR and SV (CO is dependent on HR and SV) [beats/minute].

BP (Blood Pressure): BP usually refers to the arterial pressure of the systemic circulation. It is partly dependent on CO and the vessels, and directly (strongly) depends on BV and BF (Blood Flow)). In Section 2.1 of Chapter 2 and Timischl 1998 it is discussed in detail [mmHg].

BV (Blood Volume): BV is the volume of blood (both red blood cells and plasma) in the circulatory system of any individual. It is dependent on CO.

TPR (Total Peripheral Resistance): the blood vessels provide resistance to the flow of blood. The resistance and pressure are directly (strongly) proportional to each other. If the resistance increases, then the pressure increases (TPR is dependent on CO, BV, BP, BF and MAP) [Ohms].

BF (Blood Flow): The flow of the blood through the vessels of the circulatory system is a function of the BP and TPR (BF is dependent on BP, TPR, and CO). In Section 2.1 of Chapter 2 and Timischl 1998 it is discussed in detail [l/minute].

MAP (Mean Arterial Pressure): MAP represents the average driving force for the blood flow through the arterial system (MAP is dependent on CO, BV, and directly proportional with TPR) [mmHg].

SPO₂ (Saturation Pressure of Oxygen): The muscles highly depend on SPO₂ because if the muscle starts to work, they require more oxygen (SPO₂ is dependent on muscles, CO, and BF) [Percentage].

ICI (Intra-Cardiography Impedance): Measures the cardiac output internally [Ohms].

EPG (Epicardial Potential): Internal ECG [V].

Parameters of the Respiratory System

RR (Respiration Rate): RR is the number of cycles per minute. It is not directly dependent on HR, but under certain conditions, it is dependent on HR and SPO_2 [cycles/minute].

RF (Respiration Flow): Inspiration or expiration volume of airflow in a minute. RF is also dependent on SPO_2 [l/minute].

RV (Respiration Volume): RV is the volume of air that is inhaled and exhaled per minute. It is a function of RR and RF (RV is dependent on the RR and the RF) [l/minute].

TV (Tidal Volume): TV is the volume of gas inhaled or exhaled during one respiratory cycle. It is discussed in detail in Section 2.4 of Chapter 2 and Krivošei 2009.

Parameters of the Muscular System

Muscles: The muscles' ability to work is highly dependent on oxygen supply (SPO_2).

Movement: Body movement from Biological Systems/object as prescribed.

Oxygen Usage: It is dependent on real physical load.

Short Explanation of the Cardiovascular System Parameters

The cardiovascular control centre (CCC) responds by decreasing sympathetic input and increasing parasympathetic input to the heart. This causes a drop in HR and SV, which lowers the cardiac output. The sympathetic (SPP) increases the HR and the parasympathetic (PSP) decreases the HR. Both SPP and PSP nerve fibres control the HR.

Heart Rate (HR) is the number of heartbeats per minute. The *Venous Return (VR)* is return of the blood to the heart, and is largely dependent on the total *blood volume (BV)* and the mechanisms that improve the blood flow in the veins.

Stroke Volume (SV) is the volume of blood, in millilitres (mL), pumped out of the heart with each beat. If the heart were to be filled more per beat, then it could pump out more blood on each beat and this would increase SV. Moreover, if the heart were to contract more strongly, then the heart could also pump out more blood with each beat: in other words, a stronger contraction would lead to a larger SV.

Cardiac Output (CO) is the volume of blood which is pumped by the heart in a time interval commonly given per minute (mL blood/min). The CO is an integral function (sum of CO over number of beats) of HR and SV. If either HR or SV increase, the CO also increases. The CO depends linearly on HR. The average person has a resting heartbeat of 70 beats/minute and a resting SV of 70 mL/beat. A rough estimation of the cardiac output for a person at rest is:

$$\text{CO} = 70 \text{ (beats/min)} \times 70 \text{ (mL/beat)} = 4900 \text{ mL/minute} \quad (3.1)$$

Baroreceptor Reflexes (BRR): the blood pressure is controlled on a minute-to-minute basis by BRR. Changes in blood pressure affect the frequency of action potentials sent to the CCC from the BRR.

Blood Pressure (BP) is partly dependent on CO and the vessels. It is directly dependant on BV and BF. The blood pressure is proportional to the blood volume at every instant.

Blood Volume (BV) directly affects the blood pressure. If the blood volume is increased then venous return of blood to the heart increases. An increase in venous return will, by Starling's law, causes SV to increase. As SV goes up, the cardiac output goes up and the blood pressure rises. Starling's law is discussed below in detail and in Section 2.1 of Chapter 2.

Total Peripheral Resistance (TPR): blood vessels provide resistance to the flow of blood because of the friction between moving blood and the wall of the vessel. The TPR refers to the total sum of vascular resistance to the flow of blood in the systemic circulation. Because of their small radii, arterioles provide the greatest resistance to *blood flow (BF)* in the arterial system. Adjustments in the radii of arterioles have significant effect on TPR, which in turn has a significant effect on MAP. The resistance and pressure are directly proportional to each other. If the resistance increases, then the pressure increases.

Blood Flow (BF): the blood flow through the vessels of the circulatory system is a function of the pressure in the system and the resistance to flow caused by the blood vessels. The BF is directly proportional to pressure and inversely proportional to resistance (TPR).

$$\text{Blood Flow} = \frac{\text{Pressure}}{\text{Resistance}} . \quad (3.2)$$

If the pressure in a vessel increases, then the blood flow increases. However, if the resistance in a vessel increases, then the BF decreases. The resistance in the blood vessels is affected by three parameters:

Length of the vessel – the longer the vessel, the greater the resistance.

Viscosity of the blood – the greater the viscosity, the greater the resistance

Radius of the vessel – the smaller the radius, the greater the resistance.

The relationships between the factors that affect the blood flow are described by Poiseuilles's law:

$$\text{Blood Flow} = \frac{\Delta P \pi r^4}{8 \eta L} , \quad (3.3)$$

where Δ is the change, P is the pressure, r is the radius of the vessel, π is the constant, η is the viscosity of blood, and L is the vessel length.

Mean Arterial Pressure (MAP) represents the average driving force for blood flow through the arterial system. The three most important variables affecting MAP are TPR, CO, and BV.

Saturation Pressure of Oxygen (SPO₂): if the muscles are working, the SPO₂ depends on the respiration volume. This means that more oxygen has to be supplied. This is because as the muscles start to work, they require more oxygen.

End-diastolic Volume (EDV): an increase in *venous return (VR)* of blood to the heart will result in greater filling of the ventricles during diastole. Consequently, the volume of blood in the ventricles at the end of diastole, called end-diastolic volume, will be increased.

Starling's law describes the relationship between end diastole volume and SV. It states that the heart will pump out whatever volume is delivered to it. If the EDV doubles then SV doubles.

Short Explanation of the Respiratory System Parameters

Respiration Rate (RR) is the frequency of respiration, that is, the number of breathes (inhalation-exhalation cycles) taken within a set amount of time (typically 60 seconds).

Tidal Volume (TV) is the volume of gas inhaled and exhaled during one respiratory cycle. In a healthy adult, the TV is approx. 500 ml per inspiration. It is measured in Litters and ventilation volumes are estimated based on a patient's ideal body weight. The respiration smoothing can be rectified using a low-pass filter (LPF)

Respiration Volume (RV) is a very important parameter in respiration; it is actually flow, which represents a volume variation over time. The RV is the amount of air a person breathes in a minute. The RV [l/min] is average volume of air inspired into the lungs; it can be evaluated using values of TV and respiration rate (RR [l/min]). It is discussed in detail in Section 2.4 of Chapter 2 and Krivošeš 2009.

Short Explanation of the Muscular System Parameters

Muscle is a bundle of fibrous tissue in the body that has the capability to contract, producing movement or maintaining the position of parts of the body.

Movement is changing the position of a compartment of the body. During measurement, movement is the unwanted artefact.

Oxygen Usage in this situation is the amount of oxygen consumed by the muscle.

3.2.2 Selection of the Data Source of the Interest (Step 2)

The second diagram (Figure 3.4) of the overall framework is divided into three sub-diagrams. Each sub-block is discussed below.

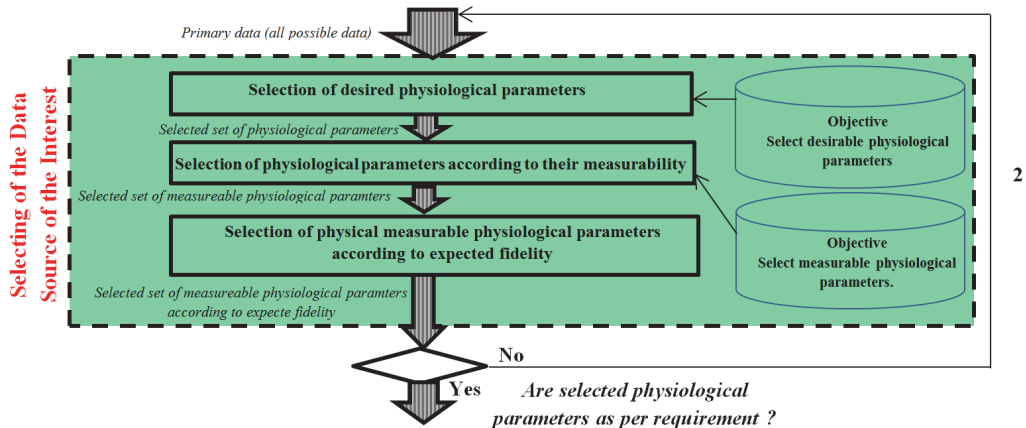


Figure 3.4 Flow diagram for selection of the data source of the interest.

In the ‘Selection of the desired physiological parameters’ sub-diagram, the objective is to select the desired physiological parameters for further use from the full set of physiological parameters, which are received from the previous diagram (Biological System/Object).

In the ‘Selection of physiological parameters according to their measurability’ sub-diagram, the objective is to select the physiological parameters according to their measurability. From an object, some parameters can be measured directly, such as ECG, HR, MAP, RR, RF, RV, and movement, etc., whereas some other parameters can be measured indirectly, such as CO, SV, BP and SPO₂, etc. However, some parameters cannot be measured, such as BV, BF, VR, and TPR.

In the ‘Selection of physical measurable physiological parameters according to expected fidelity’ sub-diagram, the objective is to select the useful physiological parameters that could be used for further analysis. It is dependent on the condition and problem in the object.

In Step 2 (Figure 3.4), the focus is to select a set of useful parameters that can be used for further analysis. After selecting the set of parameters, the question has to be answered: “Are the selected physiological parameters as per requirement?” If the answer is “Yes”, then the flow moves to the next step. If the answer is “No”, then the flow goes back and the selection of desired physiological parameters has to be reconsidered.

3.2.3 Measurement of the Parameters of Interest (Step 3)

The third diagram (Figure 3.5) is divided into four sub-diagrams. Each sub-diagram is discussed below.

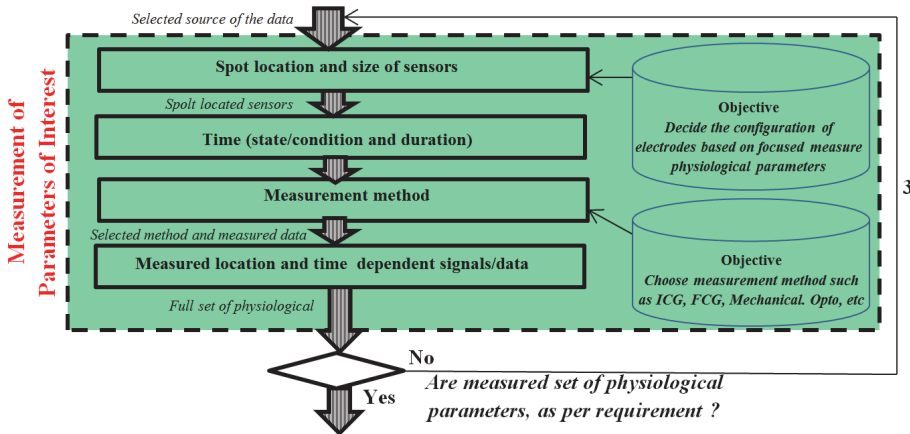


Figure 3.5 Flow diagram for measurement of parameters of interest.

In the ‘Spot location and size of sensors’ sub-diagram, the objective is to decide on the configuration of sensors based on the aim of the experiments, the criterion being which physiological parameters need to be measured.

In the ‘Time (state/condition and duration)’ sub-diagram, the objective is to decide the state and condition of measurement for parameters of interest, such as when, and duration of measurement, such as how long time data measurement is required.

In the ‘Measurement method’ sub-diagram, the objective is to decide the measurement method. The measurement method could be invasive or non-invasive. In case we consider a non-invasive method, then the specific measurement method has to be considered and selected. The non-invasive measurement methods include Electrocardiogram (ECG), Opto-Electronic Plethysmography (OEP), Electrical Impedance Tomography (EIT), impedance cardiography (ICG), Foucault Cardiography (FCG), and Electro-mechanical Wave Imaging (EWI), etc. These methods are briefly discussed in Section 2.4 of Chapter 2 and (Solà et al. 2011; Kenny & Tidy 2012; Santos et al. 2013; Grimnes & Martinsen 2014; Mughal 2014; Mughal et al. 2015; Trolla & Vedru 2001; Kohl, Peter Sachs, Frederick Franz 2011).

The final sub-diagram is ‘Measured location and time-dependent signals/data’. After deciding on the positioning of the electrodes and the measurement method, the location-dependent signals/data are measured.

The different spot location, time (state/condition and duration), and measurement methods should be carefully considered. The results can be tested and evaluated by the advanced user for further analysis. From this phase, an object could be excited in order to pass current and measure voltage or vice versa. After measuring the full set of

physiological parameters, the following question has to be answered: “Is the measured set of physiological parameters as per requirement?” If the answer is “Yes”, then the flow moves to next step. If the answer is “No”, then the flow goes back and the advanced user has to reconsider the selection of spot location, time (state/condition and duration), and measurement method.

3.2.4 Data Cleaning (Step 4)

The diagram 4 (Figure 3.6) is divided into two sub-diagrams. Each sub-diagram is discussed below.

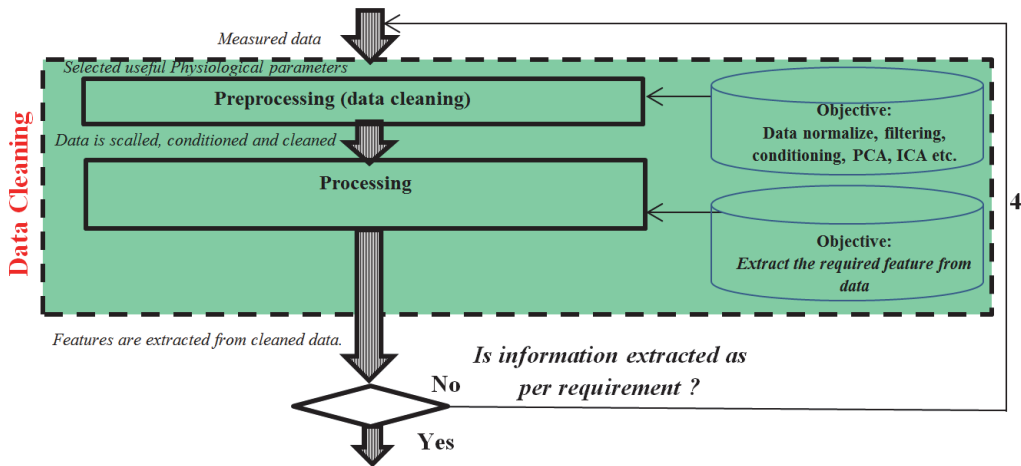


Figure 3.6 Flow diagrams of data cleaning.

In the ‘Pre-processing (data cleaning)’ sub-diagram, pre-processing should be performed to clean the data for further processing. Pre-processing includes data normalization (scaling), conditioning, and filtering to attenuate useless part(s) of the data.

In the ‘Processing’ sub-diagram, the objective is to extract the feature from signals which are saved for further processing.

In Step 4 (Figure 3.6) the features are selected. If the selected features are fulfilling the need, then the flow moves to next diagram; otherwise, this diagram could be repeated and the required feature would be selected again, i.e. measured data.

3.2.5 Modelling of the ICG and IRG Signals and Building a Corresponding Simulator (Step 5)

The modelling and simulation Step 5 (Figure 3.7) is divided into two sub-diagrams. Each sub-diagram is discussed below.

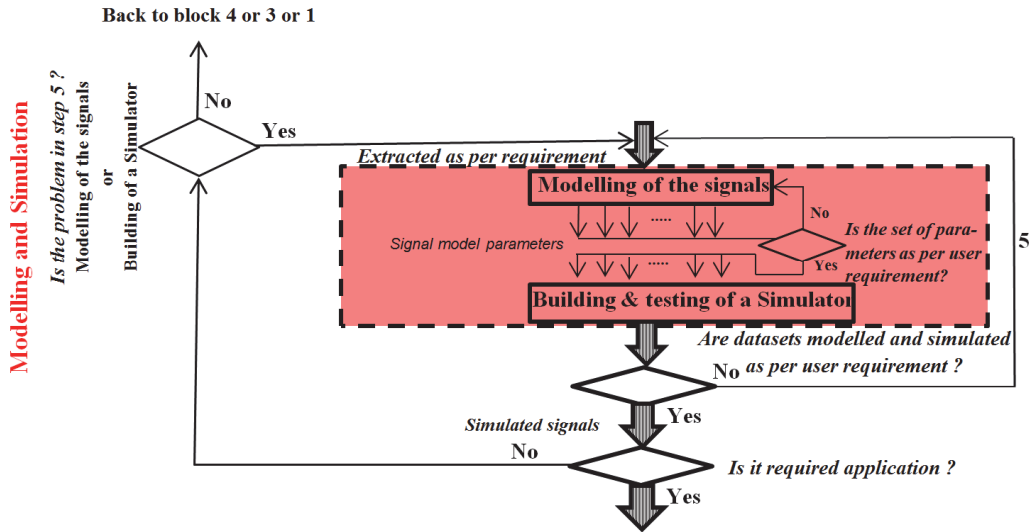


Figure 3.7 Flow diagram of modelling and simulation.

In the ‘Modelling of the signals’ sub-diagram, modelling of the signals is based on extracted information and the selected features. The objective is to choose the modelling method to construct a robust signal model. The modelling methods that could be considered include a curve-fitting method (polynomial, Fourier series, sum of sines, interpolant, smoothing, exponential, Gaussian, power, rational, Weibull, etc.), waveform generator, etc.

In the ‘Building and testing of a simulator’ sub-diagram, a simulator tool for the advanced user should be developed; it can simulate the signals as per need for further processing.

In Step 5 (Figure 3.7), the signals are modelled, tested, and simulated; if the modelled and simulated signals are as per need then they are validated. If not, then the modelling and simulation of signals could be repeated. If “Yes”, then flow moves to the next condition. If the simulated signals similar with measured and assessment, if “Yes” then flow moves to the final step, i.e. the application; if “No”, then the flow goes back to Step 4, Step 3, or Step 1 to identify which sub-diagram poses the problem.

3.2.6 Applications (Step 6)

The application diagram, which is depicted in Figure 3.8. Ideally, a wide range of bioelectrical applications could be considered, such as simulated EBI signals, Foucault Cardiography (FCG), and Photoplethysmography (PPG). The developed application could be used as follows:

- a) The simulator could be used for research to evaluate the applicability of the application.
- b) The tool could be useful for academia in teaching and training purposes. A teacher may use it for practice to provide students physiological understanding.
- c) The student could play around with the tool and understand the phenomena-related physiological parameters.

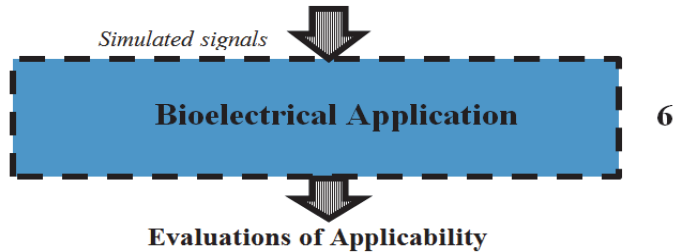


Figure 3.8 Flow diagram of bioelectrical application.

The generic framework described in this chapter is used to implement a practical EBI application, as presented in the chapter that follows, Chapter 4.

3.3 Summary of the Chapter

In this chapter a novel generic framework has been proposed, which is a pathway to model a signal and develop a simulator for the bioelectrical information.

The unique approach in the proposal of such a framework is that the framework provides a pathway between biological systems and the development of bioelectrical applications.

The process begins with selecting a biological system/object, which is needed to decide who or what will be the object.

The first step is divided into three main sub-systems. Each of these systems contains a list of parameters in which one can be interested, and show the connections, relationships, and dependencies within the system or with other systems.

The second step is the selection of the data source of the interest, where the focus is on selecting useful parameters as per the advanced user's need and to use them for further analysis.

The third step is the measurement of parameters, where the spot location, time, and measurement method should be carefully considered. The biological system/object could be excited as part of the measurement of the physiological parameters.

The fourth step regards data cleaning; it applies pre-processing and processing upon selecting the required features which need to be modelled.

The fifth step is about modelling, building, and testing the simulator: firstly, the extracted signal needs to be modelled with the help of any available method, and secondly a corresponding bioelectrical application (e.g., a simulator) must be developed.

4. IMPLEMENTATION OF THE FRAMEWORK AND EXPERIMENTAL RESULTS

As the basis for the implementation, the EBI measurement method was selected to measure the impedance cardiography (ICG) and impedance respirogram (IRG) signals in order to develop the corresponding signal models; for this purpose, different curve-fitting methods are discussed.

The corresponding simulator is built based on the modelled ICG and IRG signals, which is used to simulate the EBI signal.

The selected data measurement method, the proposed method for modelling the ICG and IRG signals, and the developed corresponding signal simulator are implemented following the proposed framework (defined in Chapter 3) as an example. The framework is used as a pathway to measure the human subject and to develop the EBI signal simulator, namely Bio-Impedance Signal Simulator (BISS). In what follows, each diagram of the framework is discussed and implemented.

4.1 Measurement of the EBI Signals

The measured EBI data is used to model the ICG and IRG signals because the implementation of this study, as an example, focuses on the modelling of these signals and the construction of a corresponding simulator.

The ICG does not separate signals from different objects during the measurement. Electrode positioning can help (at least somewhat); if the electrodes are placed properly relative to what is required to be measured and calculated, such as HR, SV, CO, RR, muscular movement, etc., then in this case ICG is one of the very prospective methods among the previously mentioned non-invasive methods (The details are discussed in Section 2.4.1 of Chapter 2).

The measurement setup and the 16-electrode configuration method are used to acquire the EBI data from the healthy male subject, as described in Mughal et al. 2015 and Mughal 2014.

4.1.1 Measurement Setup

The measurement setup shown in Figure 4.1 is used to acquire the EBI data (corresponding to the measured EBI signal). The 16-electrode belt is worn around the thorax of the subject.

The Zurich HF2IS Impedance Spectroscope (Zurich 2015) is the measurement equipment which was used in this measurement. The HF2IS is used to excite the subject and measure the EBI datasets from the subject through sense electrodes. The HF2IS is connected to the switch-box through connector cables.

The HF2IS was limited to two channels (Channel 1 and 2); because of this, at any given time four electrodes (two electrodes from each channel (Excitation A and B)) were used to excite the subject and four electrodes (two electrodes from each channel (Sense A and B)) were used to sense the EBI data. Thus, eight electrodes are active at a time. These channels are shown in Figure 4.1.

The sensed (measured) EBI datasets were stored in a computer for further analysis. The attached computer is also used to control the switch-box and HF2IS impedance spectroscopy equipment.

A program developed at T.J. Seebeck Department of Electronics was used to control the switch-box that switches/selects the electrodes' configuration for each time-step automatically. Nevertheless, the configuration of the electrode can also be set up by the advanced user.

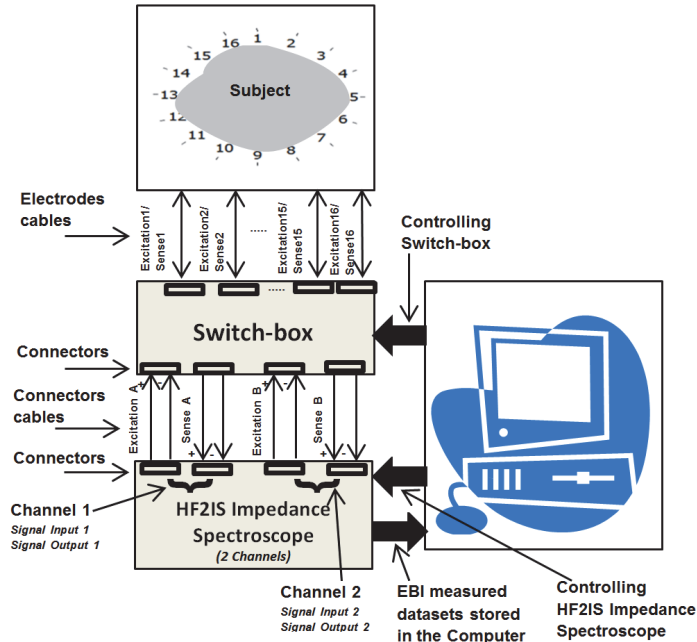


Figure 4.1 Measurement setup for measuring the EBI of a subject.

In order to make the simple representation of EBI dataset, it is assumed that the EBI data is the summation of the following four components:

$$S_{EBI}(t) = S_{ICG}(t) + S_{IRG}(t) + S_{Artefact}(t) + S_{Noise}(t), \quad (4.1)$$

where (S_{ICG}) and (S_{IRG}) are the cardiac and respiratory signals, respectively, ($S_{Artefact}$) is unwanted motion artefact caused by body movements or muscle activity, and (S_{Noise}) is noise.

The heart rate S_{ICG} (Eq. 4.1) of a healthy person can vary in the range between 60 bpm to 240 bpm (1 to 4 Hz), and the respiration rate S_{IRG} (Eq. 4.1) of a healthy person can vary from about 12 breaths/min to 30 breaths/min (0.2 to 0.5 Hz) (Mughal 2014).

4.1.2 Waveforms and Spectra of the EBI Signals

The waveform of the cardiac and respiratory components of the EBI signal are relatively smooth (Min et al. 2000); that is why only a few higher harmonics are required for representing them. Figure 4.2 shows the measured and filtered IRG signal from measured EBI, which corresponds to the subject's respiration, as well as the ICG signal, which corresponds to the cardiac activities of the subject.

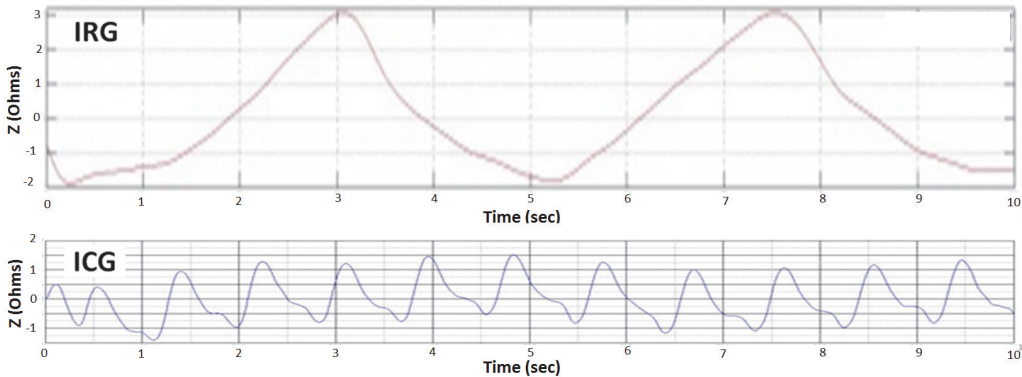


Figure 4.2 Two cycles of respiration and ~12 cycles of cardiac activity in 10 seconds

Unfortunately, muscular activities also lie on the same frequency range as that of the cardiac signal, and the higher harmonics of the respiratory signal also lie on the same frequency range of the cardiac signal, as shown in Figure 4.3 (Mughal 2014).

A simplified possible sketch of the harmonic spectrum of the EBI signal is shown in Figure 4.3. The possible spectrum is sketched for the signal components shown in Figure 4.2; in the spectrum, it is illustrated that the fifth harmonic of the respiration signal is partially overlapping with the first harmonic of the cardiac signal, and that the other higher harmonics of the respiration signal “enter” the cardiac signal frequency range.

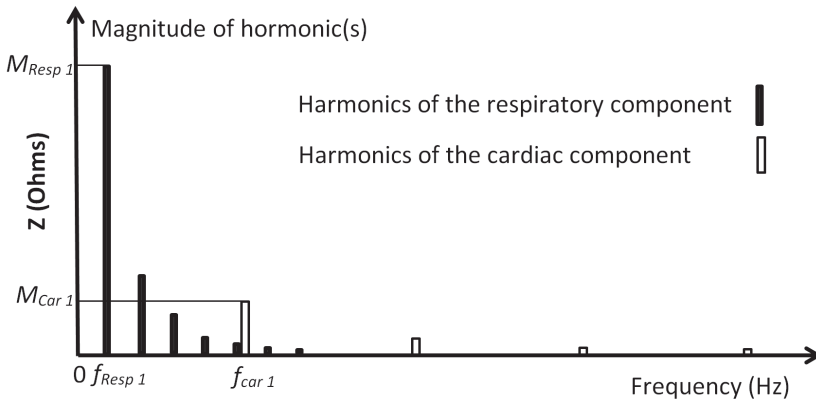


Figure 4.3 A possible sketch example of the simplified frequency spectrum of the thoracic EBI, which is based on Figure 4.2.

It contains cardiac and respiratory components (Mughal 2014).

Based on the literature survey and analysis of the existing thorax impedance models, as well as the origin of the ICG signal (Section 2.4 of Chapter 2 and in our published paper (Mughal et al. 2014)), it is assumed that none of the existing models are accurate enough to imitate the real phenomena of the ICG signal. Based on these limitations, it was therefore decided to use the 16-electrode configuration belt to measure the ICG and IRG signals instead of one of the existing models. The candidate existing configurations of electrodes are discussed in Section 2.4.4 of Chapter 2. The curve-fitting method is used to model the measured signals.

With this approach, these signal models would be more realistic and the underlying model parameters would be easily tuneable.

The models and evaluation methods are discussed below in Section 4.2. In what follows, the four measured EBI datasets and the clean ICG and IRG datasets are used.

In Figures 4.4–4.9 (Datasets 1–6), each dataset has been measured from different positioning of electrodes. Our results are published in Mughal et al. 2014.

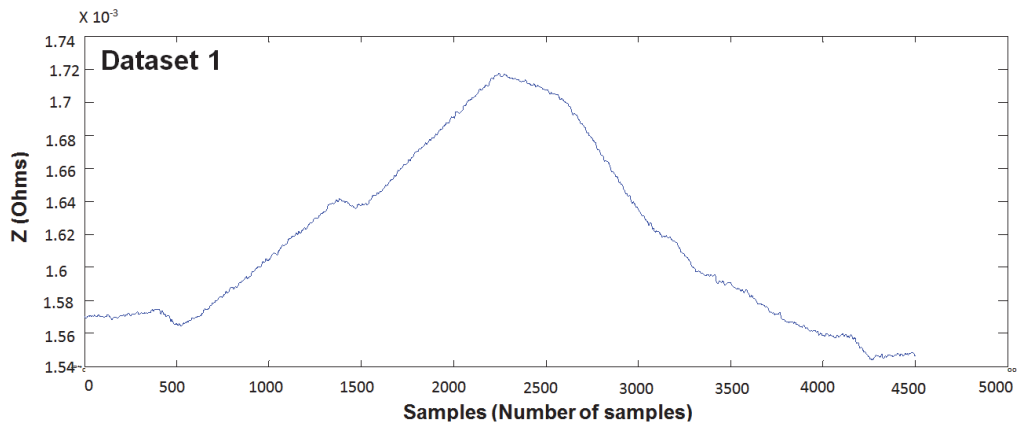


Figure 4.4 Measured EBI waveform (Dataset 1) (Mughal et al. 2014).

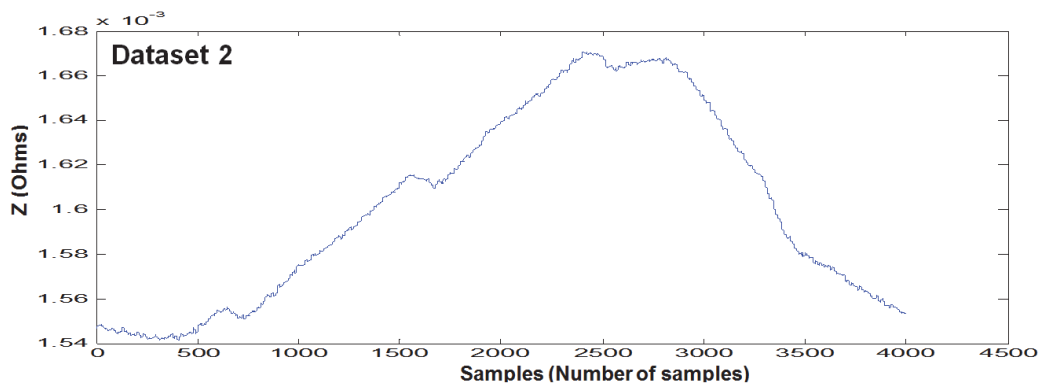


Figure 4.5 Measured EBI waveform (Dataset 2).

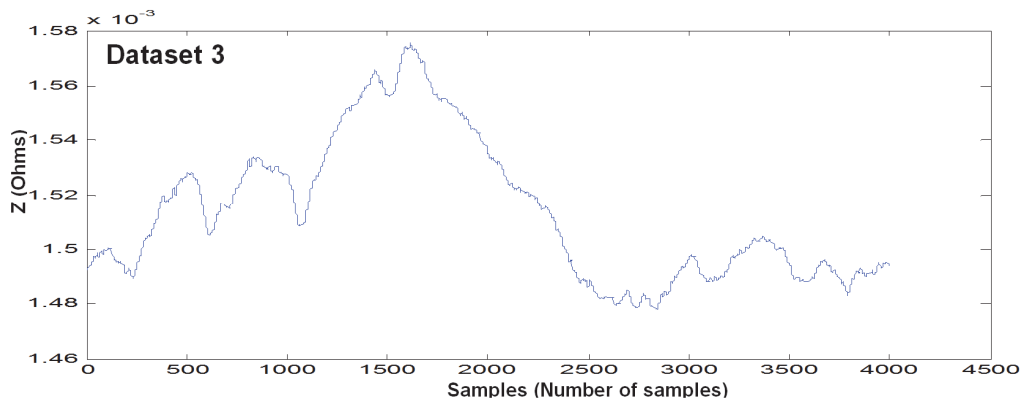


Figure 4.6 Measured EBI waveform (Dataset 3).

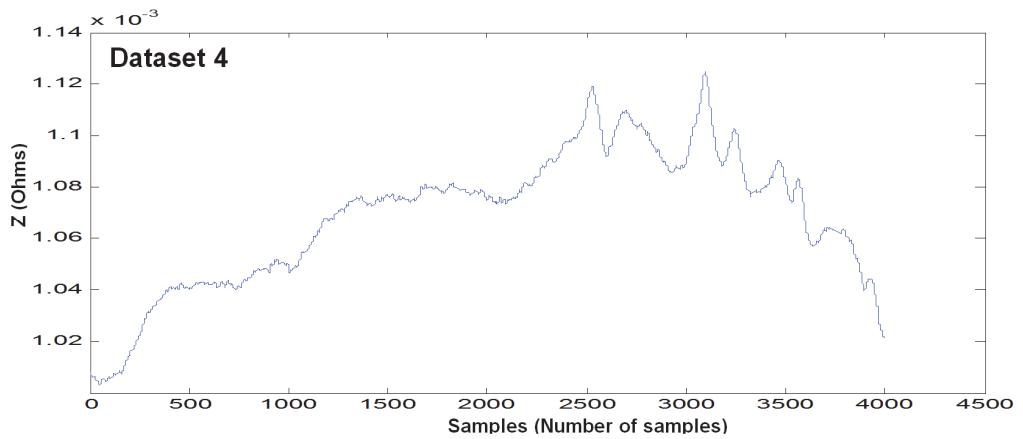


Figure 4.7 Measured EBI waveform (Dataset 4).

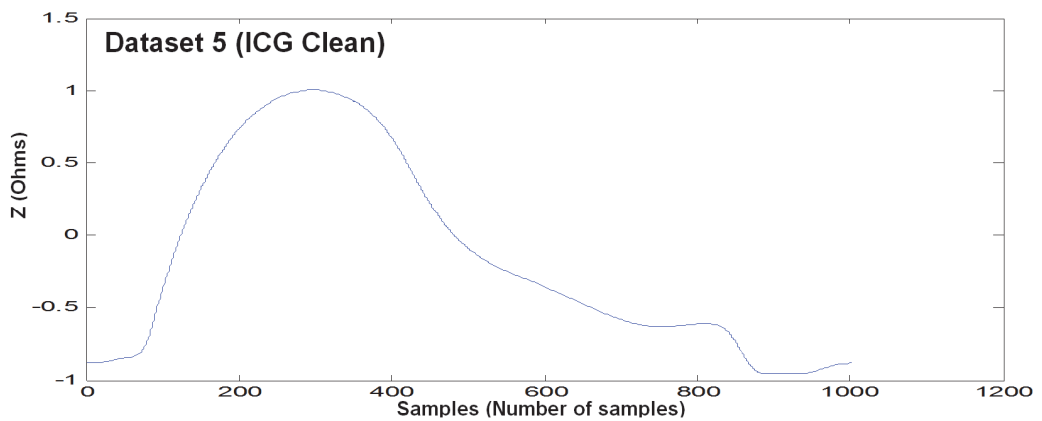


Figure 4.8 Measured EBI waveform (Dataset 5).

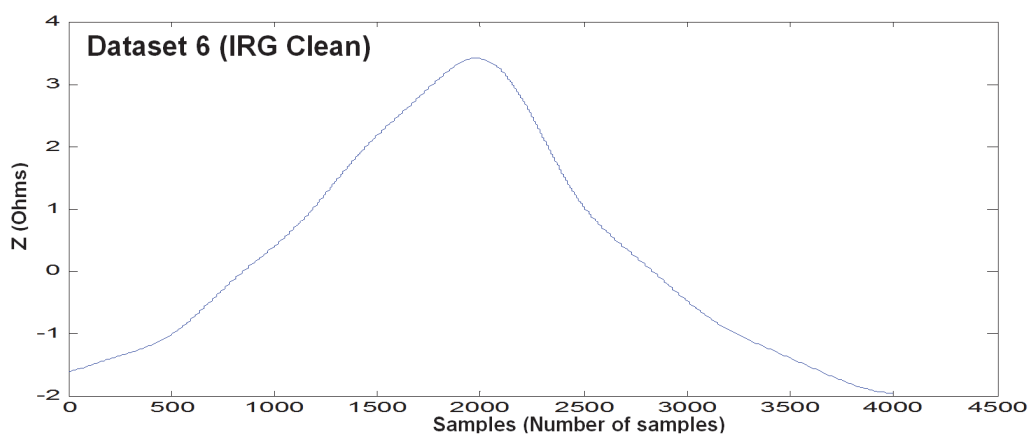


Figure 4.9 Measured EBI waveform (Dataset 6).

Datasets 1–4 (Figures 4.4–4.7) are raw measured EBI data. Datasets 5–6 (Figure 4.8 and Figure 4.9) are the cleaned ICG and IRG signals from the measured EBI datasets.

4.2 Method for Modelling the Bio-Impedance Signal

Modelling of the EBI signals can be performed by way of using template signals. This is discussed in Chapter 3 (Figure 3.1) and Section 3.2 (Modelling and Building Simulator, Step 5 of Figure 3.2).

Here the curve-fitting method is used to model the ICG and IRG signals.

Different curve-fitting models are evaluated by comparing the measured and modelled signals based on statistical parameters and visual fit.

4.2.1 Curve-Fitting Method

In the curve-fitting method, three different curve-fitting models are compared, namely polynomial, Fourier series, and sum of sines. The comparison criteria were based on visual fit and statistical parameters, namely sum of square error (SSE), correlation between the model and the corresponding dataset fitted modelled values (R-Square), and execution time. Each curve-fitting method and statistical parameters are discussed and evaluated below (Mughal et al. 2015):

Models and Evaluation Method

Each model is discussed and evaluated with the help of six EBI measured datasets. Four datasets are raw EBI measured datasets and two are cleaned ICG and IRG signals.

a) Polynomial Model

Polynomials are well suited for cases where a fairly simple empirical model is needed; they can be used for interpolation or extrapolation to characterize data by means of a global fit. The general polynomial model formula is given in Equation 4.2:

$$y = \sum_{i=1}^{n+1} p_i t^{n+1-i}, \quad (4.2)$$

where n is the degree of the polynomial (highest power of the predictor variable), $n+1$ is the order of the polynomial (number of coefficients), p_i is the coefficients, and t is time.

In this work, the polynomial model was evaluated for degrees 1 to 9 for the four EBI datasets; degree 9, which is the highest order available in the toolbox, gave the most suitable results. The comparative results are shown in Table 4.1 and Figures 4.10–4.15.

b) Fourier Series Model

A Fourier series is a sum of sine and cosine functions that describes a periodic signal. The model formula is given in Equation 4.3:

$$y = a_0 + \sum_{i=1}^n a_i \cos(i\omega t) + b_i \sin(i\omega t), \quad (4.3)$$

where a_0 is the intercept, which is a constant term in the data, ω is the fundamental frequency, and n is the number of terms in the series. The model was evaluated with 1 to 8 terms for the four EBI datasets; the most suitable results were obtained for the degree of eight, the highest available in the toolbox. The comparative results are shown in Table 4.1 and Figures 4.10–4.15.

c) Sum of Sines Waves Model

This model consists of a sum of sines terms only. The model formula is given in Equation 4.4:

$$y = \sum_{i=1}^n a_i \sin(i\omega t + c_i), \quad (4.4)$$

where a is the amplitude, ω is the frequency, c the phase, which is constant for each term and n is the total terms in the series.

The model was evaluated with 1 to 8 terms for the four EBI datasets; 8 terms (the highest available in the toolbox) gave the most suitable results. The comparative results are shown in Table 4.1 and Figures 4.10–4.15.

d) ICG and IRG Signal with Polynomial, Fourier series, and Sum of Sines Waves Models

The same approach as for the EBI datasets is used with the ICG and the IRG clean signals, and these signals are modelled with the polynomial, Fourier series, and sum of sines waves methods. The comparative results are shown in Table 4.1 (Clean ICG and IRG) and Figure 4.14 and Figure 4.15, respectively (Mughal et al. 2015).

Statistical Parameters

The performance of the three modelling methods is evaluated by means of the following three fit measures.

a) Sum of Squares Error

The sum of square error (*SSE*) statistic assesses the total deviation of the data values from the fitted model, as expressed in Equation 4.5:

$$SSE = \sum_{i=1}^n w_i (y_i - \bar{y}_i)^2, \quad (4.5)$$

where n is the number of data points, y_i is the response data, and \bar{y}_i is predictor data. SSE values close to 0 indicate that the model is fitted well and has very little random error (Matlab2012b 2014; Mughal et al. 2015).

b) R-Square

The *R-Square* measure is the square of the correlation between the data and the fitted model values. A value close to one shows a greater correlation between the data and the model, whereas a value close to zero shows a poor correlation. It is determined as the ratio of the sum of squares of the regression (*SSR*) and the total sum of squares (*SST*), where $SST = SSR + SSE$. The *R-square* measure is given in Equation 4.6 (Matlab2012b 2014):

$$R\text{-square} = \frac{SSR}{SST} = 1 - \frac{SSE}{SST}. \quad (4.6)$$

c) Execution time

The execution time is measured through Matlab “stopwatch functions (tic, toc)” and reported in Table 4.1.

4.2.2 Results of Modelling and Comparison of the Models of Curve Fitting

Table 4.1 and Figures 4.10–4.15 shows the fit of the three models with the four EBI datasets and clean ICG and IRG datasets. Generally speaking, the three models provide a reasonable fit across the four datasets: the average SSE value is 0.879e-07, and the min and max values are 0.161e-07 and 1.9417e-07, respectively

Similarly, the average R-square value across the four datasets is 0.9762; the min and max values are 0.9512 and 0.9936, respectively.

The Fourier series model minimizes the error (average SSE=0.335e-07) and also has a high correlation across the four datasets compared to the other models. However, it took 1.275 more seconds to execute compared to the polynomial model; it is nevertheless much faster (by 44.476 seconds or nearly 10 times) than the sum of sines waves model.

In this study, the most suitable results were obtained with eight terms for the Fourier series model, which gives 18 coefficients. For the polynomial model, we set the degree to 9, leading to 10 coefficients. It is preferable to limit the number of coefficients for relate to the patients' condition. However, this has to be traded-off for a lower fit and number of coefficients, as shown in Table 4.1. These results are published in our contribution (Mughal et al. 2015).

Table 4.1. Evaluation Criteria Results for the Modelled Signals

| Datasets | Sum of sine waves (24 coeff) | | Fourier (18 coeff) | | Polynomial (10 coeff) | | | | | |
|---------------------------------------|------------------------------|--------|--------------------|--------|-----------------------|--------|-----------|------------|-------------|---------|
| | SSE | R-Sq | SSE | R-Sq | SSE | R-Sq | SSE Avg | SSE Min | SSE Max | R-SqAvg |
| Dataset 1 | 1.0424e-07 | 0.9917 | 0.1612e07 | 0.9987 | 1.2270e-07 | 0.9903 | 0.810e-07 | 0.161 e-07 | 1.23 e-07 | 0.9935 |
| Dataset 2 | 0.9044e-07 | 0.9875 | 0.1786e-07 | 0.9976 | 0.3050e-07 | 0.9959 | 0.463e-07 | 0.179 e-07 | 0.904 e-07 | 0.9936 |
| Dataset 3 | 1.9417e-07 | 0.9274 | 0.6476e-07 | 0.9758 | 1.3185e-07 | 0.9506 | 1.326e-07 | 0.6476e-07 | 1.9417e-07 | 0.9512 |
| Dataset 4 | 0.8054e-07 | 0.9714 | 0.3506e-07 | 0.9876 | 1.6683e-07 | 0.9409 | 0.941e-07 | 0.3506e-07 | 1.6683 e-07 | 0.9666 |
| SSE Avg, R-Sq Avg | 1.17 e-07 | 0.970 | 0.335 e-07 | 0.9758 | 1.13 e-07 | 0.969 | 0.879e-07 | | | 0.9762 |
| SSE Min, R-Sq Min | 0.805 e-07 | 0.161 | 0.161 e-07 | 0.9758 | 0.305 e-07 | 0.941 | | 0.161 e-07 | | 0.9512 |
| SSE Max, R-Sq Max | 1.94 e-07 | 0.9917 | 0.648 e-07 | 0.9987 | 1.67 e-07 | 0.996 | | | 1.9417 e-07 | 0.9936 |
| Clean ICG Signal with different scale | | | | | | | | | | |
| Clean ICG | 0.1996 | 0.9994 | 0.0611 | 0.9999 | 2.8229 | 0.9937 | 1.0279 | 0.0611 | 2.8229 | 0.9959 |
| Ex. Time (s) | ~49.170 | | ~4.694 | | ~3.419 | | | | | |
| Clean IRG Signal with different scale | | | | | | | | | | |
| Clean IRG | 7896.1e-07 | 1 | 2890.6e-07 | 1 | 19.5782 | 0.9983 | 6.5264 | 2890.6e-07 | 19.5782 | 0.9994 |

Regarding the difference between the polynomial and the sum of sines waves models, it can be seen that for Datasets 2 and 3, the polynomial model minimizes the error (0.3050e-07 and 1.3185e-07, respectively) and is highly correlated with the datasets (0.9959 and 0.9506, respectively). On Datasets 1 and 4, the sum of sines waves model minimizes the error (1.0424e-07 and 0.8054e-07, respectively) and is highly correlated (0.9917 and 0.9714, respectively) with the datasets. However, 8 terms

were used for the sum of sines waves model, which gives 24 coefficients (versus 10 for the polynomial model) and a much longer execution time.

For the clean ICG and IRG datasets, the Fourier series model performed very well in minimizing the error (0.0611 and 2890.6×10^{-7} , respectively) and is highly correlated (0.9999 and 1, respectively) with the datasets. It is followed by the sum of sines waves model, which has the second minimum error (0.1996 and 7896.1×10^{-7} , respectively) and high correlation (0.9994 and 1, respectively) but also a larger number of coefficients (24) and longer execution time (49.170 seconds) compared to the polynomial model (Mughal et al. 2015).

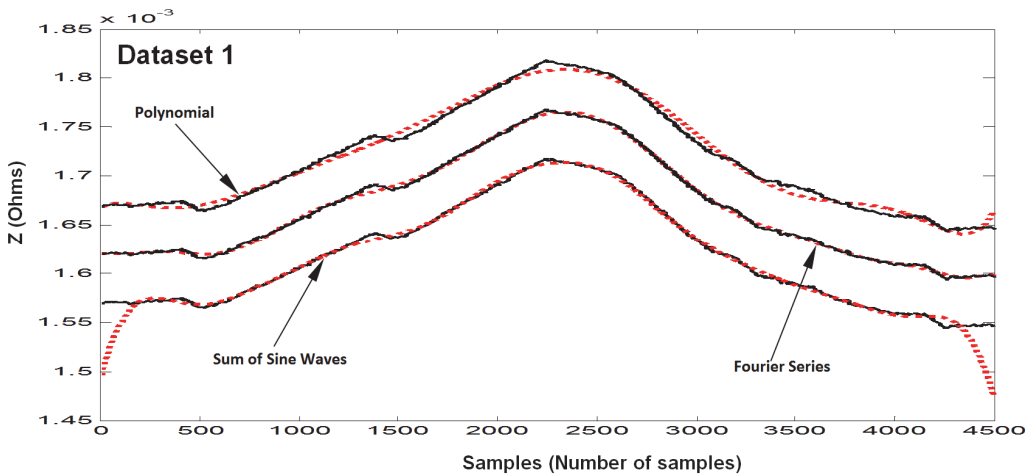


Figure 4.10 Results of fitting of the EBI dataset 1: the measured dataset 1 (solid lines, black) and fitted models (dotted lines, red) (Mughal et al. 2015).

Results for the sum of sines waves model are presented without offset.
For readability, the results for Fourier series model are offset by 0.05×10^{-3} , and the results for Polynomial model are offset by 0.1×10^{-3} .

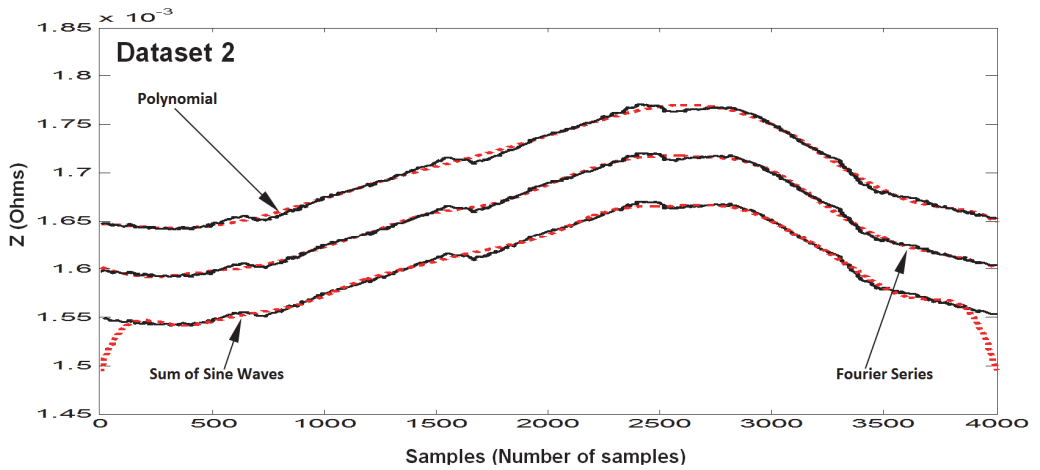


Figure 4.11 Results of fitting of the EBI dataset 2: the measured dataset 2 (solid lines, black) and fitted models (dotted lines, red) (Mughal et al. 2015).

Results for the sum of sines waves model are presented without offset.
For readability, the results for Fourier series model are offset by 0.05×10^{-3} , and the results for Polynomial model are offset by 0.1×10^{-3} .

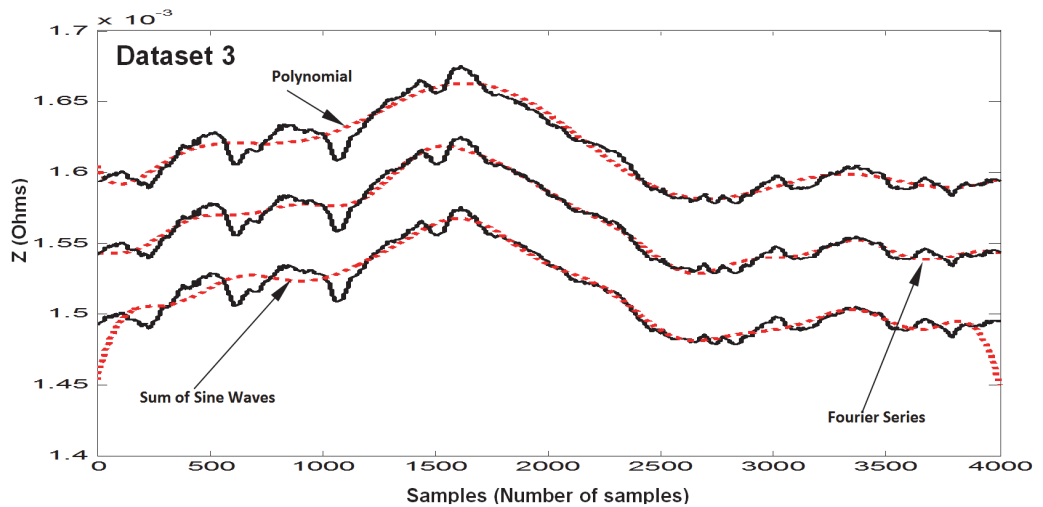


Figure 4.12 Results of fitting of the EBI dataset 3: the measured dataset 3 (solid lines, black) and fitted models (dotted lines, red) (Mughal et al. 2015).

Results for the sum of sines waves model are presented without offset.
For readability, the results for Fourier series model are offset by 0.05×10^{-3} , and the results for Polynomial model are offset by 0.1×10^{-3} .

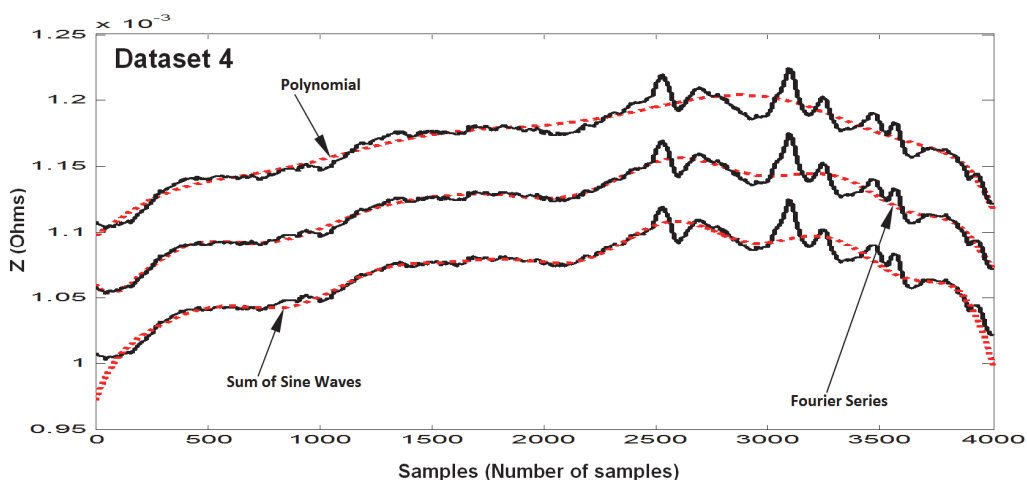


Figure 4.13 Results of fitting of the EBI dataset 4: the measured dataset 4 (solid lines, black) and fitted models (dotted lines, red) (Mughal et al. 2015).

Results for the sum of sines waves model are presented without offset.
For readability, the results for Fourier series model are offset by 0.05×10^{-3} , and the results for Polynomial model are offset by 0.1×10^{-3} .

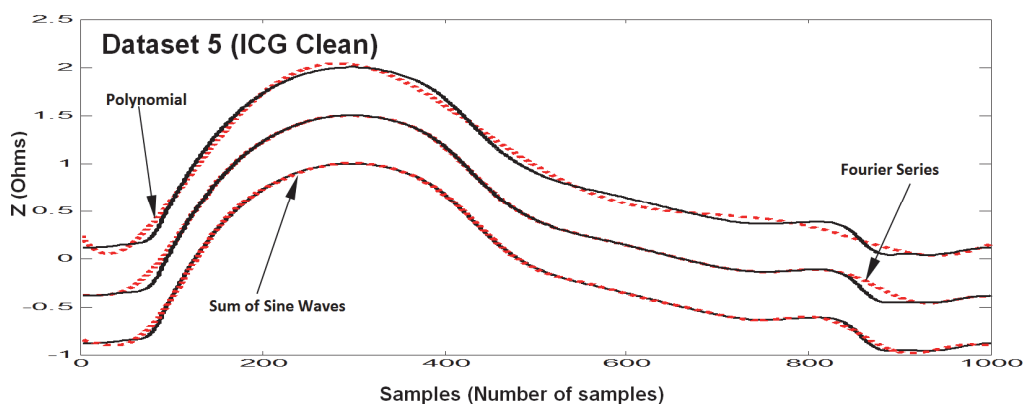


Figure 4.14 Results of fitting of the Clean ICG dataset 5: the measured Clean ICG dataset 5 (solid lines, black) and fitted models (dotted lines, red) (Mughal et al. 2015).

Results for the sum of sines waves model are presented without offset.
For readability, the results for Fourier series model are offset by 0.5 and the results for Polynomial model are offset by 1.

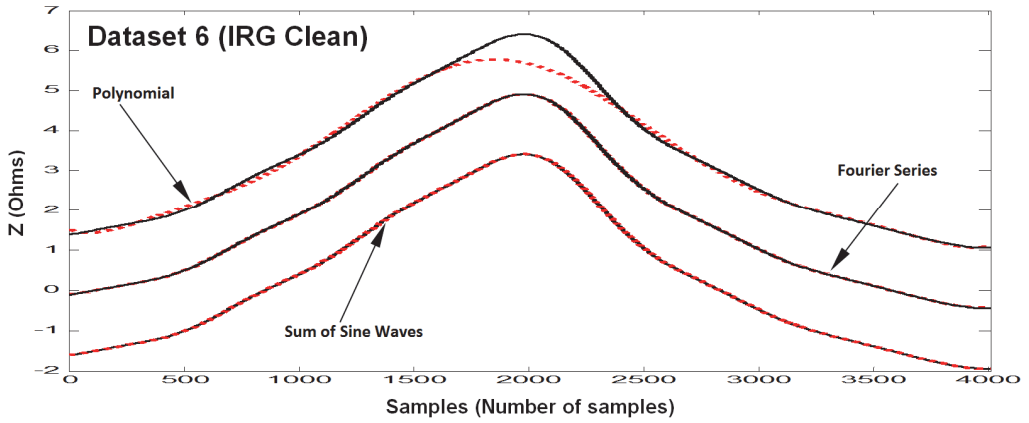


Figure 4.15 Results of fitting of the Clean IRG dataset 6: the measured Clean IRG dataset 6 (solid lines, black) and fitted models (dotted lines, red) (Mughal et al. 2015).

Results for the sum of sines waves model are presented without offset.
For readability, the results for Fourier series model are offset by 0.5 and
the results for the polynomial model are offset by 1.

Figure 4.16 depicts the ICG measured signal (red), which was cleaned, and the corresponding modelled signal with help of Fourier series (black). From the statistical parameters shown in Table 4.1 (clean ICG) and visually, it appears that the ICG signal modelled by means of Fourier series model curve-fitting method follows the measured ICG waveform quite accurately. Although it is not totally error-free, the results are deemed satisfactory for the purpose at hand.

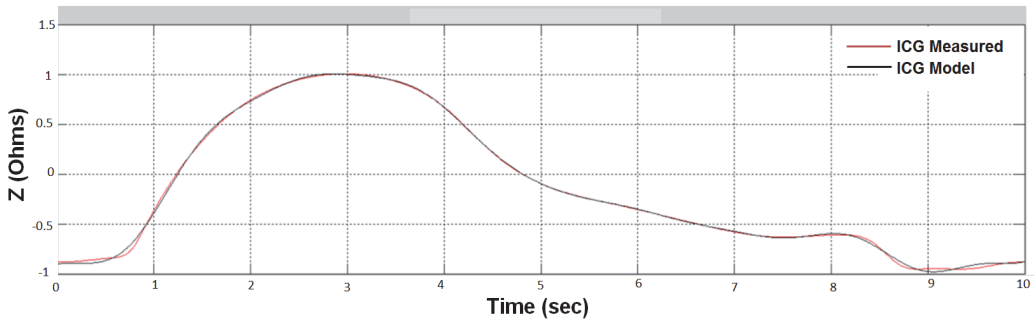


Figure 4.16 ICG signal measured (red) and ICG modelled by means of Fourier series (black).

As can be seen in Figure 4.16, both signals are overlapping most of the time, showing that only slight error exists in the modelled signal. The first derivative of both the measured and modelled signals are taken, which gives more information about the cardiac activities. Markers are used for each activity.

The first derivative of the cleaned ICG measured signal (red), and the corresponding first derivative of the modelled signal with help of Fourier series (black) is depicted in Figure 4.17.

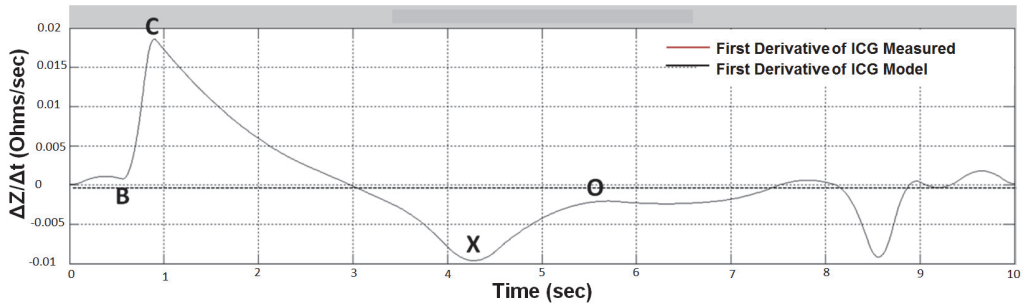


Figure 4.17 First derivative of the ICG measured (red) and ICG Fourier modelled (black).

Markers: B - opening of aortic valve; C - associated with contraction; X - closure of aortic valve, and O - diastole opening of mitral valve.

In Figure 4.17, both the curves of the first derivative of the measured and modelled ICG signals overlap each other extremely well.

Marker B is associated with the opening of the aortic valve, marker C with the contraction of heart muscles, marker X with the closure of the aortic valve, and marker O with diastole, i.e., the opening of the mitral valve to fill the heart with blood.

4.3 Proposed Bio-Impedance Signal Simulator

The bio-impedance signal simulator (BISS) is built based on the Fourier series model.

The simulator is depicted in Figure 4.18, and the simulated EBI signal is generated by summing the ICG signal (S_{ICG}), IRG signal (S_{IRG}), artefacts ($S_{Artefacts}$), and a white Gaussian noise (S_{Noise}).

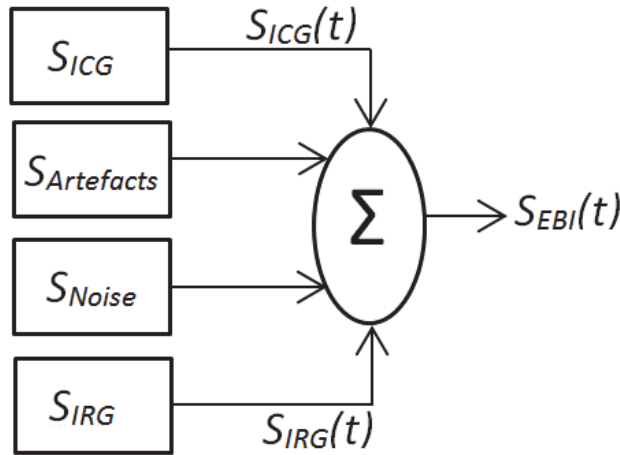


Figure 4.18 Block diagram of the Bio-Impedance Signal Simulator (BISS)

The need for summation of the components of the EBI signal is discussed above in Section 4.1 in Equation (4.1). For more details, see our published results in (Mughal et al. 2015).

4.3.1 Development of the Simulator

The EBI signal simulator is developed in the way discussed in the block diagram of the generic system for modelling of the template signals and for developing a corresponding simulator (Figure 3.1) in Chapter 3.

The first part of the generic block diagram is discussed in Section 4.2 for modelling of the template signals. In this chapter, the focus was narrowed down to one method in this study and a specific approach to develop the simulator and then present the specific implementation of the BISS.

Specific approach to develop the Bio-Impedance Signal Simulator (BISS)

The development of the specific corresponding bio-impedance signal model simulator is motivated by the desire to simulate the EBI signal to evaluate the performance of signal processing algorithms such as separation algorithms.

Figure 4.19 depicts a) the modelled ICG (S_{ICG}) and IRG (S_{IRG}), signals (modelled by means of Fourier series method) are discussed in Section 4.2, b) recorded motion artefacts ($S_{Artefacts}$) (e.g. swinging arm) added to the simulated EBI signal, and c) a white Gaussian noise (S_{Noise}) also added to the simulated EBI signal.

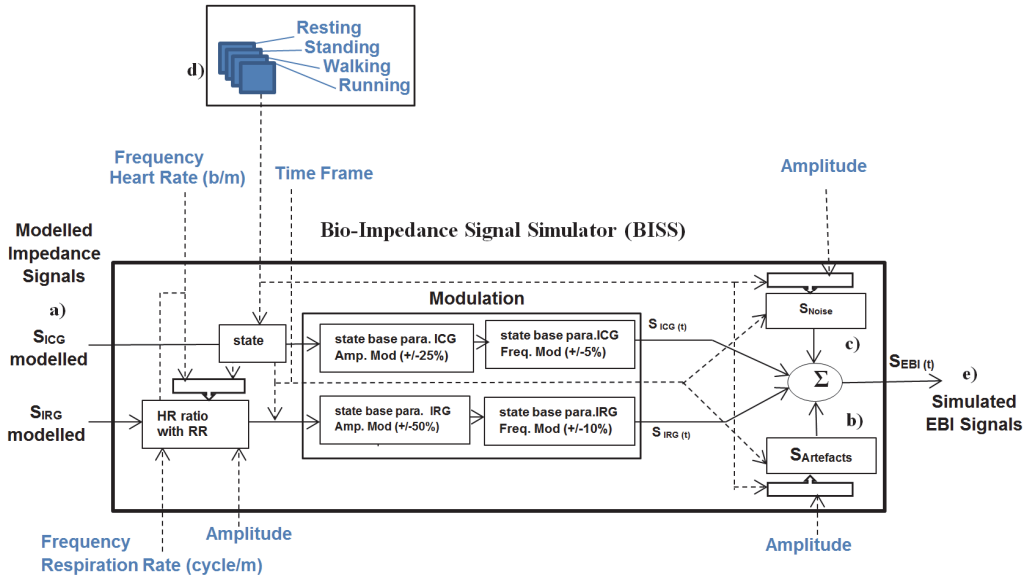


Figure 4.19 Block diagram of BISS for modelled of the ICG and IRG signals and for development of a corresponding simulator for EBI Signals.

The block diagram of BISS has different pre-recorded states d) corresponding to a healthy resting, healthy standing, healthy walking and healthy running persons are included. Each state has different parametric values and cardiac relationships with respiration, which vary with each state/condition.

Nevertheless, the end-user also has the possibility to change the parameters as per his/her needs, such as heart rate, respiration rate, timeframe, and amplitude of respiration, artefacts, and noise.

Finally, e) shows that the simulated EBI signals are a mixture of ICG, IRG, artefacts, and noise, as per Equation 4.1, and are also shown in Figure 4.18. Such simulated EBI signals can then be used for further processing (e.g. to evaluate the performance of separation algorithms).

In Figure 4.19, the outer parameters (blue colour) such as heart rate (beats/minute), timeframe (sec), respiration rate (cycles/minute), amplitude for respiration, artefacts,

and noise are controlled by the end-user (possibly overriding the values loaded from a pre-recorded state).

In Figure 4.20, a healthy running person is loaded. In this figure, the end-user interface of BISS is depicted, including:

- a) a *menu* where the end-user can load the different states of the person (e.g. healthy rest, healthy standing, healthy walking, and healthy running), open existing simulated EBI signals, save the current simulated EBI signals, and exit the simulator.
- b) is the measured and cleaned ICG signal,
- c) is the modelled ICG signal by means of Fourier series method,
- d) is the measured and cleaned IRG signal,
- e) is the modelled IRG signal by means of Fourier series method.

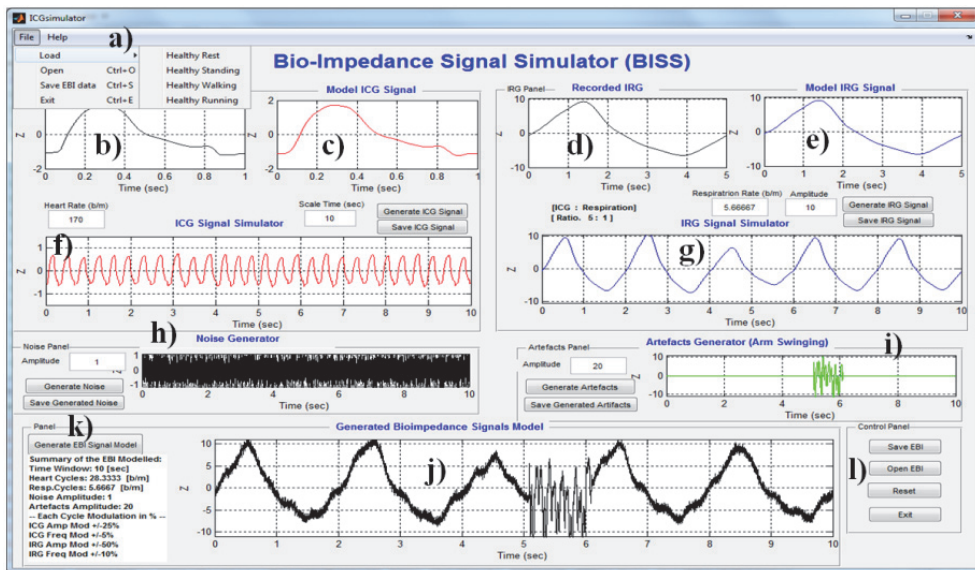


Figure 4.20 End-user graphical interface of the BISS simulator with the signals simulated for the “healthy person while running” state.

The cardiac amplitude in BISS, Figure 4.20 (f), is based on the systolic and diastolic activities in order to imitate the real phenomena of the heart.

If the heart rate increases, the amplitude of the ICG decreases and the diastole period also decreases. If the heart rate decreases, the amplitude of ICG increases and the diastole period also increases. A small variation is also introduced in systolic activities as per cardiovascular phenomena. The ICG signal is continuously moving in time and the ICG signal simulated where modulation is introduced with each cycle in amplitude and frequency.

As previously discussed in this section, the signal model parameters can also be directly configured by the advanced user.

In order to imitate the real phenomena, signal modulations are included in BISS. The ICG amplitude modulation range is $\pm 25\%$ and the frequency modulation range is

$\pm 5\%$, depending on the heart rate. This makes cycles different from each other. Similarly, modulation is also introduced for respiration (IRG) amplitude ($\pm 50\%$) and frequency ($\pm 10\%$). Medical doctors confirmed these modulation ranges as realistic.

The IRG signal is continuously moving in time and the simulated IRG signal, where modulation is introduced with each cycle.

The respiration rate is correlated to the cardiac heart rate by means of a ratio. The default ratio is taken at 5:1 (5 cardiac cycles for 1 respiration cycle). Nevertheless, the end-user can control the respiration rate as well.

Furthermore, in Figure 4.20, h) is the noise generator, i) the recorded artefacts caused by motion (in this example, by swinging the arm during the measurement) randomly moving in the defined time window, j) the simulated EBI signals model based on the end-user's entered parameters, k) the detailed summary of the simulated EBI signals model, and l) buttons that let the end-user save the simulated EBI signals, open existing simulated EBI signals, clear all the simulated model signals and start again, and exit from BISS' GUI environment.

4.4 Generic Framework for Modelling the Bio-Impedance Information

This section shows how the generic framework has been implemented, as an example, for the EBI case described previously. The generic framework is proposed in Chapter 3 (Figure 3.2); it provides guides on how to measure the EBI data from the subject, how to process to clean the measure EBI signals in order to achieve the ideal (template) of ICG and IRG signals, and how to build signal models for ICG and IRG signals.

The signal model approach is discussed in Section 4.2. It is required to have a corresponding simulator; in this work, the simulator is actually built, as discussed in detail in Section 4.3.

As an example, the flow diagram of the process to implement for the EBI case is depicted in Figure 3.2. The flow guides the advanced user step by step with the help of predefined diagrams to model the ICG and IRG signals and develop a corresponding BISS.

Each diagram has specific criteria and requirements that must be kept in mind while following the steps of the flow diagram.

In the first step (in Figure 3.2), a human was selected as a subject.

In the second step, the thorax area of the subject was selected as the data source of interest.

In the third step, the interest is how to measure the ICG and IRG signals, heart rate (HR), and respiration rate (RR) of the human (selected subject). Thus, the EBI measurement method had been selected; in the fourth step on the EBI measured dataset, filtering method was applied to clean the data and attenuate unwanted signals.

Then, after cleaning the EBI signal, namely its ICG and IRG signal components, in the fifth step, the ICG and IRG signals are modelled with the help of Fourier series (see Section 4.2.1) and the corresponding simulator, namely BISS, is built (see Section 4.3).

In the sixth, final step, the EBI signals simulator is developed, which has an application to simulate the EBI signal to evaluate the performance of separation algorithms. However, the simulator (BISS) could be used for teaching and training for the engineering, health science, and medicine students.

4.4.1 Implementation of the Proposed Novel Generic Framework for the Development of the EBI Signal Simulator

In this section, each step in the flow of the framework is described in detail to develop an EBI signal simulator.

Description of the Biological System/Object (Step 1)

The first part – the biological system or object (subject) – is presented in Figure 4.21. It is divided into three sub-systems, which represent the three main systems of the body, namely the cardiovascular, the respiratory, and the muscular systems.

Each system is described through its parameters. The relationship between the parameters is shown in the form of arrows connecting them with each other, mainly within the same system but some of them are also connected with the parameters, which belong to one or both of the two other systems.

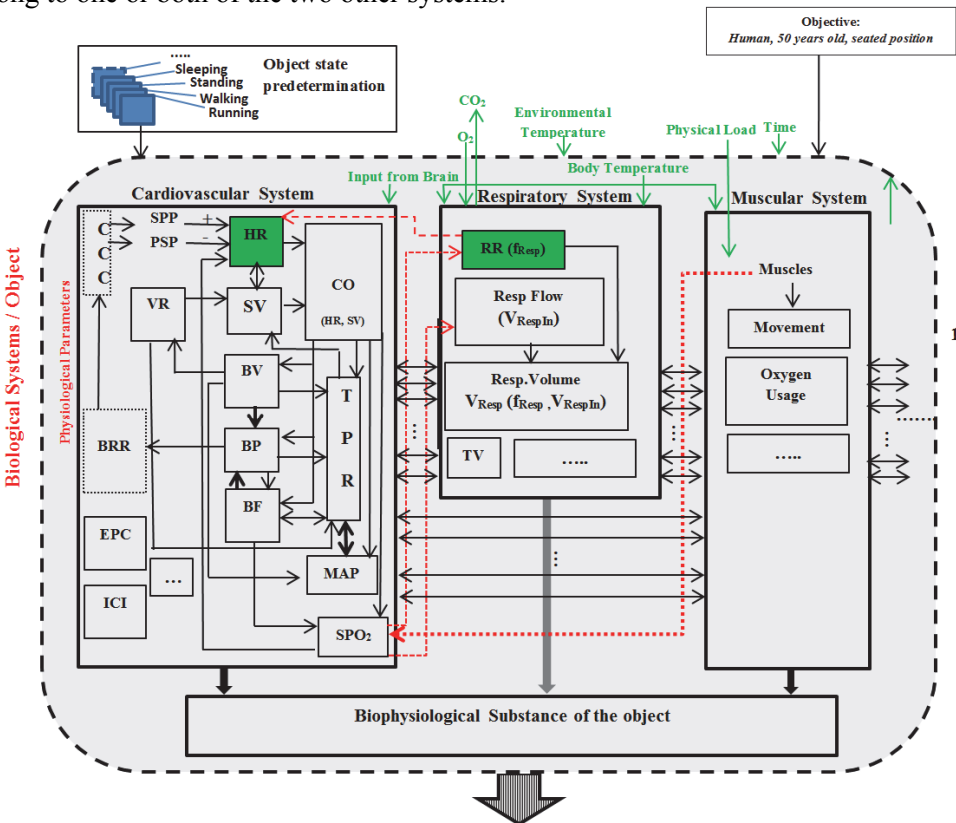


Figure 4.21 Block diagram of the relationship of parameters for the three main systems of the organism (cardiovascular, respiratory, and muscular).
The parameters of greatest interest are highlighted.

The details of the individual parameters are discussed in Section 3.2.1 of Chapter 3. Here, the interest was how to measure HR, RR, and the ICG and IRG signals from the selected subject.

Selection of the Data Source of the Interest (Step 2)

The second diagram (Figure 3.2) is divided into three sub-diagrams. Each sub-diagram is discussed, which is shown in Figure 4.22.

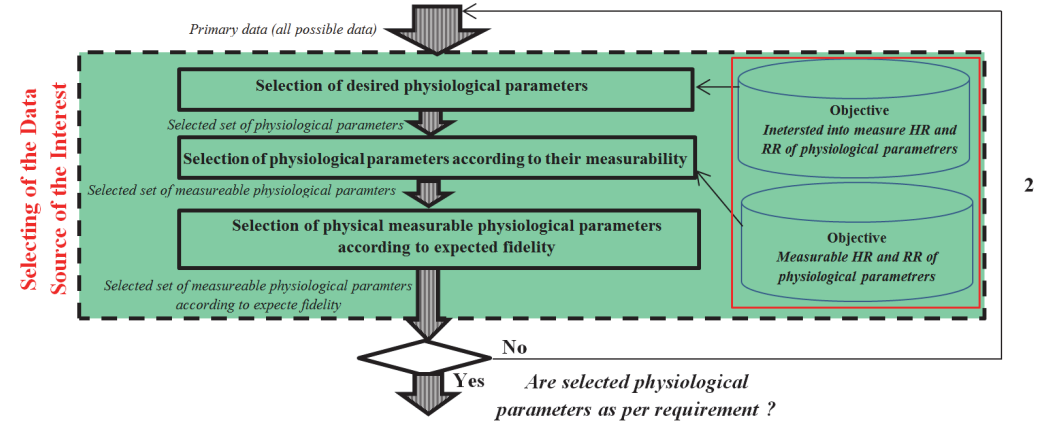


Figure 4.22 Flow diagram for selection of the data source of the interest.

The red box shows the specific parameters of interest, which are selected by the advanced user for this example.

In this diagram, the objective is to select the desired physiological parameters for further use from the full set of physiological parameters, which come from the selected subject area of the thorax. The physiological parameters of interest are HR and RR. The HR and RR are directly measurable.

Based on the selected area of the thorax, it is assumed that strong variations of the ICG and IRG signals can be obtained, and thus that it is possible to measure the physiological parameters HR and RR.

After selecting the source of data and acquiring the EBI dataset and physiological parameters, it is necessary to be sure that these selected physiological parameters are as per needs.

Measurement of Parameters (Step 3)

The third diagram (Figure 3.2) is divided into four sub-diagrams. Each sub-diagram is discussed below, which is shown in Figure 4.23.

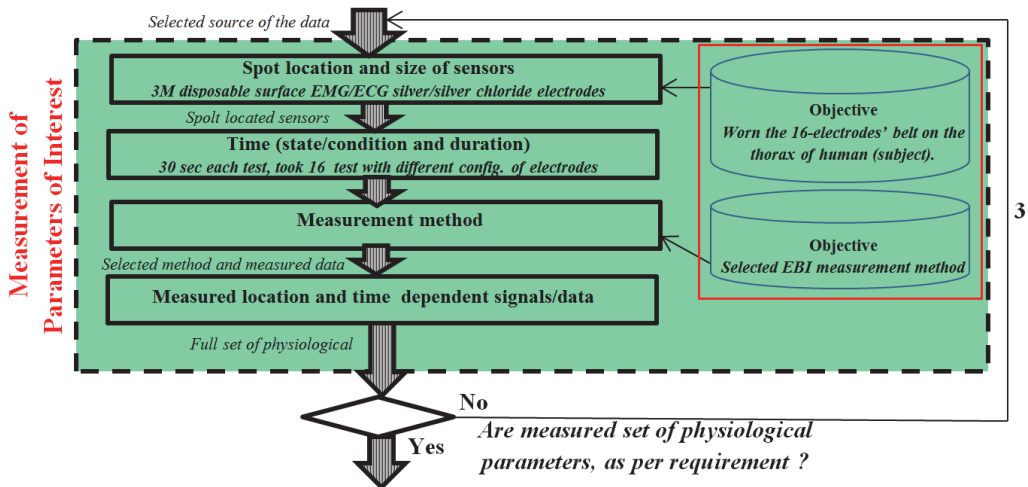


Figure 4.23 Flow diagram for measurement of parameters of interest. The red box shows the specific configuration of electrodes and measurement method, which are selected by the advanced user for this example.

In this step, the objective was to select the configuration of electrodes and select the type of electrodes.

It was decided to use the non-invasive EBI measurement method to acquire the EBI data from the subject with a different configuration of electrodes.

For acquiring the EBI dataset, a 16-electrode configuration belt was used, which was worn on the human thorax area and 3M disposable surface EMG/ECG/silver/silver chloride electrodes were chosen to measure the physiological parameters, namely HR, RR, and the ICG and IRG signals.

After deciding the parameters for all these sub-diagrams, the EBI data, which is location and time dependent, can finally be measured.

Data Cleaning (Step 4)

The fourth diagram (Figure 3.2) is divided into two sub-diagrams. Each diagram is discussed below, which is shown in Figure 4.24.

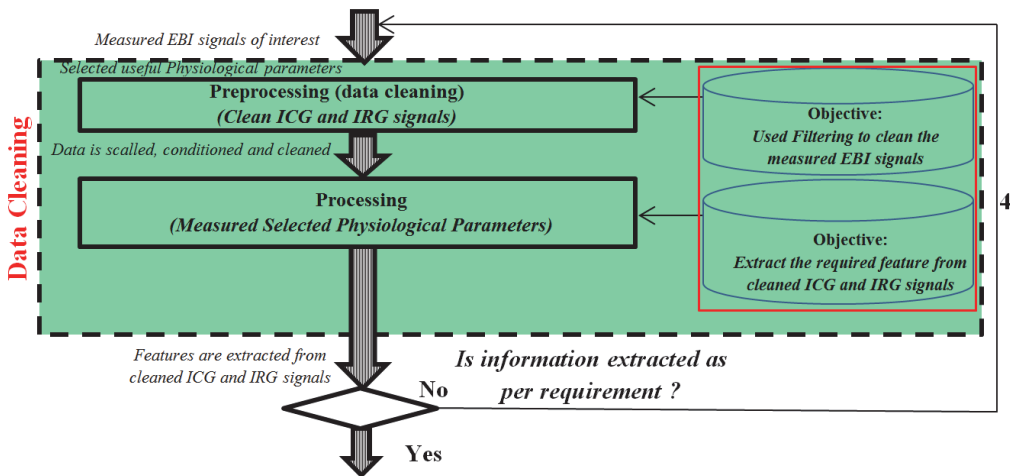


Figure 4.24 Flow diagram of data cleaning.

The red box shows cleaning of the ICG and IRG signals and extracting the feature from the cleaned signals.

In this diagram, the pre-processing was performed to clean the ICG and IRG signals. The pre-processing includes EBI signal normalization (scaling), conditioning and filtering to attenuate useless parts of the signal.

After pre-processing the EBI signal, further processing is performed to extract the features from the clean ICG and IRG signals, such as the waveform and trend of the ICG and IRG signals.

On this point, careful visualization of the ICG and IRG signals' waveform representation with the ideal ICG and IRG signal waveform templates is required.

Modelling and Building a Simulator (Step 5)

The fifth diagram (Figure 3.2) is divided into two sub-diagrams: modelling of the signals and building a corresponding simulator, as discussed below, which is shown in Figure 4.25.

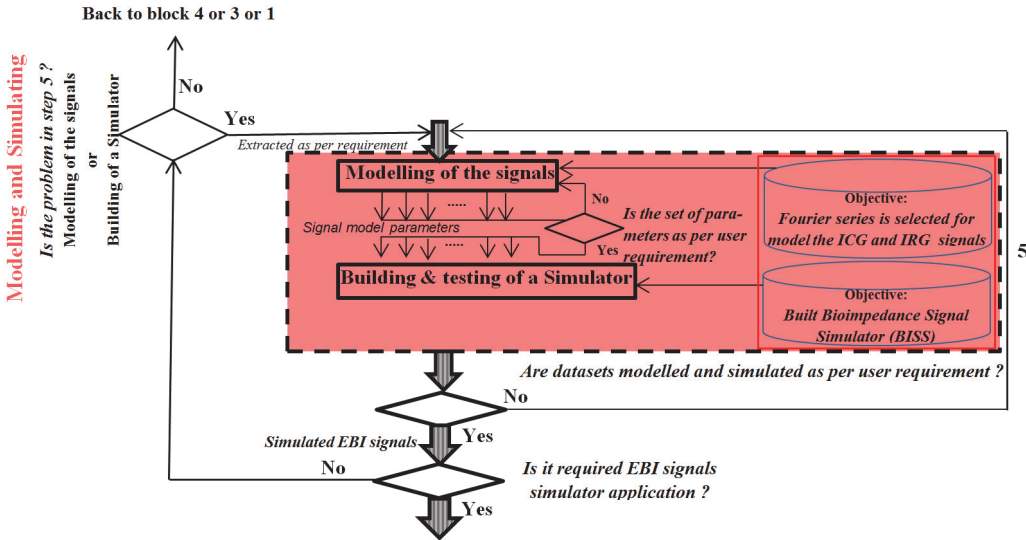


Figure 4.25 Flow diagrams for modelling the ICG and IRG signal parameters based on Fourier series and building a corresponding simulator (BISS).

In the diagram, the signals are modelled based on the clean features of the extracted ICG and IRG signals. The Fourier series method was chosen among other curve-fitting methods to model the ICG and IRG signal parameters. The Fourier series is discussed above in Section 4.2.1.

The corresponding simulator, namely BISS, is built based on the ICG and IRG signals' modelled parameters.

Applications (Step 6)

The sixth diagram (Figure 3.2) is the application, which is shown in Figure 4.26.

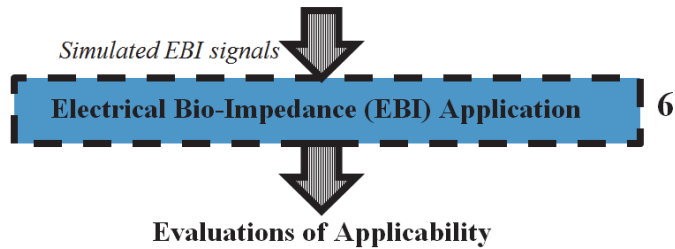


Figure 4.26 Diagram of the Electrical Bio-Impedance (EBI) application.

Finally, an application (BISS) which simulates the EBI signal is developed.

BISS can be a useful tool to simulate the EBI signals in order to evaluate the performance of signal processing algorithms, e.g. those for separation of cardiac and respiratory signals. Thus, the proposed approach can increase the level of confidence when applying the developed algorithms to real measured EBI data.

However, BISS could also be used for teaching and training in physiological courses for engineering and health science students, as it can provide a hands-on means for the students to understand the complicated physiological phenomena.

4.5 Summary of the Chapter

This chapter discussed the implementation of the framework, the experimental results related to the modelling of the ICG and IRG signals, and the developed corresponding simulator.

The EBI measurement method was selected to measure the human thorax area to record EBI datasets in order to model the ICG and IRG signals because impedance is one of the prospective methods in non-invasive methods.

Therefore, this chapter firstly described how a Zurich Instrument HF2IS Impedance Spectroscopy was used to measure the EBI (datasets).

The measured EBI data were cleaned to extract the ICG and IRG signal waveform features. The cleaning was performed with the help of a filtering method (high-pass and low-pass filters).

Then, three curve-fitting methods, namely polynomial, Fourier series, and sum of sines models were evaluated based on six EBI datasets (four measured EBI raw datasets and two cleaned (ICG and IRG signals)).

The evaluation criteria were to obtain the best fit both visually and by means of statistical parameters that were evaluated in terms of the minimization of the error (SSE), high correlation between data and model (R-Square), as well as short execution time.

Based on our evaluated results and generally speaking, the three models perform very well but Fourier series performs the best among them.

Thirdly, building on the Fourier series model, BISS has been developed to simulate the EBI signals.

BISS gives the end-user the freedom to simulate EBI signals as per his/her needs for further analysis. Nevertheless, predefined states are included in BISS. The simulator imitates the real phenomena of ICG and IRG signals, and thus the EBI simulated signals could be used to evaluate the performance of separation algorithms, for example. However, the developed BISS could also be used for teaching and training purposes.

The proposed generic framework has been implemented for the case of EBI as an example.

The framework guided the steps ranging from measuring the EBI data from the subject, the cleaning process for the measured EBI data to achieve the ideal ICG and IRG signals, and finally, based on that, to the developed corresponding simulator (BISS).

5. CONCLUSIONS

At the beginning of my PhD studies, my research was focused on developing an efficient and robust algorithm to separate the cardiac and respiratory signals from an electrical bio-impedance signal. The separated signals could then be analysed by cardiologists to understand the conditions of the heart and lungs.

With respect to this problem, different approaches and methods, namely conventional filtering, independent component analysis, principle component analysis, wavelet, etc. were analysed, tested, and tried in order to solve the problem.

During the first part of my research (Papers III and IV), it has been understood what the mechanisms for the separation algorithms are and how to evaluate them. In particular, these papers illustrated that it is not possible to evaluate the performance of the algorithms directly from measured data, because the parameters and waveform of the measured signals are uncertain, i.e. the cardiac and respiration signal parameters and waveform vary depending on the configuration of the electrodes, for example, and are subject to measurement errors.

The understanding and results of the first part of the research summarized above led to development of a signal model that can imitate the real phenomena of the cardiac and respiratory signals. The modelled signals could then be used for evaluating the performance of various signal processing algorithms, including separation algorithms.

Based on measured and cleaned extracted signals, the impedance cardiography (ICG) and impedance respirogram (IRG) signals have been modelled and a corresponding bio-impedance signal simulator (BISS) has been developed to simulate electrical bio-impedance (EBI) signals for evaluating the performance of various signal-processing algorithms on such signals.

In order to guide the development of the above signal models and simulator, a significant part of this PhD work focused on developing a physiological parametric framework for modelling measurable bioelectrical information and implement this parametric framework with a pragmatic approach on the bio-impedance example. Thus, in this study, a novel generic framework has been proposed for modelling the bioelectrical information and was then implemented for the case of EBI as an example.

From the author's point of view, the following tasks and results have been conducted and achieved, respectively:

- a) An analysis of the existing impedance thorax models and origin of the ICG signal has been carried out in order to potentially identify and use one of the models to generate the required cardiac and respiratory signals for further experiments. The analysis shows that, to the best of my knowledge, none of the models provides sufficiently accurate cardiac and respiratory signals to develop the ICG and IRG signal models (Chapter 2).
- b) A review has been performed regarding the ways in which other researchers approach the problem to build a signal model for cardiac and respiratory signals; the review also explains why these methods are not suitable in solving our

problem. This is mostly because other researchers used either a simple method, i.e. one which does not model the signal realistically, a method lacking a mathematical signal model, or a method which is computationally expensive (Chapter 2).

- c) From this study, it is concluded to be preferable to model the cardiac (ICG) and respiratory (IRG) signals based on measured EBI data rather than relying on measured data only (Chapter 2).
- d) The developed models based on measured clean ICG and IRG signals are better than the ICG and IRG signal models based on existing thorax models. The measured clean ICG and IRG signals imitate the real phenomena of the signals sufficiently accurately (as per the selected statistical measures) (Chapter 2, Chapter 4).
- e) A novel generic framework for modelling the bioelectrical information is proposed. The framework provides a pathway between biological systems and bioelectrical applications. This is the unique approach that such a framework is proposed (Chapter 3).
- f) The generic framework described in Chapter 3 is used to implement a practical EBI application (Chapter 3 and Chapter 4).
- g) Three curve-fitting models, namely polynomial, Fourier series, and sum of sines models, were evaluated based on six EBI datasets (four measured EBI raw datasets and two cleaned (ICG and IRG signals)). The evaluation criteria were to obtain the best fit both visually and by means of statistical parameters that were evaluated in terms of minimization of error (SSE), high correlation between the data and model (R-Square), as well as short execution time. Based on our evaluated results and generally speaking, the three models perform quite well but the Fourier series performed best among them (Chapter 4).
- h) Building on the Fourier series model, BISS has been developed to simulate the EBI signals. BISS gives the end-user the freedom to simulate the EBI signal as per his/her needs for further analysis. Nevertheless, predefined states are included in BISS. The simulator imitates the real phenomena of ICG and IRG signals, and thus the EBI simulated signals could be used to evaluate and assess the performance of separation algorithms, for example. However, the developed BISS could also be used for teaching and training purposes.

Based on the results summarized in a), b), and c), it is concluded that the proposed bio-impedance signal model imitates the real ICG and IRG phenomena and is more realistic than existing approaches. This is the second main contribution of this thesis (Section 1.5-b).

Moreover, based on the results presented in d) and g), it is concluded that out of the three regression models for modelling the ICG and IRG signals, the Fourier series offers the best results for modelling the ICG and IRG signals. This corresponds to the third main contribution of this thesis (Section 1.5-c).

Furthermore, based on the results listed in e) and f), it is concluded that the proposed framework provides a pathway between biological systems and bioelectrical

applications by means of steps, including the measurement of the bioelectrical data from the subject, the cleaning process for the measured bioelectrical data, and the development of the corresponding simulator. This is the first main contribution of this thesis (Section 1.5-a).

Finally, based on the results enumerated in h), it is concluded that the novel BISS EBI signal simulator implements the developed signal models and imitates the real ICG and IRG signals phenomena. BISS also gives the end-user the freedom to simulate EBI signals as per his/her needs. This corresponds to the fourth main contribution of this thesis (Section 1.5-d).

The following paragraphs discuss possible improvements and directions for future research work.

Directions for further research include:

- a) Currently, the implementation of BISS is focused on the simulation of the EBI signals and thus only EBI signals are modelled (namely ICG and IRG signals); however, BISS could be extended to other methods of bioelectrical information, such as Foucault Cardiography (FCG), Opto-Electronic Plethysmography (OEP), Electrical Impedance Tomography (EIT), and so on. This would require modelling the signals used in that method (e.g. cardiac and respirogram in the Foucault method) and integrating them in BISS. For this purpose, the proposed generic framework would provide valuable guidelines about the different steps that need to be undertaken to measure and model the signals, as well as for building the corresponding simulators.
- b) To relate the variations observed in the generated EBI signal to the actual physiological phenomenon, e.g. the relation between the model coefficients and parameters and the states/activities of the subject. This would require extensive study of the dynamics of the physiological phenomena, which is a very complex task requiring deep knowledge of the human physiology.
- c) BISS could be advanced by adding extra functionalities to calculate physiological features such as stroke volume (SV) and cardiac output (CO) from the simulated EBI signals.
- d) In the current implementation, the states are focused on healthy resting, standing, walking, and running. However, by repeating the steps described in the framework, it would be relatively easy to add other states (e.g. for someone with a heart condition) to the simulator. This would require acquiring dataset(s) from either new measurements or existing databases.

REFERENCES

- Abtahi, F. et al., 2012. Software Tool for Analysis of Breathing-Related Errors in Transthoracic Electrical Bioimpedance Spectroscopy Measurements. *Journal of Physics: Conference Series*, 407, p.012028. Available at: <http://www.scopus.com/inward/record.url?eid=2-s2.0-84874095138&partnerID=tZOtx3y1>.
- Baker, K., Hill, D. & Pale, T., 1974. Comparison of several pulse-pressure tech. for monitoring stroke volume. *Med. Biol. Eng*, 12, pp.81–8.
- Bianco, C., 2014. How Your Heart Works - HowStuffWorks. Available at: <http://health.howstuffworks.com/human-body/systems/circulatory/heart.htm> [Accessed December 4, 2014].
- Campbell, K. et al., 1982. A pulsatile cardiovascular computer model for teaching heart-blood vessel interaction. *Physiologist*, 25(3), pp.155–62.
- Chen, X. et al., 2008. Estimation of the total peripheral resistance baroreflex impulse response from spontaneous hemodynamic variability. *Am J Physiology*, 294(1), pp.293–301.
- Cotter, G. et al., 2006. Impedance cardiography revisited. *Physiological measurement*, 27, pp.817–827.
- Deborah, R. & Alvater, R., 2002. *Impedance Cardiography Mentor Resource Guide*,
- Defares, J., Osbome, J. & Hara, H., 1963. Theoretical synthesis of the cardiovascular system. Study I: The controlled system. *Acta Physiol Pharm Neerl*, 12(189-265).
- EHN, 2012. European Cardiovascular Disease Statistics 2012. Available at: <http://www.ehnheart.org/cvd-statistics.html> [Accessed February 2, 2015].
- Franz, M.R. et al., 1983. Electrical and mechanical restitution of the human heart at different rates of stimulation. *Circulation Research*, 53(6), pp.815–822. Available at: <http://circres.ahajournals.org/cgi/doi/10.1161/01.RES.53.6.815>.
- Gargasas, L. et al., 2004. Development of methods for monitoring of electrocardiograms, impedance cardiograms and seismocardiograms. *Studies in health technology and informatics*, 105, pp.131–141. Available at: <http://www.mendeley.com/research/development-methods-monitoring-electrocardiograms-impedance-cardiograms-seismocardiograms/> [Accessed November 26, 2014].

- Grimnes, S. & Martinsen, O.G., 2014. *Bioimpedance and Bioelectricity Basics*, Available at: http://www.amazon.com/Bioimpedance-Bioelectricity-Basics-Third-Edition/dp/0124114709/ref=dp_ob_image_bk [Accessed November 26, 2014].
- Grodins, F.S., 1959. Integrative Cardiovascular Physiology: A Mathematical Synthesis of Cardiac and Blood Vessel Hemodynamics. 34(2), pp.93–116.
- Harrub, B., 2005. The Unevolvable Circulatory System. Available at: <http://apologeticspress.org/APContent.aspx?category=12&article=980> [Accessed February 18, 2015].
- Heldt, T. et al., 2010. CVSim: An Open-Source Cardiovascular Simulator for Teaching and Research. *The Open Pacing, Electrophysiology & Therapy Journal*, 3, pp.45–54. Available at: <http://physionet.incor.usp.br/physiotools/cvsim/45TOPETJ.pdf> [Accessed November 16, 2014].
- Hunter, G. & Tan, F., 2006. *Advanced Topics in Global Information Management*, Idea Group Inc (IGI). Available at: <http://books.google.com/books?hl=en&lr=&id=5Vy9AQAAQBAJ&pgis=1> [Accessed November 25, 2014].
- Jurjević, M. et al., 2009. Mechanical ventilation in chronic obstructive pulmonary disease patients, noninvasive vs. invasive method (randomized prospective study). *Collegium antropologicum*, 33(3), pp.791–7. Available at: <http://www.ncbi.nlm.nih.gov/pubmed/19860105> [Accessed November 25, 2014].
- Kappel, F., 2012. Modeling the Dynamics of the Cardiovascular-respiratory System (CVRS) in Humans, a Survey. *Mathematical Modelling of Natural Phenomena*, 7(5), pp.65–77. Available at: <http://www.mmnp-journal.org/10.1051/mmnp/20127506> [Accessed December 4, 2014].
- Kappel, F. & Peer, R.O., 1993. A mathematical model for fundamental regulation processes in the cardiovascular system. *Journal of Mathematical Biology*, 31(6), pp.611–631. Available at: <http://link.springer.com/10.1007/BF00161201> [Accessed December 4, 2014].
- Karnegis, Y. & Kubicek, W., 1970. Physiological correlates of the cardiac thoracic impedance waveform. *Am Heart J*, 79, pp.519–23.
- Katz, S. et al., 1978. Computer simulation in the physiology student laboratory. *Physiologist*, 21(6), pp.41–4.

- Kauppinen, P., Hyttinen, J. & Malmivuo, J., 1998. Sensitivity Distributions of Impedance Cardiography Using Band and Spot Electrodes Analyzed by a Three-Dimensional Computer Model. *Annals of Bionedical Engineering*, 26, pp.694–702.
- Kauppinen, P.K. et al., 1999. Lead field theoretical approach in bioimpedance measurements: Towards more controlled measurement sensitivity. *Annals of the New York Academy of Sciences*, 873, pp.135–142.
- Kenny, T. & Tidy, C., 2012. Electrocardiogram (ECG) | Health | Patient.co.uk. Available at: <http://www.patient.co.uk/health/electrocardiogram-ecg> [Accessed November 28, 2014].
- Kersulyte, G., Navickas, Z. & Raudonis, V., 2009. Investigation of complexity of extraction accuracy modeling cardio signals in two ways. In *Proceedings of the 5th IEEE International Workshop on Intelligent Data Acquisition and Advanced Computing Systems: Technology and Applications, IDAACS'2009*. pp. 462–467.
- Kohl, Peter Sachs, Frederick Franz, M.R., 2011. *Cardiac Mechano-Electric Coupling and Arrhythmias*, Oxford University Press. Available at: <http://books.google.com/books?id=AgoBCHptrFYC&pgis=1> [Accessed November 26, 2014].
- Krivoshei, A., 2006. A Bio-Impedance Signal Synthesiser (BISS) for Testing of an Adaptive Filtering System. In *2006 International Biennial Baltic Electronics Conference*. IEEE, pp. 1–4. Available at: <http://ieeexplore.ieee.org/lpdocs/epic03/wrapper.htm?arnumber=4100325> [Accessed November 13, 2014].
- Krivoshei, A. et al., 2006. An Adaptive Filtering System for Separation of Cardiac and Respiratory Components of Bioimpedance Signal. In *IEEE International Workshop on Medical Measurement and Applications, 2006. MeMea 2006*. IEEE, pp. 10–15. Available at: <http://ieeexplore.ieee.org/lpdocs/epic03/wrapper.htm?arnumber=1644448> [Accessed November 12, 2014].
- Krivoshei, A., Kukk, V. & Min, M., 2008. Decomposition method of an electrical bio-impedance signal into cardiac and respiratory components. *Physiological measurement*, 29(6), pp.S15–25. Available at: <http://www.mendeley.com/catalog/decomposition-method-electrical-bioimpedance-signal-cardiac-respiratory-components/> [Accessed November 12, 2014].

- Krivošei, A., 2009. *Model Based Method for Adaptive Decomposition of the Thoracic Bio-impedance Variations into Cardiac and Respiratory Components*. Ph.D Thesis. Tallinn University of Technology.
- Kubicek, W., Kottke, F. & Ramos, M., 1974. The Minnesota impedance cardiograph-Theory & appl. *Biomed. Eng*, 9, pp.410–416.
- Lamberts, R., Visser, K. & Zijlstra, W., 1984. *Impedance cardiography*,
- Lu, Z. & Mukkamala, R., 2004. Monitoring left ventricular contractility from respiratory-induced blood pressure variability. *Comput Cardiol*, 31, pp.705–8.
- Lu, Z. & Mukkamala, R., 2005. Non-invasive monitoring of left ventricular contractility and ventilatory mechanics. In *27th Annual Conference of the IEEE Engineering in Medicine and Biology Society*. pp. 7636–9.
- Malmivuo, J. & Plonsey, R., 1995. *Bioelectromagnetism - Principles & Appl. of Bioelectric and Biomagnetic Fields*, Oxford Univ. Press.
- Matlab2012b, 2014. *manual, Curve Fitting Toolbox*,
- Matušek, A., Provaznik, I. & Fontecave-Jallon, J., 2012. *Modelling of Impedance Cardiac Signals*.
- Min, M., Martens, O. & Parve, T., 2000. Lock-in measurement of bio-impedance variations, Measurement. *IMEKO*, 27(1), pp.21–28.
- Mohapatra, S., 1988. *Impedance cardiography*. In *Encyclopedia of Med. Devices and Instrument*, NY: John Wiley & Sonss.
- Mohapatra, S., 1981. *Noninvasive Cardiovascular Monitoring of Electrical Impedance Technique*, London.
- Mughal, Y.M. et al., 2014. An Overview of the Impedance Models of the Thorax and the Origin of the Impedance Cardiography Signal and Modeling of the Impedance Signals. In *2014 IEEE Conference on Biomedical Engineering and Sciences (IECBES 2014)*.
- Mughal, Y.M., 2012. Conversation with Paul Annus, Tallinn University of Technology.
- Mughal, Y.M., 2014. *Decomposing of Cardiac and Respiratory Signals from Electrical Bio-impedance Data Using Filtering Method* Y.-T. Zhang, ed., Cham: Springer

International Publishing. Available at: <http://link.springer.com/10.1007/978-3-319-03005-0> [Accessed November 12, 2014].

Mughal, Y.M. et al., 2015. Development of a Bio-Impedance Signal Simulator on the Basis of the Regression Based Model of the Cardiac and Respiratory Impedance Signals. In H. Mindedal & M. Persson, eds. *16th Nordic-Baltic Conference on Biomedical Engineering*. IFMBE Proceedings. Gothenburg: Springer International Publishing, pp. 92–95. Available at: <http://link.springer.com/10.1007/978-3-319-12967-9> [Accessed November 12, 2014].

Mughal, Y.M., Krivoshei, A. & Annus, P., 2013. Separation of cardiac and respiratory components from the electrical bio-impedance signal using PCA and fast ICA. In *International Conference on Control Engineering & Information Technology (CEIT'13)*. Sousse, Tunisia, pp. 153–156. Available at: <http://arxiv.org/abs/1307.0915> [Accessed November 12, 2014].

Mukkamala, R. & Cohen, R., 2001. A forward model-based validation of cardiovascular system identification. *Am J Physiol*, 281(6), pp.2714–2730.

Mukkamala, R., Toska, K. & Cohen, R., 2003. Noninvasive identification of the total peripheral resistance baroreflex. *Am J Physiol*, 284(3), pp.947–959.

NIH, N., 2010. Disease Statistics - NHLBI, NIH. Available at: <http://www.nhlbi.nih.gov/about/documents/factbook/2012/chapter4> [Accessed February 2, 2015].

Parati, G. et al., 2008. European Society of Hypertension guidelines for blood pressure monitoring at home: a summary report of the Second International Consensus Conference on Home Blood Pressure Monitoring. *Journal of hypertension*, 26(8), pp.1505–26. Available at: <http://www.ncbi.nlm.nih.gov/pubmed/18622223> [Accessed November 26, 2014].

Patterson, R., 2010. Impedance cardiography: What is the source of the signal? In *Int. Conf. on Electrical Bioimpedance*. pp. 1–4.

Patterson, R., 1985. Source of the thoracic cardiogenic electrical impedance signal as determined by a model. *Med & Biol. Eng & Comput*, 23, pp.411–417.

Patterson, R., Wang, L. & McWeigh, 1993. Impedance cardiography: The failure of sternal electrodes to predict changes in stroke volume. *Biol. Psychol*, 36, pp.33–41.

- Patterson, S.W., Piper, H. & Starling, E.H., 1914. The regulation of the heart beat. *The Journal of Physiology*, 48(6), pp.465–513. Available at: <http://www.pubmedcentral.nih.gov/articlerender.fcgi?artid=1420509&tool=pmcentrez&rendertype=abstract> [Accessed December 4, 2014].
- Penny, B., 1986. Theory and cardiac applications of electrical impedance measurements. *CRC Crit. Rev. Bioeng*, 13, pp.227–81.
- Rosenberger, E., 2009. The Difference between Invasive and Noninvasive Procedures. Available at: <http://www.sciences360.com/index.php/the-difference-between-invasive-and-noninvasive-procedures-14048/> [Accessed November 26, 2014].
- Sakamoto, K. et al., 1979. Problems of impedance cardiography. *Medical & biological engineering & computing*, 17(6), pp.697–709. Available at: <http://www.ncbi.nlm.nih.gov/pubmed/317910> [Accessed January 17, 2015].
- Sakamoto, K. & Kania, H., 1979. Electrical characteristics of flowing blood. *IEEE Trans. Biomed. Eng*, 26, pp.686–695.
- Santos, N. et al., 2013. Opto-electronic plethysmography : Noninvasive and accurate measurement of the volume of the chest wall and its different thoraco-abdominal compartments. , pp.147–150.
- Solà, J. et al., 2011. Non-invasive monitoring of central blood pressure by electrical impedance tomography: first experimental evidence. *Medical & biological engineering & computing*, 49(4), pp.409–15. Available at: <http://www.ncbi.nlm.nih.gov/pubmed/21404079> [Accessed November 20, 2014].
- Soudon, P., Steens, M. & Toussaint, M., 2008. A comparison of invasive versus noninvasive full-time mechanical ventilation in Duchenne muscular dystrophy. *Chronic respiratory disease*, 5(2), pp.87–93. Available at: <http://www.ncbi.nlm.nih.gov/pubmed/18539722> [Accessed November 25, 2014].
- Sunagawa, K. & Sagawa, K., 1982. Models of ventricular contraction based on time-varying elastance. *Crit Rev Biomed Eng*, 7(3), p.193228.
- Sörnmo, L. & Laguna, P., 2005. *Model Based Method for Adaptive Decomposition of the Thoracic Bio-impedance Variations into Cardiac and Respiratory Components*, Elsevier Academic Press.
- Zurich, H., 2015. HF2IS Impedance Spectroscope - Zurich Instruments. Available at: <http://www.zhinst.com/products/hf2is> [Accessed February 12, 2015].

- Thompson, F. & Joekes, A., 1981. *Thoracic impedance cardiodynamic assessment: Validation in clinical use*, London.
- Timischl, S., 1998. *A Global Model for the Cardiovascular and Respiratory System*. Karl-Franzens University of Graz. Available at: <http://staff.technikum-wien.at/~teschl/diss.pdf>.
- Trolla, J. & Vedru, J., 2001. On the safety of foucault cardiography. In *XI Int. Conf. Electrical Bio-impedance*. Oslo, pp. 649–652.
- Ulbrich, M. et al., 2012. Simulation of Lung Edema in Impedance Cardiography. *Computing in Cardiology*, 39(1), pp.33–36.
- Wang, L. & Patterson, R., 1995. Multiple Source of the Impedance Cardiogram Based on 3-D Finite Difference Human Thorax Models. *IEEE Trans. on Biomedical Engineering*, 42(2), pp.141–148.
- Wang, L., Patterson, R. & Raza, B., 1991. Respiratory effects on cardiac related impedance indices measured under voluntary cardio-respiratory synchronization. *Med. Biol. Eng & Comput*, 29, pp.505–510.
- Wittoe, D. & Kottke, F., 1967. The origin of cardiogenic changes in thoracic electrical impedance (del Z). In *Feder. Proc.*
- Woltjer, H.H., Bogaard, H.J. & de Vries, P.M., 1997. The technique of impedance cardiography. *European heart journal*, 18, pp.1396–1403.
- Wu, H. et al., 2008. Three dimensional electrical impedance tomography in thorax complete model. *Conference proceedings : Annual International Conference of the IEEE Engineering in Medicine and Biology Society. IEEE Engineering in Medicine and Biology Society. Conference*, 2008, pp.466–469.
- Wu, T.-H., 2011. Personalized eHealth: Status and Challenges - IEEE Life Sciences. Available at: <http://lifesciences.ieee.org/articles/43-personalized-ehealth-status-and-challenges> [Accessed November 26, 2014].
- Xu, D. et al., 2011. Improved pulse transit time estimation by system identification analysis of proximal and distal arterial waveforms. *AJP: Heart and Circulatory Physiology*, 301, pp.H1389–H1395.

APPENDIX

Copies of the main published papers

This appendix provides copies of the papers listed on page 11.

Paper I

Yar M. Mughal, Yannick Le Moullec, Paul Annus, Mart Min

“Development of a Bio-Impedance Signal Simulator on the basis of the Regression based Model of the Cardiac and Respiratory Impedance Signals”

in *IFMBE Proceedings*, Volume 48,

16th Nordic-Baltic Conference on Biomedical Engineering, 16. NBC & 10. MTD 2014 Joint Conferences, Gothenburg, Sweden, October 14–16, 2014, pages 92-95.



The conference participants amounted to 430, this paper was selected as a finalist in the Young Investigator Award (YIA) competition for scientific contribution. The award was given by Springer and IFMBE

YOUNG INVESTIGATOR AWARD

The Award Committee of the NBC16 and MTD10 is pleased award this book prize to

Yar M. Mughal

for being selected as a finalist in the YIA competition for their scientific contribution.

This award entitles the recipient a Springer book in the amount of Euro 140€.

To redeem 140€ value book entitlement, contact Dr. Christoph Baumann (Springer)

E-Mail: christoph.baumann@springer.com

CB
Dr. Ch. Baumann, Springer

The committee
flerk-Jes

NBC16
MTD10

 **IFMBE**

 **Springer**
the language of science

Springer Verlag GmbH
Tiergartenstr. 17
69121 Heidelberg
Germany
www.springer.com

Expires: December 31, 2014
Not redeemable for cash.

Development of a Bio-Impedance Signal Simulator on the Basis of the Regression Based Model of the Cardiac and Respiratory Impedance Signals

Y.M. Mughal¹, Y.L. Moullec¹, P. Annus^{1,2}, and M. Min^{1,2}

¹ Thomas Johann Seebeck Department of Electronics, Tallinn University of Technology (TUT), Tallinn, Estonia

² Competence Centre in Electronics-, Info- and Communication Technologies (ELIKO), Tallinn, Estonia

Abstract—A software implemented bio-impedance signal simulator (BISS) is proposed, which can imitate real bio-impedance phenomena for analyzing the performance of various signal processing methods and algorithms. The underlying mathematical models are built by means of a curve-fitting regression method. Three mathematical models were compared polynomial, Fourier series and sum of sine waves with four different measured impedance cardiography (ICG) datasets and two clean ICG and impedance respirography (IRG) datasets were taken as the basis of the signals. Statistical analysis (sum of squares error, correlation and execution time) implies that Fourier series is best suited. The models of the ICG and IRG signals are integrated into the proposed simulator.

In the simulator the correlation between heart rate and respiration rate are taken into account by means of ratio between them (5:1 respectively).

Keywords— Regression based model, Signal Simulation and Modeling, Electrical Bio-Impedance, Impedance Cardiography, Respiratory Signal.

I. INTRODUCTION

Impedance cardiography (ICG) measurement has been offered as a cost effective and noninvasive method for monitoring haemodynamical parameters. The time variant part of the bioimpedance (BI) phasor reflects processes in patient physiological state since some changes in BI can be caused by normal activity or pathological reasons [1, 2].

Extracting information from impedance signals for diagnosing diseases and assessing heart function is essential for exploiting this method.

Working on real signals can be difficult; it is desirable to provide a simulation tool to enable simulation and control of such signals for analyzing the performance of various signal processing methods such as cardiac and respiratory separation algorithms, e.g. independent component analysis (ICA), adaptive filtering, ensemble averaging, and spectral methods [3, 4].

Modeling of the ICG signal has captured the interest of several researchers in the past few years, using different approaches such as described in [4, 5, 6].

In [4], Krivoshei proposed a simple bio-impedance signal synthesizer to generate cardiac and respiratory signals. The author used a piece-wise linear triangular function to model the cardiac signal and a trapezium to model the respiratory signal. The model, however, is too simple to fully imitate the cardiac and respiratory signals, and thus does not allow testing e.g. separation algorithms.

Kersulyte et al. [5] proposed a cardio model based on the sum of exponential functions. The purpose of their

work was to find out a model for cardio signals as precise as possible and compare complexity parameters of the real signals and that of the model for both healthy and sick persons. They compared two function types polynomial and sum of exponentials. Their results indicate that both methods lead to similar results in terms of fidelity; however, the authors also indicate that the polynomial equation depends on the signal length and number of intervals, which could lead to too many coefficients and increased computational requirements for complex signals.

In [6] Matušek et al. proposed a cardiac signal model based on a series of real signals. By filtering and averaging the series of real signals, they estimated one average ICG signal cycle and simply replicated this cycle over time to get the final signal model. One limitation of this approach is that it lacks a mathematical model and thus the user cannot easily change the parameters of the model.

Given the limitations of the above works, it was decided to compare the suitability of three mathematical models (polynomial, Fourier series, sum of sine waves) by means of Matlab's Curve Fitting Toolbox.

II. MODELING THE ICG AND IRG SIGNALS

The impedance cardiography and impedance respirography (IRG) signals are nearly periodic signals that can be approximated through various mathematical models. In this study, first were evaluated ten models, which are available in the toolbox and found out that three of these gave the better results, namely polynomial, Fourier series, and sum of sine waves. Then these three models were applied on four measured ICG datasets and two clean ICG and IRG datasets for evaluation and comparison purposes. What follows briefly describes the electrical bio-impedance (EBI) measurement procedure and then discusses each model separately.

A. EBI Measurement Procedure

The datasets were obtained using multiple pairs of electrodes with different electrode configurations. The EBI measurement electrode setup is shown in Figure 1.

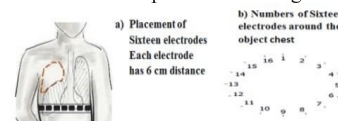


Fig 1. Sixteen electrodes configured belt, which is used for the EBI measurement procedure [2].

Such type of electrodes' setup is presumed to allow raising strong enough variations of the EBI in order to record the cardiac and respiration signals, which are caused by the heart and lungs. Further details about the EBI measurement setup can be found in [2].

The measured datasets are obtained from a healthy male subject aged between 40 and 50 years, in a seated position.

The total EBI dataset was divided into three different segments. Each segment contains 10 seconds of the total EBI raw data, about 10,000 samples. Accordingly, the structure of the three segments is as follows:

- a) cardiac only (breathing was held),
- b) cardiac + respiration (deep breathing),
- c) cardiac + respiration + motion artefacts (normal breathing with added motion artefacts).

In what follows, the four ICG datasets correspond to b) and the clean ICG and IRG datasets correspond to filtered versions of a) and b), respectively.

B. Models and Evaluation Method

a) Polynomial Model

Polynomials are well suited for cases where a fairly simple empirical model is needed; they can be used for interpolation or extrapolation to characterize data by means of a global fit. The general polynomial model formula is given in Equation 1:

$$y = \sum_{i=1}^{n+1} p_i t^{n+1-i} \quad (1)$$

where n is the degree of the polynomial (highest power of the predictor variable), $n+1$ is the order of the polynomial (number of coefficients), p_i are the coefficients and t is time.

In this work, the polynomial model was evaluated for degrees 1 to 9 for the different datasets; degree 9, which is the highest order available in the toolbox, gave the best suitable results. The comparative results are shown in Table 1 and Figures 2 & 3.

b) Fourier Series Model

The Fourier series is a sum of sine and cosine functions that describes a periodic signal. The model formula is given in Equation 2:

$$y = a_0 + \sum_{i=1}^n a_i \cos(i\omega t) + b_i \sin(i\omega t) \quad (2)$$

where a_0 is the intercept, which is constant term in the data, ω is the fundamental frequency and n is the number of terms in the series. The model was evaluated with 1 to 8 terms for the different ICG datasets; the best suitable results were obtained for the degree of 8, the highest available in the toolbox. The comparative results are shown in Table 1 and Figures 2 and 3.

c) Sum of Sine Waves Model

This model consists of a sum of sine terms only. The model formula is given in Equation 3:

$$y = \sum_{i=1}^n a_i \sin(i\omega t + c_i) \quad (3)$$

where a is the amplitude, ω is the frequency, c the phase, which is constant for each term and n is the total terms in series.

The model was evaluated with 1 to 8 terms for the different datasets; 8 terms (the highest available in the toolbox) gave the most suitable results. The comparative results are shown in Table 1 and Figures 2 and 3.

d) IRG Signal with Polynomial, Fourier Series and Sum of Sine Waves Models

Following the same approach as for the ICG signal, the IRG clean dataset is also modeled with the polynomial,

Fourier series and sum of sine waves methods. The comparative results are shown in Table 1 (Clean IRG) and Figure 3(c).

C. Statistical Parameters

The performance of the three modeling methods is evaluated by means of the following fit measures.

a) Sum of Squares Error (SSE)

The SSE statistic assesses the total deviation of the data values from the fitted model, as expressed in Equation 4:

$$SSE = \sum_{i=1}^n w_i (y_i - \bar{y}_i)^2 \quad (4)$$

where n is the number of data points, y_i is the response data, and \bar{y}_i is predictor data. SSE values close to 0 indicate that the model is fitted well and has a very small random error [7].

b) R-Square

R-Square measure is the square of the correlation between the data and the fitted model values. A value close to 1 shows a greater correlation between the data and the model whereas a value close to 0 shows a poor correlation. It is determined as the ratio of the sum of squares of the regression (SSR) and the total sum of squares (SST), where $SST = SSR + SSE$. The R-square measure is given in Equation 5 [7]:

$$R\text{-square} = \frac{SSR}{SST} = 1 - \frac{SSE}{SST} \quad (5)$$

c) Execution time

The execution time is measured through Matlab stopwatch functions (tic, toc) and reported in Table 1.

III. EXPERIMENTAL RESULTS

Table 1 and Figures 2 and 3 show the fit of the three models with the various datasets. Generally speaking, the three models provide a reasonable fit across the four datasets: the average SSE value is 0.879e-07, the min and max values are 0.161e-07 and 1.9417e-07, respectively

Similarly, the average R-square value across the four datasets is 0.9762, the min and max values are 0.9512 and 0.9936, respectively.

The Fourier series model minimizes the error (average SSE=0.335e-07) and has also a high correlation across the four datasets as compared to the other models. However, it took 1.275 more seconds to execute as compared to the polynomial model; it is nevertheless much faster (by 44.476 seconds or nearly 10 times) than the sum of sine waves model.

In this study, the most suitable results were obtained with eight terms for the Fourier series model, which gives 18 coefficients. For the polynomial model, we set the degree to 9, leading to ten coefficients. It is preferable to limit the number of coefficients for relating them to the patients' condition. However, this has to be traded-off for a lower fit, as shown in Table 1.

Table 1. Evaluation Criteria Results for the Modeled Signal

| Datasets | Sum of sine Waves (24 coeff) | | Fourier (18 coeff) | | Polynomial (10 coeff) | | | | | |
|---------------------------------------|------------------------------|--------|--------------------|--------|-----------------------|--------|-----------|------------|------------|---------|
| | SSE | R-Sq | SSE | R-Sq | SSE | R-Sq | SSE Avg | SSE Min | SSE Max | R-SqAvg |
| Dataset 1 | 1.0424e-07 | 0.9917 | 0.1612e07 | 0.9987 | 1.2270e-07 | 0.9903 | 0.810e-07 | 0.161e-07 | 1.23e-07 | 0.9935 |
| Dataset 2 | 0.9044e-07 | 0.9875 | 0.1786e-07 | 0.9976 | 0.3050e-07 | 0.9959 | 0.463e-07 | 0.179e-07 | 0.904e-07 | 0.9936 |
| Dataset 3 | 1.9417e-07 | 0.9274 | 0.6476e-07 | 0.9758 | 1.3185e-07 | 0.9506 | 1.326e-07 | 0.6476e-07 | 1.9417e-07 | 0.9512 |
| Dataset 4 | 0.8054e-07 | 0.9714 | 0.3506e-07 | 0.9876 | 1.6683e-07 | 0.9409 | 0.941e-07 | 0.3506e-07 | 1.6683e-07 | 0.9666 |
| SSE Avg, R-Sq Avg | 1.17e-07 | 0.970 | 0.335e-07 | 0.9758 | 1.13e-07 | 0.969 | 0.879e-07 | | | 0.9762 |
| SSE Min, R-Sq Min | 8.05e-08 | 0.161 | 0.161e-07 | 0.9758 | 0.305e-07 | 0.941 | | 0.161e-07 | | 0.9512 |
| SSE Max, R-Sq Max | 1.94e-07 | 0.9917 | 0.648e-07 | 0.9987 | 1.67e-07 | 0.996 | | | 1.9417e-07 | 0.9936 |
| Clean ICG Signal with different scale | | | | | | | | | | |
| Clean ICG | 0.1996 | 0.9994 | 0.0611 | 0.9999 | 2.8229 | 0.9937 | 1.0279 | 0.0611 | 2.8229 | 0.9959 |
| Ex. Time (s) | ~49.170 | | ~4.694 | | ~3.419 | | | | | |
| Clean IRG Signal with different scale | | | | | | | | | | |
| Clean IRG | 7896.1e-07 | 1 | 2890.6e-07 | 1 | 19.5782 | 0.9983 | 6.5264 | 2890.6e-07 | 19.5782 | 0.9994 |

Regarding the difference between the polynomial and the sum of sine waves models, it can be seen that for Datasets 2 and 3, the polynomial model minimizes the error (0.3050e-07 and 1.3185e-07, respectively) and is highly correlated with the datasets (0.9959 and 0.9506, respectively). On Datasets 1 and 4, the sum of sine waves model minimizes the error (1.0424e-07 and 0.8054e-07, respectively) and is highly correlated (0.9917 and 0.9714 respectively) with the datasets. However, 8 terms were used for the sum of sine waves model, which gives 24 coefficients (versus 10 for the polynomial model) and a much longer execution time.

For the clean ICG and IRG datasets, the Fourier series model performed very well among all to minimize the error (0.0611 and 2890.6e-07, respectively) and is highly correlated (0.9999 and 1, respectively) with the datasets. It is followed by the sum of sine waves model, which has the second minimum error (0.1996 and 7896.1e-07, respectively) and high correlation (0.9994 and 1, respectively) but also has a larger number of coefficients (24) and larger execution time (49.170 seconds) as compared to the polynomial model.

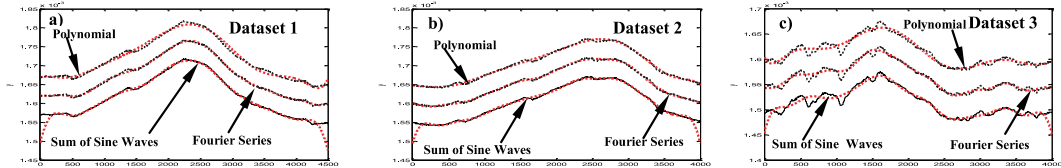


Fig 2. Measured datasets (solid-lines) and fitted models (dotted-lines) for three EBI datasets:

a) results of fitting of the EBI dataset 1, b) results of fitting of the EBI dataset 2, c) results of fitting of the EBI dataset 3. Results for the sum of sine waves model are presented without offset, results for Fourier series model are offset by 0.05×10^{-3} and results for Polynomial model are offset by 0.1×10^{-3} .

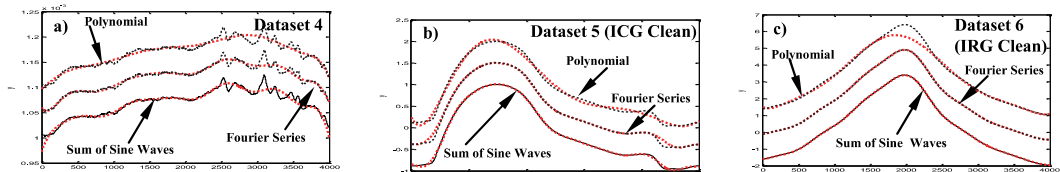


Fig 3. Measured (a) and cleaned (b, c) datasets (solid-lines) and fitted models (dotted-lines) for other three EBI datasets:

a) results of fitting of the EBI dataset 4, b) results of fitting of the cleaned ICG dataset 5, c) results of fitting of the cleaned IRG dataset 6. Results for the sum of sine waves model are presented without offset, results for Fourier series model are offset by offset a) 0.05×10^{-3} , b) offset 0.5, c) offset 1.5) and results for Polynomial model are offset by (a) 0.1×10^{-3} , b) 1, c) 3].

IV. THE BIOIMPEDANCE SIGNAL SIMULATOR (BISS)

This section describes how the Fourier series model was included in our Bioimpedance Signal Simulator (BISS).

As shown in Figure 4, the simulated bio-impedance signal is generated by summing the ICG signal ($S_{AZ\ ICG}$), artefacts ($S_{Artefacts}$), a white Gaussian noise (S_{Noise}) and the IRG signal ($S_{AZ\ IRG}$) such as:

$$S_{EBI(t)} = S_{AZ\ ICG} + S_{Artefacts} + S_{Noise} + S_{AZ\ IRG} \quad (6)$$

The BISS' GUI is shown in Figure 5, where a) is the menu used to perform different operations such as loading different datasets (ICG/FCG) to simulate the signal, saving the final generated EBI signal model for further processing and exiting from the BISS environment, b) a recorded clean ICG period, c) a period of the ICG signal model, d) a recorded respiration period e) a period of the IRG signal model f) the continuously simulated ICG signal.

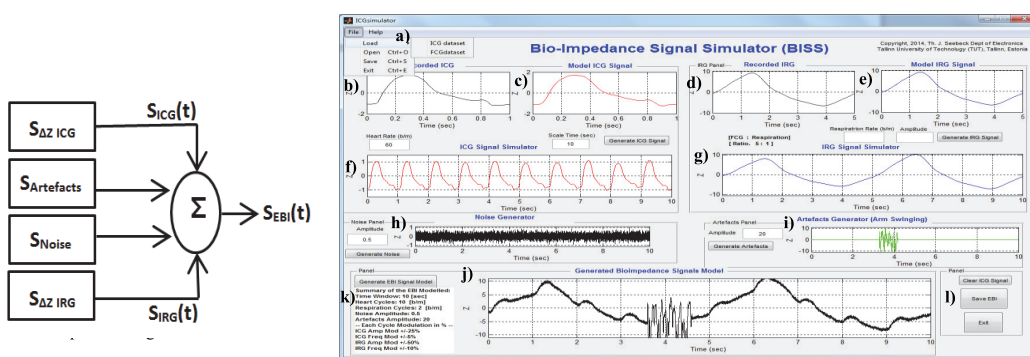


Fig 5. User Interface of the Bioimpedance Signal Simulator (BISS).

The heart rate, time scale, respiration rate, noise and artefacts amplitude parameters are user-Controlled

In order to take the real phenomena of BI signals into account, a random modulation is introduced with each cycle (amplitude ± 25 , frequency ± 5). Moreover, the user should specify the heart rate in beats/min and time window. g) is the continuously simulated respiration signal where a random modulation is introduced with each cycle (amplitude ± 50 , frequency ± 10).

The respiration rate is correlated to the cardiac heart rate by means of the ratio. The default ratio is 5:1 (5 cardiac cycles for 1 respiration cycle). Nevertheless, the user can control the respiration rate as well. h) is the noise generator, i) the recorded artefacts caused by swinging the arm during the measurement (randomly moving in the defined time window, j) the generated bio-impedance signal model based on the user entered parameters, k) the detailed summary of the generated bio-impedance signal model and l) buttons that let the user clear all simulated model signals and start again, save the EBI signal model and exit from BISS' GUI environment.

Figures 5 f), g), h) and i) illustrate the effect of the user-controlled parameters such as time scale window, heart rate (b/m), respiration rate (b/m), noise amplitude and artefacts amplitude.

V. CONCLUSIONS

The polynomial model is relatively simple, but it does not provide the best results for our application. The sum of sine waves model produces better results than the polynomial one, but is less suitable than the Fourier series one because it has a higher number of coefficients, higher SSE values, lower R-Square values, and higher execution times.

Overall, the Fourier series model fits with the measured datasets very well, minimizes the error and has high correlation values as compared to the two other models; only its execution time is slightly higher than that of the polynomial model.

Furthermore, the correlation between the heart rate and the respiration rate is implemented by means of a ratio (default 5 ICG cycles for 1 IRG cycle).

Finally, the user can enable the insertion of the recorded artifact in the final EBI model.

Nevertheless, the resulting simulated signal does not model all aspects of the real bioimpedance data yet. Thus,

future work will refine the model by means of piece-wise segmentation of the datasets for finer grain curve-fitting while maintaining the number of coefficients to the required minimum for reflecting the pathological conditions (i.e. not necessarily 24, 18, and 10 as shown in Table 1).

The Starling's and Poiseuille laws will be taken into account in the model to reflect the systolic and diastolic phenomena respectively.

ACKNOWLEDGMENT

The authors thanks, Prof. T. Rang, Dr. T. Parve and Dr. A. Krivoshei, for providing valuable advices.

Research supported by the European Union through the European Regional Development Fund in frames of the research center CEBE, the competence center ELIKO, the ESF DoRa, the Estonian Ministry of Education and Research (Institutional Research Project IUT19-11) and Tiger University.

REFERENCES

1. Grimnes S. and Martinsen. Ø. G. (2008). Bioimpedance & Bioelectricity Basics. London: Academic Press.
2. Mughal Y. M. (2014) Decomposing of Cardiac and Respiratory Signals from Electrical Bio-impedance Data Using Filtering Method The Int. Conf. on Health Inf. IFMBE Proc. Vol. 42, pp 252-255
3. Mughal Yar M., Krivoshei A, Annus P. (2013) Separation of cardiac and respiratory components from the electrical bio-impedance signal using PCA and fast ICA Int. Conf. on Control, Engineering & Information Technology, Proc. Eng. & Tech., Vol.1,
4. Krivoshei A. (2006) A Bio-Impedance Signal Synthesiser (BISS) for Testing of an Adaptive Filtering System", Proc. of the BEC . p. 1-4.
5. Kersulyte G, Navickas Z, Raudonis V (2009) Investigation of Complexity of Extraction Accuracy Modeling Cardio Signals in Two Ways IEEE Int. Workshop on Intelligent Data Acquisition and Advanced Computing Systems: Tech. and Appl. 21-23.
6. Matušek A, (2012) Modelling of Impedance cardiac Signals M.S. thesis, Faculty of Electrical Eng and Comm. Dept. of Biomedical Eng, Brno university of Technology, Czech Republic.
7. Matlab (2012b) manual, Curve Fitting Toolbox, (June 15, 2014).

Author: Y. M. Mughal

Institute: Thomas Johann Seebeck, Department of Electronics, TUT

Street: Ehitajate tee 5

City: Tallinn

Country: Estonia

Email: yar@elin.ttu.ee.

Paper II

Yar M. Mughal, Paul Annus, Mart Min, Rauno Gordon

“An Overview of the Impedance Models of the Thorax and the Origin of the Impedance Cardiography Signal and Modeling of the Impedance Signals”,

in *Proceeding* of 2014 IEEE Conference on Biomedical Engineering and Sciences (IECBES 2014), 2014, Miri, Malaysia, December 8-10.



An Overview of the Impedance Models of the Thorax and the Origin of the Impedance Cardiography Signal for Modelling of the Impedance Signals

Yar M. Mughal, Jr-EMBS Member, IEEE Member, Paul Annus, IEEE Member, Mart Min, Senior IEEE Member and Rauno Gordon

Abstract—This paper presents our work in the search for a realistic thorax impedance model that is suitable for the simulation of an impedance cardiography (ICG) signal model. The developed ICG signal model would be useful to evaluate the performance of e.g. algorithms for the separation of cardiac and respiratory signals. Five different impedance models of the thorax were studied to evaluate their suitability with respect to the development of the ICG signal model. We found out that none of the models would be accurate enough to imitate the real human thorax phenomena in the context of ICG. In addition, we also reviewed the generation of (bio-) impedance signal in order to understand the origin of the ICG signal waveform. It is found that although a consensus exists in the scientific community, several researchers have expressed doubts about the generally admitted origin of impedance signal waveform. The present study concludes that the ICG signal model could be mathematically derived from measured electrical bio-impedance (EBI) data obtained with a specific electrodes configuration.

I. INTRODUCTION

The measurement of thoracic electrical impedance has been practiced since the 1930s. As a measurement technique, the impedance method is generally viewed as a promising non-invasive method for measuring cardiac output (CO) [1] and other physiological and biological parameters.

Nevertheless, the anatomical structure of the human thorax is very complex and its electrical properties are related to anisotropic and inhomogeneous structures in it [2].

The formation of the ICG waveform is essential for understanding the physiological activities and anatomy of the human thorax as well as the origin of the ICG signal. In the formation of the impedance signal, each organ and tissue makes its contribution [3]. Several methods have been used to understand the origin of the ICG signal [4] and relate it to physiological activities. The main obstacle in cardiovascular impedance measurement is the incapability to precisely associate the measured impedance waveforms to the original mechanical and physiological activities of the heart and following blood volume changes (ΔBV) happening in it [3].

This research was supported by the European Union through the European Regional Development Funding in the frames of the research center CEBE and the competence center ELIKO, the Estonian Ministry of Education and Research (Institutional Research Project IUT19-11) the Found. Archimedes ESF DoRa and Estonian Science Found. Grant (9394).

Y. M. Mughal, P. Annus, M. Min and R. Gordon are with Thomas Johann Seebeck Department of Electronics, Tallinn University of Technology, Ehitajate tee 5, Tallinn, Estonia. (email: yar@elin.ttu.ee phone: +37258026086) and also with the competence center ELIKO.

In order to determine the variations from basal impedance (Z_0), one can detect the resistivity variations in the thorax (or construct a model of it) from the potential of the ICG leads field that can be obtained by changing the conductivity values of the thorax or constructed model [3].

This study focuses on the selection of a thorax impedance model suitable for generating an ICG signal model. In principle, the signal model development could be based on existing selected thorax impedance model or measured electrical bio-impedance (EBI) data.

In this paper, five thorax impedance models and the origin of the ICG signal waveforms are discussed with respect to the ICG signal model development.

Such ICG signal model could be used to evaluate the performance of e.g. algorithms for the separation of cardiac and respiratory signals instead of relying on measured EBI data, which have been shown to be impractical [5].

II. IMPEDANCE MODELS OF THE THORAX

The existing impedance models vary from the simplest (e.g. two or more compartments) ones to the 3D model of the thorax. They were studied to evaluate their suitability for developing a realistic ICG signal model that is as accurate as possible.

A. Simplified Model of the Thorax

This is a very simplified thorax model in which the thorax is considered to be divisible into two parts: tissue (A_t) and fluids (A_b). The parts are characterized by area A of the cross-section of each, as depicted in Fig. 1. This model was developed to find the relationship between change in blood volume (ΔBV) and impedance change (ΔZ). The following equation was found to describe this relationship [2]:

$$dv_b = \rho_b l^2 / Z^2 dZ \quad (1)$$

where d_{vb} is the change of blood volume, ρ_b is the resistivity of blood, l is the distance between the measurement electrodes, Z is the thorax impedance, and dZ is the impedance change.

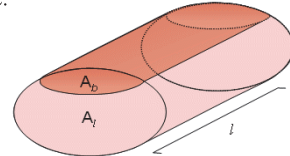


Figure 1. A simple thorax's cylindrical model, which contains a uniformly distributed blood and tissue compartments for determining the net torso impedance [2].

B. Ideal Cylindrical Models

The cylindrical models can have one- or two-compartment. The one- and two-compartment cylinder models are depicted in Fig 2(a-b). The cross sectional area of the ideal cylinder models may be elliptic, circular, or could have any plane [6].

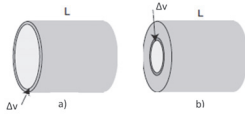


Figure 2. Ideal Cylindrical Models [6]:

a) One-compartment cylinder model, b) Two-compartment cylinder model

In the simple cylindrical model, the thorax is divided into either one or two compartments with the same resistivity. In Fig. 2, L is the length and Δv is the parallel volume increment such that:

$$\Delta / = \Delta v / v \quad (2)$$

Equation (2) is for one compartment (Fig 2a). It is clear that the relative ΔBV can be found without knowing the dimensions of the cylinder:

$$\Delta / = \Delta v / \Delta v + v_A + v_t \quad (3)$$

In the two-compartment model (Fig 2b), the two cylinders are physically in parallel and the conductance model preferred where $\Delta v + v_A$ is the volume of the inner cylinder, and v_t is the volume of the outer cylinder. Equation (3) shows that the sensitivity decreases with a larger surrounding volume (v_t) [6].

C. Kinnen's Thorax Model

Kinnen et al. developed their model based on a cylindrical thorax model [2]. The purpose of this model is to examine the generation of the impedance signal. The model is depicted in Fig. 3, in which the thorax model is divided into two cylindrical parts. The inner part of the model characterizes the BV of the heart and primary arteriovenous system of the thorax. The lungs are characterized by the medium outside the inner part. The resistance for the inner part of the model was taken equal to 495Ω , and 32Ω for the other part.

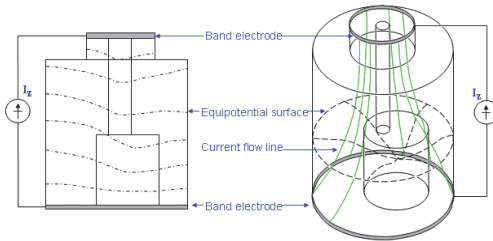


Figure 3. Kinnen's Thorax Model [2]

D. Sakamoto's Thorax Model

Sakamoto et al. [7] developed a model that is anatomically more realistic. This model consists of the heart, aorta, lungs, vena cava and torso shape, as depicted in Fig. 4 (b-c). The model allows investigating the effect of

conductivity variations of the tissues on the measured impedance. These results showed that the information connected to the blood circulation in the human thorax could be measured by potential distribution changes on the body surface.

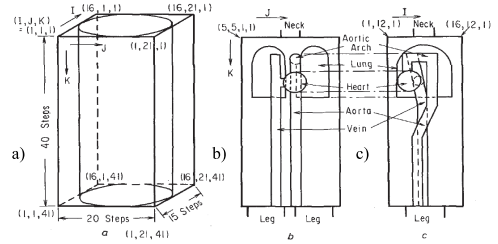


Figure 4. Simplified Sakamoto's thorax model:

a) model of human body, b) cross-section at $I=5,5$, c) cross-section at $J=12$ [7].

The impedance waveform is affected not only by the CO or the ΔBV in the aorta, but also by the ΔBV in the heart and lungs [7].

In Fig. 5, the solid lines depict the impedance signal waveform ΔZ , which is recorded through different pairs of point electrodes around the human thorax, and the dotted line represents the signal waveform recorded through the pair of band electrodes. This impedance signal waveform is affected through the ΔBV in both the heart and the aorta [7].

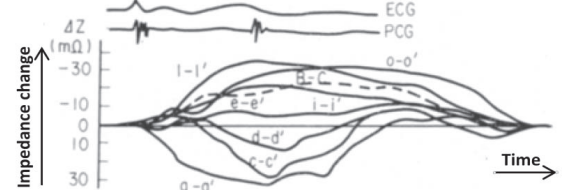


Figure 5. Impedance signal recorded by different pairs of point and band electrodes around the thorax [7].

E. 3-D Thorax Model

The 3-D thorax model is composed of lungs, muscle, heart and spinal column, as depicted in Fig. 6. The potential distribution can reflect different effects when inhaling (Fig. 6(a)) and exhaling (Fig. 6(b)); the lungs become smaller when exhaling and larger when inhaling. The potential distribution fluctuates with the change of resistivities caused by the activities in the thorax, for example, inspiration and expiration (cf. Fig. 7). Thus, the model is helpful to judge whether there are more or less physiological activities or pathologic variations in the studied subject [8].

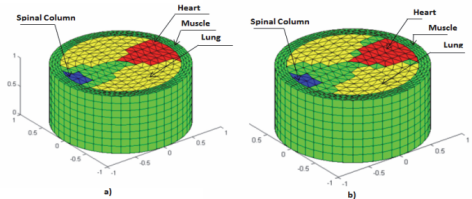


Figure 6. 3D thorax model at the end of phase: a) inhaling b) exhaling [8]

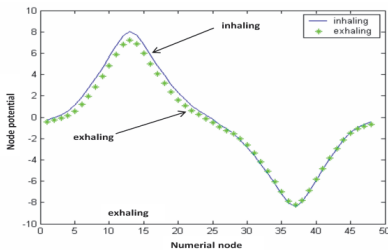


Figure 7. Changing of the node potentials during haling [8].

III. ORIGIN OF THE ICG SIGNAL

This section reviews the history of the ICG signal origin generation; understanding and waveform markers are discussed. In particular, it is found that although there exists a consensus within the scientist community, doubts and critical analyses about the origin of ICG signal have been expressed.

A. Analysis of Original ICG Signal Waveform

A typical impedance signal (ΔZ) and its first derivative (dZ/dt) can give detailed information about the physiological activities of thorax. Fig. 8 [9] depicts the different marks on the waveform which indicate the important points. The corresponding ECG is also depicted in Fig. 8. Research efforts have focused on discovering the physiological correlation with the ICG signal and its origin. It has been studied together with its first derivative [1, 36].

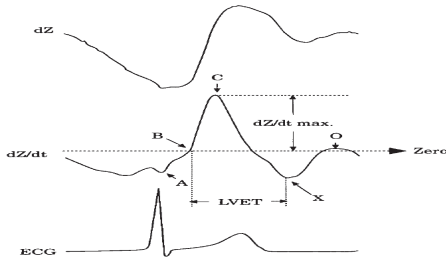


Figure 8. Characteristic impedance (ΔZ) signal, first derivative (dZ/dt) of impedance signal and ECG signal [1].

In 1970, Karnegis and Kubicek first indicated that the A-wave of the dZ/dt is associated with the P-wave of the ECG and that the C-wave of dZ/dt is associated with ventricular contractions [9]. During diastole, it was noticed another upward deflection of the O-wave in the dZ/dt signal. During the study, they found that the B point of dZ/dt corresponds to the aortic valve opening and the X point to the aortic valve closure. Several researchers make use of echocardiography and aortic pressure recordings and have confirmed these observations.

Furthermore, studies are required to confirm the exact physiological and anatomical origin of the impedance cardiography signal. Several investigators have dealt with this topic in the past, including a modelling and study performed on animals [1].

Witso & Kottke conducted these experiments in 1967 with dogs, using venous occlusion achieved by inflated ball [10].

Baker et al. reported experimental results in 1974. During their experiment, the ventricles were operated either at the same time or individually. From the experiment, it is concluded that the contribution of the left ventricle (LV) to the impedance signal waveform was 62% of the total impedance signal; on the other hand, the contribution from the right ventricle (RV) was 38% [11].

Kubicek et al. concluded in 1974 that the systolic portion of the dZ/dt impedance signal waveform was mainly contributed to by left ventricle ejection (LVE) into the aorta [12]. However, Thompson and Joeke reported in 1981 that both sides of the heart, left and right, make a main contribution to the systolic dZ/dt impedance signal waveform [13]. Wang et al. in 1991 presented that the impedance signal waveform was perhaps related to the right heart instead of left heart [14].

In 1979 Sakamoto proposed that the contribution of the BV variation in the lungs was very small [7], although Patterson in 1985 suggested that the lungs were one of the two largest origin source of the impedance signal waveform [15].

In 1979, Sakamoto and Kania reported that another possible reason of the impedance variations is resistivity change of the subsequent blood caused by a preferred orientation of the red blood cell [16].

Sakamoto et al. in 1979 and Lemberets et al. in 1984 point out that the blood resistivity change in the main arteries and veins contributed approximately one half to the overall ΔZ signal [16], [17]. The movement of the thoracic organ may also be a contributor to the impedance change [7].

In 1981, Mohapatra conducted a critical analysis on several of the hypotheses regarding the origin of the cardiac impedance signal waveform. In this study, he concluded that the signal is due to cardiac hemodynamics only. Moreover, the impedance signal reflects both changes in the blood velocity as well as changes in blood volume (ΔBV). The changing speed of forcing out affects the systolic behaviour of ΔZ , while changing volume (mostly of the atria and great veins) affects the diastolic portion of the impedance signal waveform curve [18].

In 1986, Penney concludes several studies which are based on the observations of contributions to the impedance signal waveform; his findings are reported in Table I [19].

TABLE I. ORIGIN OF THE IMPEDANCE SIGNAL IN ICG [19]

| Tissue/Organ | Contribution in % |
|--------------------------------|-------------------|
| Aorta and thoracic musculature | +60% |
| Pulmonary artery & lungs | +60% |
| Vena cava and right atrium | +20% |
| Pulmonary vein and left atrium | +20% |
| Left ventricle | -30% |
| Right ventricle | -30% |

In 1988, Mohapatra reported in his critical analysis that the evidence that the impedance plethysmography is at the origin of the impedance signal is very weak; but this is not exactly known until now [20]. In 1995, Wang and Patterson reported that the exact origin(s) or a region in the thorax that causes the impedance change during cardiac cycle, are unknown. It is suggested that contributions from many regions or origins invest to the formation of the impedance change [21].

Later, Kauppinen et al., as well as Patterson, reported controversial research findings. In 1998, Kauppinen et al. reported results that state that it is likely that more than 55% of the time-varying signal originates from the skeletal muscle even though that amount of measurement sensitivity originates in it. The contribution from the ventricle, aortas, carotid artery and jugular vein in 4 cases was 3.06%, 2.36%, 3.66% and 3.39%, respectively [3]. The obtained results also confirm the reported measurement problem when using sternal electrode for impedance cardiography [22].

In 2010, Patterson reported new controversial results: the aorta is a very weak contributor to the source of the impedance signal. The aorta contributes approximate only 1% to the total impedance measurement [23]. These reported results are closely agreeing with that of Kauppinen et al. [3]. The comparisons of contribution of tissues/organs are shown in Table II.

TABLE II. IMPEDANCE CONTRIBUTION FROM EACH TISSUE [3], [23].

| Tissue/Organ | Kauppinen et al 1998 | Patterson 2010 |
|-------------------|----------------------|----------------|
| Skeletal muscle | 67.00% | 52.90% |
| Left lung | 4.64% | 3.17% |
| Right lung | 4.15% | 3.48% |
| Liver | 1.59% | 3.62% |
| Aortic arch/Aorta | 0.26% | 0.89% |
| Others | 22.36% | 35.94% |
| Total | 100.00% | 100.00% |

Both studies reported the large contribution of the skeletal muscle to total impedance signal and a small contribution by the aorta in impedance waveform.

B. Waveform Markers

Waveform markers are the physiological indicators of different activities (see Fig. 8) [1]. The B waveform marker is the standard B points for the ICG waveform [36].

1) The A-wave marker

A wave associates with the contraction of atria, as found by Karnegis et al. [9] and others who found undoubted evidence. The hypothesis rose that the source of the A-wave marker is due to the back flow of blood from the atria into central veins. The A-wave marker is depicted in Fig. 8.

In 1979, Takada et al. found evidence that the left atrium might be the major contributor to this wave [24]. However, the exact contributions of the right and left atria are not known [1].

2) The C-wave marker

Several studies have taken place to unravel the origin of the systolic C-wave in the impedance cardiogram, since the

absolute height (dZ/dt_{max}), depicted in Fig. 8, is used to calculate stroke volume (SV). These studies took place on animals and models by several researchers using different approaches, such as described in [17, 25, 26, 27, 28, 29, 30, 31 and 32].

In order to unravel a more elaborate explanation of the origin of the C-wave marker, researchers have attempted to imitate impedance cardiographic variations in a model. Still, these are far from reliable evidence, and most fail to give details of the relationship between dZ/dt_{max} and other physiological variables as aortic peak flow velocity. More study is required on the contributors to dZ/dt_{max} as predicted by a model [1].

3) The O-wave marker

The O-wave marker corresponds to the diastolic upward deflection of the dZ/dt signal, which is depicted in Fig. 8. In 1970, Lababidi Ehmke and Rurnin published their findings and many researchers prove its origin, which is described in [33].

IV. DEVELOPMENT OF THE TARGETED ICG MODEL

Based on the literature survey and analysis of the existing thorax impedance models and origin of the ICG signal, it can be concluded that none of these models are accurate enough to imitate the real phenomena in the ICG signal. A summary and the limitations of each model are discussed in Table III.

TABLE III. SUMMARY AND LIMITATION OF EXISTING MODELS

| Model | Summary and limitations |
|----------------------------|---|
| Simplified Model of Thorax | This thorax model is highly simplified since the division into only two uniform tissues is used and geometrically it is not realistic. On the contrary, the real structure of the human thorax is very complicated. |
| Ideal Cylindrical Model | This model is also very simple because a simple cylinder is used to represent the thorax structure. In particular, the cross sectional point of view is not taken into account. |
| Kinnen's Thorax Model | Kinnen's model is simple; it indicates only two conductivity zones (blood volume of heart & primary arteriovenous system, and lungs). Most of the current flow would pass by the lungs. In this case, the generation of the impedance signal waveforms is primarily based on right ventricular (RV), which is not true if we consider the real thorax physiology. |
| Sakamoto's Thorax Model | This is not an accurate enough thorax impedance model because the blood pumps more toward the left leg side. |
| 3-D Thorax Model | The model is not accurate enough because it uses a cylinder as the structure of the thorax. Furthermore, it does not take the variation of heart size during inhaling and exhaling into account. |

Given these limitations, it is thus decided to use a sixteen electrodes' configuration belt to measure the ICG signal instead of the above models. Such a type of electrodes' setup is presumed to allow raising strong enough variations of the EBI in order to record the cardiac and respiration signals, which are caused by the heart and lungs. Further details about the EBI measurement setup can be found in [34].

The curve fitting method is used to develop an ICG signal model. With this approach, the ICG signal model would be more realistic and the underlying model parameters could be easily tuneable.

The EBI measurement procedure and the models and evaluation methods are discussed below.

A. EBI Measurement Procedure

The impedance measurement system consists of sixteen active electrodes; each of them can be used for measurement as well as excitation. The electrodes are connected to the impedance analyzer using a switch-box that can cross-switch any of the 16 electrode-inputs to any of the four analyzer-outputs, which is depicted in Fig. 9.



Figure 9. Switchbox with four capacitive and four active electrodes are attached

The datasets were obtained using multiple pairs of electrodes with four different positioning of the electrodes. The electrode setup is used for EBI measurement, which is shown in Fig. 10.

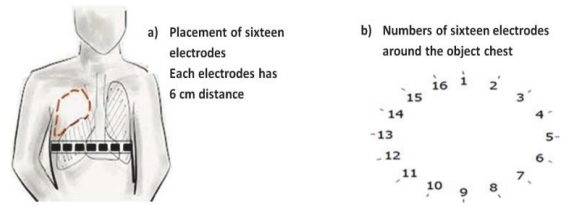


Figure 10. Sixteen electrodes configured belt, which is used for the EBI measurement procedure [34].

The measured datasets are obtained from a healthy male subject aged between 40 and 50 years, in a seated position.

The total EBI dataset was divided into three different segments. Each segment contains 10 seconds of the total EBI raw data, about 10,000 samples. Accordingly, the structure of the three segments is as follows:

- cardiac only (breathing was held),
- cardiac + respiration (deep breathing),
- cardiac + respiration + motion artefacts (normal breathing with added motion artefacts).

In what follows, the four ICG datasets correspond to b) and the clean ICG and IRG datasets correspond to filtered versions of a) and b), respectively.

In Fig. 11 (Datasets 1-6), each dataset has been measured from different positioning of electrodes.

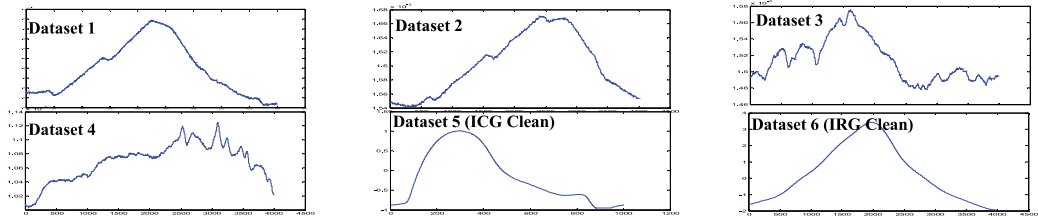


Figure 11. Measured EBI datasets with different configuration of electrodes.

B. Models and Evaluation Methods

Different curve fitting methods such as polynomial with different orders, Fourier series and sum of sine with different terms have been evaluated. The best-fit model performance has been selected based on the Sum Square Error (SSE), correlation (R-square) and execution time. Further details can be found in [35].

1) Polynomial Model

Polynomials are well suited for cases where a fairly simple empirical model is needed; the general polynomial model formula is given in Equation 4:

$$y = \sum_{i=1}^{n+1} p_i t^{n+1-i} \quad (4)$$

where n is the degree of the polynomial (highest power of the predictor variable), $n+1$ is the order of the polynomial (number of coefficients), p_i are the coefficients and t is time.

2) Fourier Series Model

The Fourier series is a sum of sine and cosine functions that describes a periodic signal. The model formula is given in Eq. 5:

$$y = a_0 + \sum_{i=1}^n a_i \cos(i\omega t) + b_i \sin(i\omega t) \quad (5)$$

where a_0 is the intercept, which is constant term in the data, ω is the fundamental frequency and n is the number of terms in the series.

3) Sum of Sine Waves Model

This model consists of a sum of sine terms only. The model formula is given in Equation 6:

$$y = \sum_{i=1}^n a_i \sin(i\omega t + c_i) \quad (6)$$

where a is the amplitude, ω is the frequency, c the phase, which is constant for each term and n is the total terms in series.

V. DISCUSSION, CONCLUSION AND FUTURE WORK

It is concluded that the simplified, Ideal Cylindrical, and Kinnen's models are too simple models that only take a few basic parameters into account. Sakamoto's and the 3-D model are more advanced and closer to reality, but still not accurate enough to imitate the complicated structure of the human thorax and different electrical properties of tissues such as anisotropy and inhomogeneity. Thus, we consider that none of these models is complete enough for developing the targeted ICG signal model.

Based on the reviewed existing thorax models and controversial statements regarding the origin of the impedance signal, we have started to evaluate how measured electrical bioimpedance (EBI) data can be used to develop an ICG signal model which closely imitates the real phenomena.

For this, we have built upon our previous study in which the EBI data was measured through a sixteen electrodes configuration belt from a normal human thorax [34]. The various curve-fitting methods have been used to process the collected data and in turn derive a mathematical model of the ICG signal. A practical application of this work can be found in [35] where a Bio-Impedance Signal Simulator (BISS) is described and implemented.

In future work, we will further investigate the modelling of the relation between cardiac and respiratory signals depending on human activity and health condition.

ACKNOWLEDGMENT

The authors thank Prof. T. Rang, Dr. T. Parve, Dr. Y. Le Moullec, Dr. A. Krivoshei and M. Rist for providing valuable advice. The authors are associated with, and all work has been done at, Th. J. Seebeck Dept. of Electronics, Tallinn University of Tech. and competence center ELIKO, Estonia.

This research was supported by the European Union through the European Regional Development Funding in the frames of the research center CEBE and the competence center ELIKO, the Estonian Ministry of Education and Research (IUT19-11), Foundation Archimedes ESF DoRa program and Estonian Science Foundation (9394).

REFERENCES

- [1] H. Woltjer, H. Bogaard, and P. Vries, "The technique of impedance cardiography," *European Heart Journal*, vol. 18, pp.1396-1403, 1997.
- [2] J. Malmivuo and R. Plonsey, *Bioelectromagnetism - Principles & Appl. of Bioelectric and Biomagnetic Fields*, NY, Oxford Univ. Press, 1995.
- [3] P. Kauppinen, J. Hyttinen and J. Malmivuo, "Sensitivity Distribution of Impedance Cardiography Using Band and Spot Electrodes Analyzed by a Three-Dimensional Computer Model", *Annals of Biomedical Engineering* Vol. 26, 694-702, 1998.
- [4] A. Sherwood, M.T. Allen, J.R.M.K. Fahrenberg, W. Lovallo, & L. Doornen, "Methodological Guidelines for Impedance Cardiography", *Psychophysiology*, Vol. 27, No. 1, 1-23, 1990
- [5] Y.M. Mughal, A. Krivoshei & P. Annus, "Separation of cardiac and respiratory components from the electrical bio-impedance signal using PCA and fast ICA", *Int. Conf. on Control, Eng & Info Tech IPCO*, 2013
- [6] S. Grimnes, & Ø. G. Martinsen. "Bioimpedance and Bioelectricity Basics", Elsevier. Academic Press 2015
- [7] K. Sakamoto, K. Muto, H. Kanai and M. Lizuka, "Problems of impedance cardiography", *Med & Biol. Eng. & Comp.*, 17,697-709, 1979
- [8] W. Huanli, X. Guizhi, Y. Hongli et al., "Three Dimensional Electrical Impedance Tomography in Thorax Complete Model", 30th Annual IEEE EMBS Conference. British Columbia: pp 466-469, 2008
- [9] J. Kamegis, and W. Kubicek, "Physiological correlates of the cardiac thoracic impedance waveform", *Am Heart J*, vol 79, pp 519-23, 1970
- [10] D. Wittoe, and F. Kottke, "The origin of cardiogenic changes in thoracic electrical impedance (del Z)", *Feder. Proc*; 26, 1967.
- [11] K. Baker, D. Hill, and T. Pale, "Comparison of several pulse-pressure tech. for monitoring stroke volume", *Med. Biol. Eng.*; 12, 81-8, 1974.
- [12] W. Kubicek, F. Kottke, M. Ramos, et al., "The Minnesota impedance cardiograph-Theory & appl.", *Biomed. Eng*, Vol 9, 410-416, 1974.
- [13] F. Thompson & A. Joekes, "Thoracic impedance cardiodynamic assessment: Validation in clinical use", London: St. Peter's Hospital, Geigy Pharmaceuticals, 1981.
- [14] L. Wang, R. Patterson and B. Raza, "Respiratory effects on cardiac related impedance indices measured under voluntary cardio-respiratory synchronization", *Med. Biol. Eng & Comput*, vol 29, 505-510, 1991.
- [15] R. Patterson, "Source of the thoracic cardiogenic electrical impedance signal as determined by a model", *Med & Biol. Eng & Comput*, Vol 23, 411-417, 1985.
- [16] K. Sakamoto and H. Kania, "Electrical characteristics of flowing blood", *IEEE Trans. Biomed. Eng*, Vol. 26, 686-695, 1979.
- [17] R. Lamberts, K. Visser, and W. Zijlstra, "Impedance cardiography", Assen, The Netherlands; Van Gorcum, 1984.
- [18] S. Mohapatra, "Noninvasive Cardiovascular Monitoring of Electrical Impedance Technique", London: Pitman, 1981.
- [19] B. Penny, "Theory and cardiac applications of electrical impedance measurements", *CRC Crit. Rev. Bioeng.*; 13, 227-81, 1986.
- [20] S. Mohapatra, "Impedance cardiography. In *Encyclopedia of Med. Devices and Instrument*", NY, pp. 1622-32, John Wiley & Sonss, 1988.
- [21] L. Wang, & R. Patterson, "Multiple Source of the Impedance Cardiogram Based on 3-D Finite Difference Human Thorax Models", *IEEE Trans. on Biomedical Engineering*, Vol. 42, No. 2, 141-148, 1995.
- [22] R. Patterson, L. Wang, McWeigh, et al. "Impedance cardiography: The failure of sternal electrodes to predict changes in stroke volume", *Biol. Psychol.* Vol. 36, pp. 33-41, 1993.
- [23] R. Patterson, "Impedance cardiography: What is the source of the signal?", *Int. Conf. on Electrical Bioimpedance* pp. 1-4, IOP Pub, 2010.
- [24] K. Takada, T. Fujinami, K. Senda, & et al., "Clinical study of 'A waves' (atrial waves) in imp. Cardiograms", *Am Heart J*, 94, 710-7, 1979.
- [25] F. Bonjer, J. Berg, MNJ, D. "The origin of the variations of body impedance occurring the cardiac cycle", *Circulation*, 415-20, 1952.
- [26] L. Geddes & L. Baker, "Thoracic impedance changes following saline injection into right & left ventricles", *J Appl Physiol*, 33, 278-81, 1972.
- [27] H. Ito, K. Yamakoshi and A. Yamada, "Physiological and fluid dynamic investigation of the transthoracic impedance plethymograph for measuring cardiac output", *Med. Eng Comp*; 14, 373-8, 1976.
- [28] Y. Saito, T. Goto, and H. Terasaki, "The effects of pulmonary circulation pulsatility on the impedance cardiogram", *Arch Internat Physiol Biol*; 91, 339-44, 1983.
- [29] W. Kubicek, "On the source of peak first time derivative (dZ/dt) during impedance cardiography", *Ann of Biomed Eng*, 459-62, 1989.
- [30] F. Spinal, A. Smith, and F. Crawford, "Relationship of bioimpedance to thermomodulation and echocardiographic measurements of cardiac functions", *Crit Care Med*; 18, 414-8, 1990.
- [31] N. Ohashi, Noninvasive estimation of aortic flow by bioelectrical impedance method and its clinical use for assessment of aortic atherosclerosis. *Nagoya Med J*; 31, 193-207, 1986.
- [32] P. Kezakevich, S. Teague and D. Nissman, "Comparative measures of systolic ejection during treadmill exercise by impedance cardiography and Doppler echocardiography", *Bio Psychol*; 36, 51-61, 1993.
- [33] Z. Lababidi, D. Ehmke, and R. Rurmin, "The first derivative thoracic impedance cardiogram", *Circulatio*; 41, 651-8, 1970.
- [34] Y.M. Mughal, "Decomposing of Cardiac and Respiratory Signals from Electrical Bio-impedance Data Using Filtering Method", *The Int. Conf. on Health Info. Springer*, vol 42, pp 252-255. IFMBE Proc 2013
- [35] Y.M. Mughal, Y. Le Moullec, P. Annus and M. Min, "Development of a Bio-Impedance Signal Simulator on the basis of the Regression based Model of the Cardiac and Respiratory Impedance Signals", *The 16th Nordic Baltic Conference on Biomedical Engineering and Medical Physics (NBC16)*, Springer, vol. 48, pages 92-95, IFMBE proc, Gothenburg, Sweden, October 14-16, 2014.
- [36] Da Xu, Kathy L. Ryan, Caroline A. Rickards et al. "Improved pulse transit time estimation by system identification analysis of proximal and distal arterial waveforms" *American Journal of Physiology - Heart and Circulatory Physiology* Published, Vol. 301 no. 4, October 1, 2011

Paper III

Yar M. Mughal

“Decomposing of cardiac and respiratory signals from electrical bio-impedance data using filtering method”,

in *IFMBE Proceedings*, Volume 42,

International Conference on Health Informatics (ICHI’13),

November 07 – 09, 2013, Vilamoura, Portugal, pages 252 – 255.



Decomposing of Cardiac and Respiratory Signals from Electrical Bio-impedance Data Using Filtering Method

Y.M. Mughal

Thomas Johann Seebeck, Department of Electronics, Tallinn University of Technology, Tallinn, Estonia

Abstract— This paper presents an attempt to decompose cardiac and respiratory signals from an electrical bio-impedance (EBI) dataset. To accomplish this task, the conventional filtering method is used. FIR (low pass filter (LPF) and high pass filter (HPF)) was intended to decompose the impedance respirogram (IRG) and impedance cardiogram (ICG), (the clean ECG was also extracted by filtering method). The decomposed components can be analysed and processed further, each one separately. Investigation was accomplished under the assumption that the total EBI dataset is the summation of cardiac and respiratory components, motion artefacts, stochastic disturbance and noise. The impedances were measured using a Zurich Instruments HF2IS Impedance Spectroscope. A sixteen electrodes configuration belt was used around a human thorax, to measure the EBI. This study showed that it is not possible to decompose cardiac and respiratory signals completely through conventional filtering method.

Keywords— Cardiac Signal, Electrical Bio-impedance; FIR Filter; Respiratory Signal.

I. INTRODUCTION

This study is focused on the decomposition of cardiac and respiratory components from a mixed electrical bio-impedance (EBI) raw dataset, by suppressing disturbing components such as motion artefacts, stochastic disturbance and noise by filtering.

By means of EBI measurements one can assess physiological activities and structural configurations of a tissue, as well as offer possibility to analyze dynamic processes in organs such as a) impedance cardiogram (ICG) of the heart, and b) impedance respirogram (IRG) from the thorax. The EBI measurement is a non-invasive and cost effective method.

The assumption is that, the total EBI data is the sum of:

$$S(t) = S_{car(t)} + S_{resp(t)} + N_{mot(t)} + M_{stoch} + S_{bas(t)} \quad (1)$$

where $S_{car(t)}$ and $S_{resp(t)}$ are the cardiac and respiratory components, $N_{mot(t)}$ unwanted motion artifact caused by body movement or muscle activity, M_{stoch} stochastic disturbance and $S_{bas(t)}$ basal (average) signals.

The cardiac and respiration components are correlated due to their nature [1]. However, they can be viewed as uncorrelated under the assumption that the correlation is relatively weak because both components have different sources [2]. The filtering method was tested as a mean for accomplishing a) ICG and IRG from the total EBI dataset and b) simultaneously suppressing the artefacts.

II. ELECTRICAL BIO-IMPEDANCE (EBI)

The study of the EBI is very important in the medicine to develop robust, efficient and practical measurement apparatus, which can be based on the electrical bio-impedance [1, 3]. The signal processing area has acquired promising achievements which help to estimate components of the EBI and to further analyze and process them. Impedance devices with digital signal processing capability can be used to estimate and analyze the EBI components efficiently, precisely, reliably and online with the measurements.

The measurement of EBI is a scientifically relevant topic nowadays. The prefix bio in the electrical bio-impedance is due to the biological essence of an object [3]. In addition to galvanic path, the EBI measures dielectric polarization on a tissue, which arises from intrinsic polarizability, which is the manner that the biological tissue resists to an electrical current.

In a typical impedance measurement setup, a known current is supplied on the tissue under test. The EBI measures the dielectric response of the tissue under examination [3].

The EBI measurement is used to get an input dataset to which the filtering method was applied in this study.

The EBI is measured by applying electrical current across the thorax region and measuring the voltage drop (Figure 1).

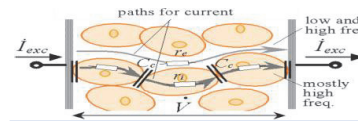


Fig. 1 Schematic of the high and low frequency current distribution in a cell tissue [5].

At a selected frequency, the EBI can be expressed as the ratio of the voltage drop to the excitation current, which has caused the voltage drop [4]:

$$\dot{Z} = \frac{V}{I} \quad (2)$$

where V is the voltage drop which measures the resistance, and I is the electrical current, which is used to excite the tissue.

It has become clear that the EBI on living tissue is frequency dependent because of the capacitive effect of tissue. In addition, each tissue region and even each cell has different dielectric response as well as spectral characteristics in the frequency domain.

The cardiac and respiratory components from the human thorax can be measured as the time variation of the EBI. From the total EBI, the useful components, like cardiac and respiratory ones, can be extracted for further analysis and separate processing [4].

III. EBI MEASUREMENT PROCEDURE

The dataset of the total EBI is measured using multiple pairs of electrodes. The excitation current was applied to the body through one pair of electrodes. The voltage drop was measured through the other pairs of electrodes.

The EBI measurement setup is depicted in Figure 2. Such kind of electrodes' setup is assumed, allow to produce strong enough variations of the EBI in order to measure the cardiac and respiration activities, which are caused by heart and lungs.

A. Configuration of Electrodes

The sixteen electrodes configuration was used in the experiment, which was performed in the Thomas Johan Seebeck Department of Electronics, at Tallinn University of Technology. The electrodes were positioned at 6 cm distance from each other. This belt was worn around a person's thorax. Figure 2 illustrates the configuration of electrodes.

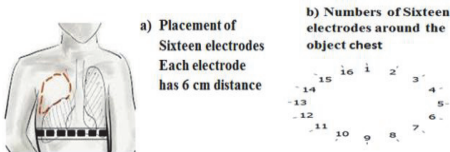


Fig. 2 Sixteen electrodes configured belt, which is used at the EBI measurement procedure.

The impedances were measured using a Zurich Instruments HF2IS Impedance Spectroscopy.

Current source excitations, of 8 slightly different frequencies, were used in every electrode pairs in order to minimize mutual influence of simultaneous impedance measurements between the channels.

The measurement current was confined under 1mA at all times for ensuring patient's safety. Electrical contact to the thorax was achieved by 3M disposable surface EMG/ECG silver/silver chloride electrodes, followed by proprietary front-end electronics close to the electrodes.

B. Pre-processing of Data Gathering Experiment

A person was instructed at the beginning of the experiment to hold his breathing around 10s (from 1s to 10s),

after the 10th second he starts to take deep breathing around 10s (from 10s to 20s) and finally, while taking the breathing, added motion artefacts around 10s (from 20s to 30s).

According to this, the total EBI dataset was divided into three different segments. Each segment contained 10 sec of the total EBI raw data, about 10,000 samples. Accordingly the structure of each segment is as follows:

- only cardiac,
- cardiac + respiration,
- cardiac + respiration + motion artefacts.

IV. FINITE IMPULSE RESPONSE (FIR) FILTERS

The FIR filters are assure to be stable BIBO and generally used in applications that require the filter to have linear phase frequency response to the desired signal passed [6]. Types of FIR filters are the LPF, HPF and BPF. These filters are used in this study to filter out the IRG and ICG signals.

The LPF is a filter that allows the harmonic components of low frequencies up to cut-off (f_c) to pass and attenuates all components of higher frequencies [7]. The LPF is used to filter out the IRG component which has low frequency, and to attenuate all higher frequencies, because respiration can take place only at low frequency range often below 1 Hz.

The HPF is a filter that allows the harmonic components of high frequencies above the f_c and attenuates all components of lower frequencies [7]. The HPF is used to filter out the ICG. f_c frequency is selected to attenuate all lower frequencies because those are out of interest.

V. FILTERING METHOD

The decomposition of cardiac and respiratory components was accomplished from Segment (b) of the total EBI dataset. We assume that the total EBI dataset is the summation, as shown in Equation 1.

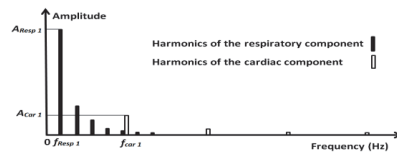


Fig. 3 An example of frequency spectrum of EBI, which contains cardiac and respiratory components. [4].

The heart rate S_{car} (Eq.1) of a healthy person can vary in the range between 60 bpm to 240 bpm (1 to 4 Hz) [8], and the respiration rate S_{resp} (Eq.1) of a healthy person can vary from 12 breaths/min to 30 breaths/min (0.2 to 0.5 Hz). Unfortunately, muscular activities also lie on almost on the same frequency

range, and the higher harmonics of the respiratory signal also lie on the same frequency range with the cardiac signal [8 - 9]. The harmonic spectrum of EBI signal is shown in Figure 3.

The waveform of the cardiac and respiratory components of the EBI signal are relatively smooth [10] and that is why only few higher harmonics are required for representing them.

In this study, LPF and HPF were used to extract the impedance respirogram (IRG) and impedance cardiogram (ICG) from the total EBI dataset (Segment b). The electrical cardiograph (ECG) was also filtered separately as a reference signal for ICG.

In accordance with the characteristics of the signals, given above to separate the respiratory and cardiac signals, a structure of filtering device, given in the block diagram in Figure 4 was used.

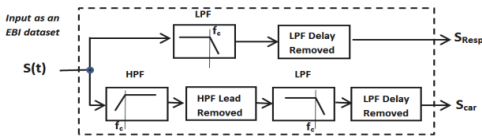


Fig. 4 Flow diagram of the filtering method

To filter out the ICG waveform, the HPF is used to attenuate the lower frequencies, mainly to suppress the respiration components, and the LPF is used to attenuate the higher frequencies, which are out of interest. The Equation (3) is used to determine the high pass and low pass FIR filters delay:

$$td = \frac{N-1}{2}, \quad (3)$$

where N is the number of filter coefficients and td is the time delay.

VI. RESULTS

The filtering method according to Figure 4 was used to decompose the cardiac and respiratory components from the total EBI, and simultaneously to suppress the stochastic disturbance, motion artefacts and noise.

A. Decomposition of the IRG

The IRG component contains harmonics with low frequencies of relatively high amplitudes (Figure 3). On the basis of spectrum analysis, the LPF was designed to filter out the IRG component. For IRG, the pass-band was set to 1.5 Hz and attenuation of higher frequencies was set to 80 dB. Figure 5 (dotted line, blue colour) and Figure 6 (a) show the decomposed IRG signal from the total EBI dataset. To some extent, cleaner IRG signal is extracted, and it is slightly smoother as well.

B. Decomposition of the ICG

The cardiac component contains low amplitude harmonics at relatively higher frequencies. The spectra of cardiac

and respiration signals often overlap with each other (Figure 3). Based on spectrum analysis, the LPF was designed and tuned to separate the ICG component. For the ICG, the pass-band was set to 20 Hz, stop-band was set 22 Hz and attenuation of all higher frequencies was set to 80 dB.

Figure 5 (solid line, red colour) and Figure 6 (b), shows the separate output ICG signal. The ICG signal is corrupted by the respiration: because respiration has high influence, we just can see the rippling. The LPF permits all low frequency components to pass. Accordingly the respiration components, which exist at low frequencies, will also pass (Figure 3).

In order to decompose just cardiac components, first a HPF was designed to attenuate the low frequencies of the respiration component. After attenuating the low frequencies, the LPF was designed to attenuate the higher frequencies; i.e only passed the range of interest. This is shown in the flow diagram of the filtering method in Figure 4.

The Figure 5 (solid line, black colour) and Figure 6 (c) shows the filtered ICG signal which is extracted from the total EBI dataset; but the extracted ICG signal is not clean enough. It contains some noise.

The first harmonic of the cardiac component is very close to some of the higher respiration harmonics (Figure 3). In order to suppress the respiratory component, the cut-off frequency of the HPF was taken closer to the first cardiac harmonic. It was 0.8 Hz.

C. Decomposition of the ECG

The electrical cardiogram (ECG) was recorded during the experiment, and added to the total EBI dataset. The ECG is included in this study as a reference signal for ICG.

Based on the spectrum analysis, the LPF was designed to clean the ECG component. For the ECG, the pass-band was set to 25 Hz and stop-band was set 30 Hz, and attenuation of all higher frequencies set to 80 dB.

Figure 5 (dotted line, green colour) and Figure 6 (d), show the cleaned ECG signal. To the some extent the ECG signal is clean.

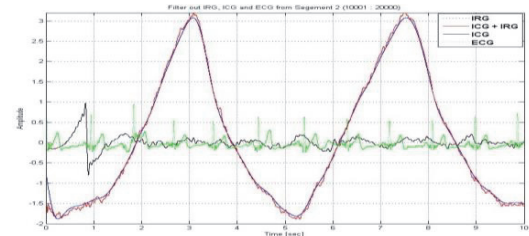


Fig. 5 Filter out the signals (IRG and ICG) from the total electrical bio-impedance (EBI) dataset on the same scale.

- a) Impedance Respirogram (IRG),
- b) Impedance Cardiogram (ICG) corrupted by respiration,
- c) Impedance Cardiogram (ICG),
- d) Electrical Cardiogram (ECG)

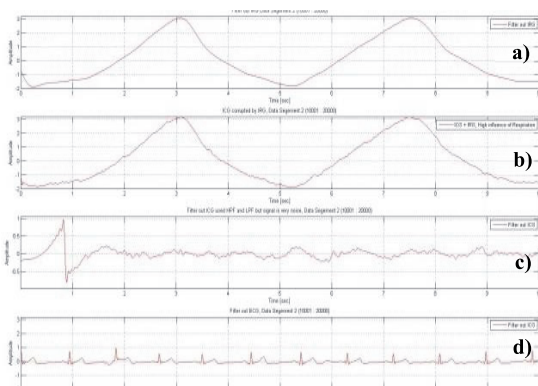


Fig. 6 Filter out the signals (IRG and ICG) from the total electrical bio-impedance (EBI) dataset.

- a) Impedance Respirogram (IRG),
b) Impedance Cardiogram (ICG) corrupted by respiration,
c) Impedance Cardiogram (ICG),
d) Electrical cardiogram (ECG)

VII. DISCUSSIONS, CONCLUSIONS AND FUTURE WORK

The first LPF, which was designed to separate out the IRG signal and attenuate the higher frequencies because respiration (IRG) exists at low frequencies, to some extent separated the IRG signal, which became smoother and cleaner. The results are shown in Figure 5 (dotted line, blue colour) and Figure 6 (a).

The second LPF was used to separate the ICG signal. In Figure 5 (solid line, red colour) and Figure 6 (b) are shown the separated ICG signal. The results seem to be corrupted by respiration because respiration has influence to the ICG through its higher harmonics.

In order to filter out the cardiac component, the HPF was designed and tuned to attenuate the low frequencies first those frequencies which are out of interest. We again applied a LPF to attenuate the higher frequencies; those which are also out of interest. Figure 5 (solid line, black colour) and Figure 6 (c) are shown the ICG signal, which is separated. The ICG is not clean enough, it contains some noise.

The ECG was extracted to use as a reference signal for the ICG. The LPF was designed to separate the clean ECG component. Figure 5 (dotted line, green colour) and Figure 6 (d) is shown the decomposed ECG signal. At the same extent the ECG signal is very clean.

It seems that it is difficult to solve the decomposition problem through conventional filtering method. The filtering method could be used as pre-processing for the total EBI. Further development of the method is required to approach

better decomposition of the cardiac and respiration signals from the total EBI dataset. For example, one could try to take the advantage of blind source separation (BSS) because BSS works on correlated and dependent sources. The cardiac (S_{car}) and respiratory (S_{resp}) components are correlated. Moreover, machine learning techniques could be used to approach the problem.

ACKNOWLEDGMENT

The author thanks Dr. P. Annus, Dr. A. Krivoshei, Prof. T. Rang, Dr. T. Parve, Prof. M. Min and Dr. A. T. Giannitsis for providing valuable advices.

This research was supported by ESF DoRa, the Estonian Ministry of Education and Research (the target oriented project SF0140061s12), the Estonian Science Foundation (the research grants G8592 and G8905), the Foundation Archimedes through the CEBE (TK05U01) and IT Academy.

REFERENCES

1. L. Sörnmo, and P. Laguna. (2005) Bioelectrical Signal Processing in Cardiac and Neurological Application. Elsevier Academic Press.
2. Yar M. Mughal, A. Krivoshei, P. Annus. (2013) Separation of cardiac and respiratory components from the electrical bio-impedance signal using PCA and fast ICA, Proc. International Conf. on Control, Engineering & Information Technology, vol. 1.
3. S. Grimnes and Ø. G. Martinsen. (2008) Bioimpedance & Bioelectricity Basics. London: Academic Press.
4. A. Krivoshei. (2009) Model Based Method for Adaptive Decomposition of the Thoracic Bio-Impedance Variations into Cardiac and Respiratory Components. PhD thesis, Tallinn: TUT Press.
5. M. Min., T. Parve, P. Annus, and T. Paavle. (2006) Method of Synchronous Sampling in Multifrequency Bioimpedance Measurements, Proc. of the 23rd IEEE Instrumentation and Measurement Technology Conference (IMTC/06), p. 1699-1703.
6. J. G Proakis, and V. K Ingle, Student Manual for Digital Signal processing with MATLAB. Pearson Prentice Hall, 2007
7. A. V. Oppenheim and A. S. Willsky. (1997) Signal and System, 2nd ed. Prentice-Hall, Inc, USA.
8. A. Krivoshei, M. Min, T. Parve and A. Ronk. (2006) An Adaptive Filtering System for Separation of Cardiac and Respiratory Components of Bioimpedance Signal, Proc. of the Medical Measurement and Application (MeMeA), p. 10 - 15.
9. A. Krivoshei. (2006) A Bio-Impedance Signal Synthesiser (BISS) for Testing of an Adaptive Filtering System, Proc. of the Baltic Electronics Conference (BEC), p. 1-4.
10. M. Min, O. Märtens, T. Parve, (2000) Lock-in measurement of bio-impedance variations, Measurement (Journal of IMEKO), Volume 27, Issue 1, p. 21-28.

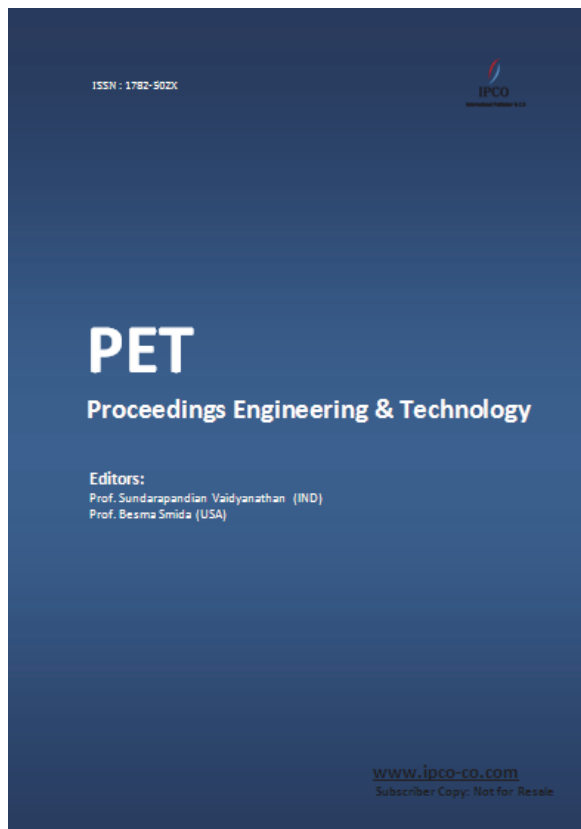
Author: Y.M. Mughal
Institute: Thomas Johann Seebeck, Department of Electronics, TUT
Street: Ehitajate tee 5
City: Tallinn
Country: Estonia
Email: yar@elin.ttu.ee

Paper IV

Yar M. Mughal, A. Krivoshei, P. Annus

“Separation of cardiac and respiratory components from the electrical bio-impedance signal using PCA and fast ICA”,

in PET (Proceedings Engineering & Technology), Volume 1, 2013,
The International Conference on Control, Engineering & Information
Technology (CEIT’13), June 04 – 07, 2013, Sousse, Tunisia.



Separation of cardiac and respiratory components from the electrical bio-impedance signal using PCA and fast ICA

Yar M. Mughal ^{#1}, A. Krivoshei ^{#1 *2}, P. Annus ^{#1 *2}

[#]Thomas Johann Seebeck, Department of Electronics, TUT
Ehitajate tee 5, 19086 Tallinn, Estonia

¹yar@elin.ttu.ee

²andreik@elin.ttu.ee

³paul.annus@elin.ttu.ee

^{*}E LIKO Competence Centre in Electronics, Info- and Communication Technologies
Mäealuse 2/1, 3rd floor, 12618 Tallinn, Estonia.

Abstract— This paper is an attempt to separate cardiac and respiratory signals from an electrical bio-impedance (EBI) dataset. For this two well-known algorithms, namely Principal Component Analysis (PCA) and Independent Component Analysis (ICA), were used to accomplish the task. The ability of the PCA and the ICA methods first reduces the dimension and attempt to separate the useful components of the EBI, the cardiac and respiratory ones accordingly. It was investigated with an assumption, that no motion artefacts are present. To carry out this procedure the two channel complex EBI measurements were provided using classical Kelvin type four electrode configurations for the each complex channel. Thus four real signals were used as inputs for the PCA and fast ICA. The results showed, that neither PCA nor ICA nor combination of them can not accurately separate the components at least are used only two complex (four real valued) input components.

Keywords— Principal Component Analysis, fast Independent Component Analysis, Electrical Bio-impedance, Cardiac Signal and Respiratory signal

I. INTRODUCTION

The Blind Source Separation (BSS) is forth-coming field of interest to separate useful components in the case of using the multi-source signals. The BSS is an approach which allows estimating original statistically independent sources from only observed mixture of these sources without any known *a priori* information.

The BSS can be found in many applications, such as biomedical, telecommunication, image and speech signal processing [1-4]. Many algorithms are used to implement the BSS. They are based on a statistical independence property of the separated signals [3, 4].

The Principal Component Analysis (PCA) algorithm is a useful technique to uncorrelate the components, but the Independent Component Analysis (ICA) algorithm as an implementation of the BSS; it is suitable to separate the original independent components [1-4].

The purpose for combining the both algorithms (PCA and ICA) is to decrease the dimension of the electrical bio-

impedance (EBI) data set before implementing the ICA algorithm, hence to make easier for the ICA to separate the cardiac and respiratory components.

In this study, it was tried to apply the Principal Component Analysis (PCA) and fast Independent Component Analysis (ICA) algorithms to the electrical bio-impedance (EBI) dataset, which consist of two simultaneously measured complex EBI signals containing both the respiratory and cardiac components, as well as certain amount of motion artefacts and disturbances from the surrounding environment.

The impedances were measured using Zurich Instruments HF2IS Impedance Spectroscope. The classical Kelvin type four electrode configurations were used.

Current source excitation at slightly different frequencies was used in both of them to minimize mutual influence of simultaneous impedance measurements between two channels.

The measurement current was kept under 1mA at all times for safety reasons. Connection to the chest was made using Kendall/Tyco ARBO disposable surface EMG/ECG silver/silver chloride electrodes, followed by proprietary front end electronics close to the electrodes.

Biologically modulated impedance signals were collected from two orthogonal directions. One set of electrodes was placed on belt surrounding the chest, and another on vertical line between heart tip and neck.

The later analysis was accomplished in MATLAB environment on PC. The purpose of this study is to use the PCA and fast ICA individually or in combination in order to observe their capability to separate the cardiac and respiratory components of the total EBI. It is known that the spectra of the both components are overlapping each other, and thus it is a challenging task to separate these components in frequency and time domain.

The rest of this paper is structured as follows. Section 2 and 3 presents the related work of PCA and ICA. Section 4 discusses the block diagram and steps of the trial method. Section 5 demonstrates the results which are obtained. Finally, Section 6 concludes with the summary of the main contributions of the paper and future work.

II. PRINCIPAL COMPONENT ANALYSIS (PCA)

PCA, which is sometimes also called the Karhunen-Loève transformation, is broadly used for the representation of high-dimensional data and is commonly used as a preprocessing step to a projection of high-dimensional data into a low-dimensional subspace [12]. As well the PCA is frequently used for data reduction in statistical pattern recognition and to visualize the comparisons between the biological samples, and for filtering out noise [6, 7].

The mixing matrix equation is:

$$Y=AS', \quad (1)$$

where Y is data modelled as the product of A (scores are the amount of artefact's variable for particular sample) and S' (loading) is define new coordinate, which has highest variation).

The principal component analysis projects the data into a new space and finds the principal components (PCs) like s_1, s_2, \dots, s_N , which are uncorrelated and orthogonal [7]. The PCs can effectively extract the related information form the data [7], so that they carry the maximum amount of variance likely by N linear transformed components [1, 6]. Each PC consists of one score and one loading and PCs are given by $s_i = w_i^A \cdot y$, where y and w_i are observation vector and i -th the PCA weight vector, and $(\cdot)^A$ represents the transposition [1, 6].

The computation for the w_i can be achieved by making the use of covariance matrix $E\{xx^A\} = R_x$, where $E\{\cdot\}$ is the expectation operator. w_i are the eigenvectors of R_x that relate to the N largest eigenvalues of R_x . The first PC s_1 points in the direction where the input has the highest variance, and second PC s_2 is orthogonal to the first PC and points a direction of highest variance when the first project has been subtracted, and so on [1, 6].

III. INDEPENDENT COMPONENT ANALYSIS (ICA)

The ICA algorithm is an implementation of the Blind Source Separation (BSS) approach and it is a valuable technique to find the independent components (ICs) of a multivariate random variable. These components are in the direction, which the element of the random variable has no dependency. The ICs are used to decrease effects of noise and artefacts of signals [7, 9]. Because of this, ICA becomes good application of the BSS.

In contrast to the correlation based transformation the PCA, the ICA also reduces higher-order statistical dependencies for non-Gaussian distributed signals [1]. In latest literature, it has been presented that the independent components (ICs) from the ICA were better in separating the different kinds of biological groups than principal components (PCs) from the PCA [7, 10, 11].

IV. METHOD

In this study the well-known algorithms used such as the PCA and fast ICA, were selected to investigate their ability to extract the information about the two components of the EBI dataset corresponding to the cardiac and respiratory activities of a human. The cardiac and respiratory signals are correlated

due to their nature [Ch. 8 in 13]. However they could be viewed as uncorrelated under assumption that the correlation is relatively weak to cause sufficient errors.

The complex EBI was measured on two channels. The obtained four real valued signals were used as input dataset for the selected methods.

The block diagram of trial method, which was used to investigate the separation of cardiac and respiratory components, is shown in the Figure 1.

The first part is the PCA algorithm, is intended to uncorrelate the EBI dataset, whilst the second part is the ICA algorithm, which tries to separate the cardiac and respiratory components the total EBI.

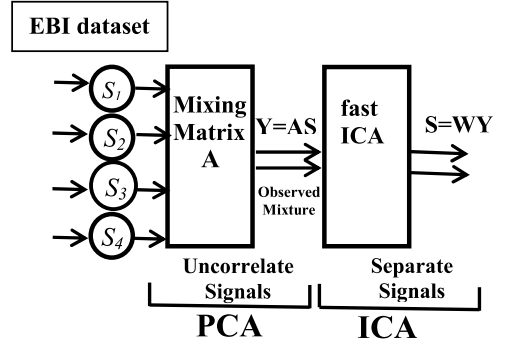


Figure 1. Block diagram of trial method, which consists the combination of PCA and ICA steps to solve the BSS problem.

It was observed that the PCA is capable to un-correlate and reduce the dimensionality of the EBI dataset but it is not efficient to separate the cardiac and respiratory signals accurately. However, ICA is more suitable for separation of independent components from a mixture of input signals [7, 10, 11]. The PCA and ICA algorithms complement each other since if only the PCA is used; no separation can be achieved, because the PCA only uncorrelates the data, it does not mean independence. However, if fast ICA is applied alone, it is too hard for fast ICA to solve problem.

The raw EBI signals were sampled at rate 1000 samples/s.

It was observed in this study that without preprocessing the raw data the ICA's convergence is slow.

The following steps were followed for solving the problem:

Step 1: The EBI dataset is loaded and divided into frames of 10,000 samples each.

Step 2: Frames of the EBI data are sampled down by factor 10.

Step 3: The second order low-pass Butterworth filter is applied to suppress the noise.

Step 4: The PCA is applied to un-correlate the filtered data.

Step 5: The fast ICA is applied to separate the cardiac and respiratory components.

Assume the EBI dataset is a centred $n * p$ matrix (the mean of each column has been subtracted), where n is the number of samples (or observations) and p is the number of variables or parameters that are measured.

$$Y = UDV^T, \quad (2)$$

where U is an $n * p$ matrix, columns of which are uncorrelated ($U^T U = I_p$), D is a $p * p$ diagonal matrix with diagonal elements d_j and the V is a $p * p$ orthogonal matrix ($V^T V = I_p$).

After un-correlating the EBI dataset by the PCA method, the uncorrelated data Y is passed as input to the fast ICA algorithm. The fast ICA algorithm maximizes the non-Gaussian form for each component and separates the independent data [5, 7].

Let Y ($n * p$) be the centred data and S ($n * p$) the matrix containing the independent components (ICs). It can solve the ICA problem by introducing a mixing matrix A of size $n * n$.

$$Y = AS. \quad (3)$$

The mixing matrix A shows how the ICs of S are linearly joined to make Y . If it reorder the equation above to get

$$S = WY, \quad (4)$$

where the un-mixing matrix W ($n * n$) describes the inverse process of mixing the ICs, if assuming A is a square and orthonormal matrix and then the W is basically the transpose of A . In practice, it is very beneficial to whiten the data matrix Y . In this study PCA is used as pre-processing step to

centring and whitening the data matrix for fast ICA algorithm [5, 7]. However, fast ICA uses the PCA as a preprocessing by default.

After adopting the method, the convergence of the entire algorithm became faster and results are enhanced as well with regard to results obtained by applying the fast ICA algorithm alone as it is visible from Figure 2 (a).

V. RESULTS

This study investigates the performance of both algorithms, the PCA and the fast ICA, to separate the EBI signals corresponding to cardiac and respiratory activities.

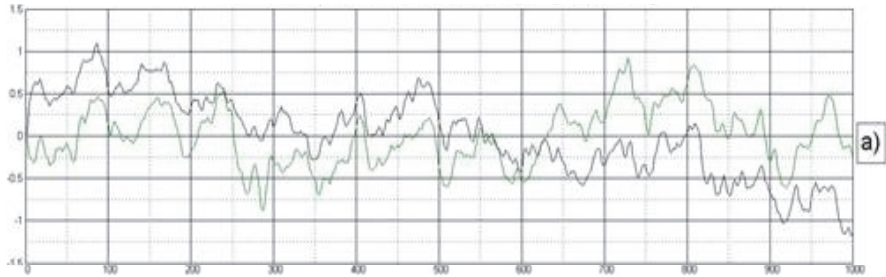
After some attempts and observations, it was understood that sequential use of both algorithms (PCA and ICA) are required in order to take advantage of BSS. The required steps are discussed in the method section IV.

In the Figure 2 the comparison of results achieved by applying both algorithms and described steps are depicted.

After following the steps described in method section, fast ICA performance was tested without the PCA. The results are depicted in the Figure 2 (a). However, fast ICA uses the PCA by default.

The results are depicted in the Figure 2 (b) for the case PCA separately was used as the preprocessing step for the fast ICA.

Result of the fast ICA without using PCA as pre-processing



Result of the fast ICA with using PCA as pre-processing

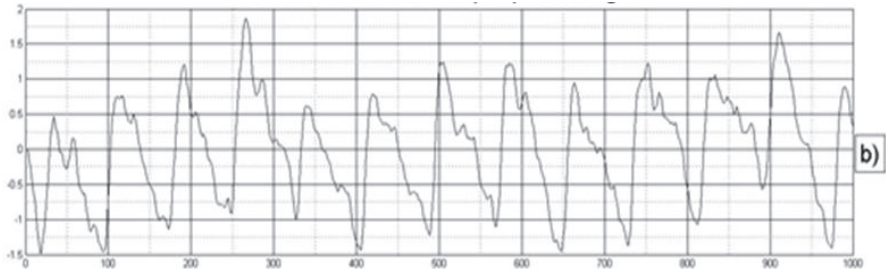


Figure 2. Results of investigation of the fast ICA applied on a frame of the EBI dataset:

- (a) without using the PCA for pre-processing,
- (b) with using the PCA for pre-processing.

Figure 2 (a) depicts the performance of fast ICA after applying only centring procedure to the EBI dataset. It is difficult to predict anything based on shown signals in Figure 2 (a) because signals are not clear. The results were discussed with cardiologist. The cardiologist said that based on figure 2 (a), it is difficult to perceive anything. However, based on figure 2 (b), could be some useful information.

On the other hand, it is observed that fast ICA alone is not efficient. The results are not so promising, which are depicted in Figure 2 (a).

In the second trial the PCA has been used as preprocessing step in order to reduce the dimension of the EBI dataset before applying the fast ICA algorithm. The more promising results were obtained, but not accurate enough to solve the task. The cardiac component still contains the respiratory one, but with lower amplitude.

However, the respiratory signal was not separated by both methods.

VI. CONCLUSIONS AND FUTURE WORK

The complex EBI measured using two orthogonal placed electrode pairs. Thus four real valued signals were used as inputs for the PCA and ICA.

It was understood that the sequential use of both algorithms and proper steps of preprocessing is required to outcome the fast execution of algorithms; the steps are discussed in the method section. Firstly, it is required to reduce the demission of the EBI dataset, and then to separate the cardiac and respiratory signals.

The investigation showed that neither the PCA nor ICA nor combination of them can not accurately and robustly separate the components, at least when using only two complex valued (four real valued) input components. But the combination of the PCA and ICA algorithms showed more promising results, than the ICA alone, however the estimate of the cardiac component still contains the respiratory one.

The PCA uncorrelate and reduce the dimension of data. It does not mean the separation of components. The ICA works on the assumption of independence among source signals; if the source signals do not satisfy the condition then ICA would not be able to separate the components. In this case more investigation is required to understand the nature of cardiac and respiratory components.

It was the first attempt to use the PCA and fast ICA in order to separate cardiac and respiratory components from the electrical bio-impedance (EBI) dataset, measured using two orthogonal placed electrode pairs simultaneously.

Development of the method is required to approach better separation of cardiac and respiratory components from the EBI in order to take advantage of the BSS, machine learning techniques and understand the nature of cardiac and respiratory components.

ACKNOWLEDGMENT

The authors express thanks to Prof. T. Rang, Dr. T. Parve, Prof. M. Min, Dr. R. Land, and Dr. R. Gordon for providing valuable advices and practical information and others for the fast ICA package which is used in this study.

This research was supported by European Social Fund's Doctoral Studies, Internationalization Program DoRa, the Estonian Ministry of Education and Research (the target oriented project SF0140061s12), the Estonian Science Foundation (the research grants G8592 and G8905) and the Foundation Archimedes through the Center of Excellence CEBE (TK05U01).

REFERENCES

- [1] M. Berg, E. Bondeesson, S. Y. Low; S. Nordholm, I. Claesson, "A Combined On-Line PCA-ICA Algorithm for Blind Source Separation". In Proc Communications Asia-Pacific Conf., Oct. 2005.
- [2] P. Comon, "Independent component analysis: A new concept?" *Signal Processing*, vol. 36, no. 3, pp. 287–314, 1994.
- [3] J. F. Cardoso, "Blind signal separation: Statistical principles". *Proc. of the IEEE*, vol. 86, no. 10, pp. 2009–2025, October 1998.
- [4] S. Y. Low, S. Nordholm, and R. Togneri, "Con-volutive blind signal separation with post processing". *IEEE Trans. on Speech and Audio Process.*, vol. 12, no. 5, pp. 539–548, Sept. 2004.
- [5] A. Hyvärinen, E. Oja, "Independent Component Analysis: Algorithms and Applications". *Neural Networks*, vol. 13' no. 4-5, pp. 411-430, 2000.
- [6] S. Haykin, *Neural Networks: A Comprehensive Foundation*. 2nd ed. Upper Saddle River, New Jersey, USA: Prentice-Hall, 1999.
- [7] F. Yaho, J. Coquery and K.-A. Le Cao, "Independent Principal Component Analysis for biologically meaningful dimension reduction of large biological data sets". In Proc. BMC Bioinformatics, 2012.
- [8] M. Scholz, S. Gatzek, A. Sterling, O. Fiehn, J. Selbig, "Metabolite fingerprinting: detecting biological features by independent component analysis". *Bioinformatics*, vol. 20, no. 15, pp. 2447-2454, 2004.
- [9] A. Hyvärinen, J. Karhunen, E. Oja, *Independent Component Analysis*. John Wiley & Sons, 2001.
- [10] S. Lee, S. Batzoglu, "Application of independent component analysis to micro arrays". *Genome Biology*, vol. 4, no. 11, R76, 2003.
- [11] A. Frigyesi, S. Veerla, D. Lindgren, M. Höglund, "Independent component analysis reveals new and biologically significant structures in micro array data". *BMC bioinformatics*, no. 7, p. 290, 2006.
- [12] R. He, B. G. Hu, W.S. Z. X Wei Kong "Robust Principal Component Analysis Based on Maximum Correntropy Criterion". *Proc. of the IEEE Trans. on Image Processing*, vol. 4, no. 6, p. 1485, 2011.
- [13] L. Sörm, P. Laguna, *Bioelectrical Signal Processing in Cardiac and Neurological Application*. Elsevier Academic Press, 2005.

The following paper is also published in the same field, but does not form the main part of this thesis.

Paper V

P Annus, R Land, M Reidla, J Ojarand, **Y Mughal**, M Min
“Simplified signal processing for impedance spectroscopy with spectrally sparse sequences”,

in Journal of Physics: Conference Series, Volume 434, Conference 1, Proceedings

The XV International Conference on Electrical Bio-Impedance (ICEBI) and XIV Conference on Electrical Impedance Tomography (EIT), Heilbad Heiligenstadt, Germany, April 22–25, 2013.



Simplified signal processing for impedance spectroscopy with spectrally sparse sequences

P Annus^{1,2}, R Land^{1,2}, M Reidla², J Ojarand², Y Mughal¹ and M Min^{1,2}

¹Thomas Johann Seebeck Department of Electronics, Tallinn University of Technology, Ehitajate tee 5, 10919 Tallinn, Estonia

²ELIKO Competence Centre, Mäealuse 2/1, 12618 Tallinn, Estonia

E-mail: paul.annus@elin.ttu.ee

Abstract. Classical method for measurement of the electrical bio-impedance involves excitation with sinusoidal waveform. Sinusoidal excitation at fixed frequency points enables wide variety of signal processing options, most general of them being Fourier transform. Multiplication with two quadrature waveforms at desired frequency could be easily accomplished both in analogue and in digital domains, even simplest quadrature square waves can be considered, which reduces signal processing task in analogue domain to synchronous switching followed by low pass filter, and in digital domain requires only additions. So called spectrally sparse excitation sequences (SSS), which have been recently introduced into bio-impedance measurement domain, are very reasonable choice when simultaneous multifrequency excitation is required. They have many good properties, such as ease of generation and good crest factor compared to similar multisinusoids. Typically, the usage of discrete or fast Fourier transform in signal processing step is considered so far. Usage of simplified methods nevertheless would reduce computational burden, and enable simpler, less costly and less energy hungry signal processing platforms. Accuracy of the measurement with SSS excitation when using different waveforms for quadrature demodulation will be compared in order to evaluate the feasibility of the simplified signal processing. Sigma delta modulated sinusoid (binary signal) is considered to be a good alternative for a synchronous demodulation.

1. Introduction

Complex electrical impedance has been widely used to characterize properties of biological tissues for many years [1]. One of the promising application areas is postoperative monitoring of the healing process. Bioimpedance reflects changes in the tissue state, which can be used to characterize the revivability or resuscitation ability of the tissue. Typically simultaneous measurement at several frequencies is required. Low and high frequency currents flow through the resistive interstitial space between the cells (extracellular component), but only the high frequency current can flow through the electrical capacitances of the insulating cell membranes (intracellular current). Ratio of these currents will reflect the state of the cells, accumulation of fluid in extracellular space, amount of swelling and ultimately warn before massive edema is about to develop. Generally it is desirable to monitor tissue parameters from different tissue locations simultaneously. These multifrequency and multisite measurements may be relatively rare and slow due to the dynamics of the underlying processes, and can be even sequential. Monitoring is warranted during the first few days after the surgical intervention, and possible changes take several minutes to occur. One of the critical tasks is restoration of the spontaneous blood circulation postoperatively. Cardiac activity will cause modulation of the

measured bioimpedance due to varying amounts of blood pushed through the tissue. Therefore faster changes in impedance need to be monitored as well, in order to assess whether the blood vessels are connected, and blood flow is restored. Extensive laboratory experiments have been conducted during longer period on isolated tissue samples, such as pigs heart, tongue etc. of pigs, for preclinical investigation of the impedance changes in the biological tissues. Device prototype has been developed for conducting these bioimpedance measurements in laboratory conditions (figure 1). Device has the ability to conduct measurements simultaneously on 16 frequencies in the range from 1 Hz to 100 kHz. Spectrally sparse sequences have been proven to be viable excitation signals for such a device [2]. SSS as two level or binary signal has many good properties, such as ease of generation, and good crest factor compared to similar multisinusoids. They can have tens of almost arbitrarily chosen, spectral lines with tailored magnitudes. The drawback is that there is also certain amount of energy on unwanted spectral lines, on so called snow lines, which extend well beyond the highest measurement frequency of interest. Combination of oversampling and correction is used in order to avoid large measurement errors. Another drawback is that real time calculation of that many discrete Fourier coefficients puts a heavy burden even on the internal resources of the used digital signal processor (DSP) and has been main limiting factor so far. Therefore simplification of the signal processing step is highly desirable.

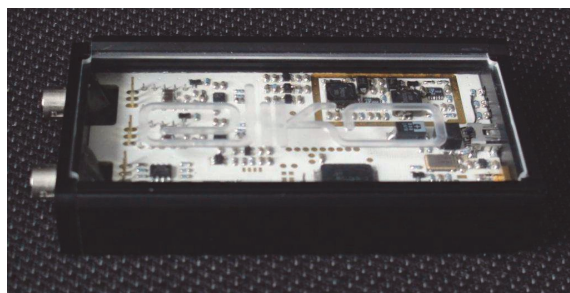


Figure 1. Two channel tissue monitor with spectrally sparse sequence as an excitation signal.

2. Description of simplification steps and the test

One of the possibilities is replacement of the sinusoidal signals used for quadrature demodulation with suitable binary counterparts. In an essence it would enable usage of simple summation (or switching in analogue domain) instead of more complex multiply and accumulate (MAC) operations. Eliminating MAC from the signal processing chain widens choice of possible signal processing platforms. It has been shown that simple low power complex programmable logic device (CPLD) can be used to process acquired signals if only summation is involved [3]. Three of the possible candidates are considered for replacement, and resulting measurement errors are compared (figure 2, table 2). First is the set of simple quadrature square waves, second is the set of shortened square waves (SSW) [3] with shortening angle of 22.5 degrees, and lastly sinusoids modulated with first order sigma delta circuit are considered. Simple first order RC low pass circuit is used with varying corner frequency to make simulations in LabVIEW environment more realistic, since impedance of various biological tissues can be modelled as RC circuitry. Filter corner frequency is swept from 1 Hz to 1.1 kHz, covering wide variety of possible target impedances. SSS, used in simulation, contains ten measurement frequencies (2, 4, 8, 16, 32, 64, 128, 256, 512, and 1024 Hz) with equal magnitudes. Result of the demodulation of the response to the SSS excitation with binary signals is compared against measurements with classical single sinusoidal excitation signal which is demodulated by multiplying it with two quadrature sinusoids.

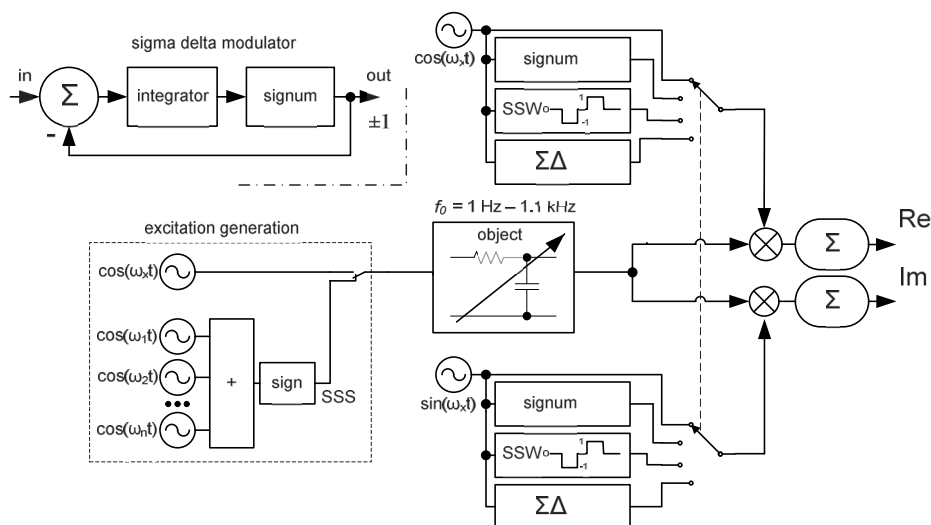


Figure 2. Simplified first order sigma delta modulator (upper left), and block diagram of the experiment with excitation generation, object and demodulation, where f_0 is filter corner frequency, $\omega_1 - \omega_n$ frequencies of the SSS components, and ω_x is an actual measurement frequency.

Quadrature sinusoids were also used for demodulation of the response to SSS excitation, however resulting errors were very low compared to purely sinusoidal case, and are therefore omitted from analysis. It should be noted that results are not general and depend on chosen excitation sequence, nevertheless similar tests can be conducted for any arbitrary sequence needed and results compared.

3. Results

Since RC circuit is modelled using exponential function certain caution is in order. Measured real and imaginary components of the response signal should be equal exactly when the corner frequency of the sweeping RC filter coincides with the measurement frequency. In reality there is some discrepancy between these frequencies due to limited resolution of the simulation. To assess simulation accuracy this discrepancy is calculated for purely sinusoidal measurement case:

Table 1. Measurement frequency versus frequency when real and imaginary parts coincide in case of sinusoidal excitation and demodulation with sinusoidal signals.

| $f_{\text{samplings}}$, kHz | Frequency when real and imaginary parts coincide in Hz | | | | | | | | | |
|------------------------------|--|------|------|-------|-------|-------|-------|-------|-------|--------|
| | Measurement frequency in Hz | | | | | | | | | |
| | 2 | 4 | 8 | 16 | 32 | 64 | 128 | 256 | 512 | 1024 |
| 100 | 1.99 | 3.99 | 7.99 | 15.97 | 31.92 | 63.74 | 126.9 | 251.9 | 495.8 | 960.8 |
| 1000 | 1.99 | 3.99 | 7.99 | 15.99 | 31.99 | 63.99 | 127.9 | 255.6 | 510.3 | 1017.4 |

The sampling frequency should exceed maximal filter corner frequency roughly 1000 times according to table 1. Raising it further would make simulation too slow to complete within reasonable time.

Generally relative errors are presented in literature, whereas deviation from the correct value is divided by the correct value. In some cases these errors exceed 50% for real and imaginary parts.

However closer examination shows that it happens when the value of the measurand is very small. In real measurement situation it could mean that it is already buried in the noise. Therefore it seems reasonable to compute full scale errors instead, whereas deviation from the correct value is divided by maximal value of the measurand. Resulting errors are shown in table 2. Also absolute phase errors in degrees are included in italics for better clarity.

Table 2. Demodulation quality with square wave (SQW), shortened square wave (SSW), and sigma delta modulated sinusoid is compared against demodulation of the response to the sinusoidal excitation with pure sinusoids. Errors below 0.001% are denoted by “-“. Absolute phase errors are added in italic.

| Signal component detected, signal used for detection | Maximal full scale measurement error in % / <i>absolute phase error</i> | | | | | | | | | |
|---|---|--------------|--------------|--------------|--------------|--------------|--------------|--------------|--------------|-------------|
| | <i>Measurement frequency in Hz</i> | | | | | | | | | |
| | 2 | 4 | 8 | 16 | 32 | 64 | 128 | 256 | 512 | 1024 |
| Re, SQW | 1.42 | 3.85 | 3.23 | 3.48 | 2.65 | 2.80 | 1.95 | 0.048 | 0.63 | 0.47 |
| Im, SQW | 3.24 | 5.00 | 5.27 | 2.89 | 1.79 | 1.32 | 0.22 | 0.85 | 0.55 | 1.22 |
| Magnitude, SQW | 1.36 | 3.85 | 3.23 | 3.48 | 2.64 | 2.78 | 1.93 | 0.18 | 0.39 | 0.38 |
| <i>Phase, SQW (deg, abs)</i> | <i>0.96</i> | <i>1.55</i> | <i>1.63</i> | <i>1.00</i> | <i>0.61</i> | <i>0.55</i> | <i>0.2</i> | <i>0.25</i> | <i>0.29</i> | <i>0.48</i> |
| Re, SSW | 3.81 | 2.60 | 2.36 | 2.52 | 1.54 | 0.81 | 0.85 | 0.42 | 0.32 | 0.27 |
| Im, SSW | 1.11 | 1.79 | 2.13 | 1.81 | 1.77 | 1.10 | 0.15 | 0.29 | 0.92 | 0.54 |
| Magnitude, SSW | 3.81 | 2.60 | 2.36 | 2.52 | 1.52 | 0.78 | 0.83 | 0.36 | 0.05 | 0.15 |
| <i>Phase, SSW, (deg, abs)</i> | <i>0.24</i> | <i>0.56</i> | <i>0.63</i> | <i>0.56</i> | <i>0.56</i> | <i>0.34</i> | <i>0.09</i> | <i>0.14</i> | <i>0.33</i> | <i>0.23</i> |
| Re, sigma-delta | 0.002 | 0.007 | 0.006 | 0.001 | - | 0.024 | - | 0.005 | 0.004 | - |
| Im, sigma-delta | 0.005 | 0.005 | 0.01 | 0.02 | 0.007 | 0.009 | 0.005 | 0.004 | 0.003 | 0.007 |
| Magnitude, sigma-delta | 0.002 | 0.007 | 0.006 | 0.001 | - | 0.024 | - | 0.005 | 0.004 | 0.003 |
| <i>Phase, sigma-delta, (deg, abs)</i> | <i>0.002</i> | <i>0.002</i> | <i>0.004</i> | <i>0.006</i> | <i>0.004</i> | <i>0.002</i> | <i>0.002</i> | <i>0.003</i> | <i>0.004</i> | <i>0.12</i> |

4. Discussion

Even though error calculation results depend on actual SSS used, and on actual object to be measured, some observations are in order. First of all, when comparing measurement results with those of pure sinusoidal excitation and classical Discrete Fourier Transform (DFT), SSS perform almost exactly as well when DFT is applied. Secondly, sufficient oversampling is in order when SSS is used for measurement, due to higher harmonic content. Regarding demodulation with different binary signals it is probably fair to say that sigma delta modulated sinusoids perform almost as well as real sinusoids, with both relative and full scale magnitude errors being below 0.1% and absolute phase error below 0.2 degrees. Even measurement results with simple square waves are within 4% of actual magnitude and 2 degree of real phase. Question remains if the usage of shortened square waves is justified due to little improvement over simple square waves, and added complexity.

5. Acknowledgments

This research was supported by the European Union through the European Regional Development Fund in frames of the research centre CEBE and competence centre ELIKO, partly also by Estonian target financed project SF0140061s12.

References

- [1] Kun S, and Peura R A 1994 Tissue ischemia detection using impedance spectroscopy *Proc. IEEW/EMBS 16th Ann. Conf.* pp 868–9
- [2] Min M, Ojarand J, Martens O, Paavle T, Land R and Annus P 2012 Binary signals in impedance spectroscopy *Proc. IEEE EMBC 2012* pp 134–7
- [3] Paavle T, Annus P, Kuusik A, Land R and Min M 2007 Bioimpedance monitoring with improved accuracy using three-level stimulus *Proc. of ECCTD '07* pp 412–5

Curriculum vitae

1. Personal data

Name: Yar Muhammad (Yar M. Mughal)
Date and place of birth: 09 June 1980, Shikarpur, Pakistan
E-mail address: yar.mughal@hotmail.com

2. Education

| Educational institution | Graduation year | Education (field of study/degree) |
|-------------------------|-----------------|--------------------------------------|
| Mid Sweden University | 2009 | MS (CE) |
| PIMSAT | 2004 | MS (IT) |
| PIMSAT | 2003 | BS (CS) |

3. Language competence/skills (fluent, average, basic skills)

| Language | Level |
|----------|----------------------------|
| Sindhi | Native |
| Urdu | Fluent (National Language) |
| English | Fluent |

4. Professional employment

| Period | Organisation | Position |
|-------------------------|--|--|
| 2014 – to date | Tallinn University of Technology | Engineer |
| Jan 2011 – Sept 2011 | Institute of Business and Technology, Karachi, Pakistan | Assistant Professor and Head of Program |
| 2009 – 2011 | SZABIST ⁷ , Karachi, Pakistan | Lecturer & Researcher |
| 2008 – 2009 | Efficient AB, Stockholm, Sweden | Software Engineer |

5. Research activity, including honours and thesis supervised

- Young Investigator Award (YIA) awarded by Springer at 16th Nordic-Baltic Conference on Biomedical Engineering & Medical Physics and Medicinteknikdagarna 2014, Sweden. In the conference, 430 papers were presented.
- IEEE SZABIST Student Branch Counsellor, SZABIST

⁷ SZABIST – Shaheed Zulfiqar Ali Bhutto Institute of Science and Technology.

- c) IEEE TUT Student Branch Founder member and Chairman at Tallinn University of Technology
- d) Thesis supervised: Abdul Basit Abdul Qadir, Master's Degree student, 2011, "A Novel Key Generation for FMET" at Institute of Business and Technology.
- e) Complex Project supervised: Shiva Gowda, Master's Degree student, 2014, "Model based separation of Cardiac and Respiratory Signals" at Tallinn University of Technology.

Elulookirjeldus

1. Isikuandmed

Ees- ja perekonnanimi: Yar Muhammad (Yar M. Mughal)
Sünniaeg ja -koht: 09 June 1980, Shikarpur, Pakistan
Kodakondsus: Pakistan
E-posti aadress: yar.mughal@hotmail.com

2. Hariduskäik

| Õppeasutus (nimetus lõpetamise ajal) | Lõpetamise aeg | Haridus (eriala/kraad) |
|---|----------------|---------------------------|
| Mid Sweden University | 2009 | MS (CE) |
| PIMSAT | 2004 | MS (IT) |
| PIMSAT | 2003 | BS (CS) |

3. Keelteoskus (alg-, kesk- või kõrgtase)

| Keel | Tase |
|---------|-----------------------|
| Sindhi | Emakeel |
| Urdu | Kõrgtase (rahvuskeel) |
| English | Kõrgtase |

4. Teenistuskäik

| Töötamise aeg | Tööandja nimetus | Ametikoht |
|----------------------|---|--------------------------------|
| 2014 – | TTÜ | Insener |
| 2011 jaan– 2011 sept | Institute of Business and Technology, Karachi, Pakistan | Abiprofessor ja Programmi juht |
| 2009 – 2011 | SZABIST, Karachi, Pakistan | Õppejõud ja teadur |
| 2008 – 2009 | Efficient AB, Stockholm, Sweden | Tarkvarainsener |

5. Teadustegevus, sh tunnustused ja juhendatud lõputööd

- Young Investigator Award (YIA) awarded by Springer at 16th Nordic-Baltic Conference on Biomedical Engineering & Medical Physics and Medicinteknikdagarna 2014, Sweden. In the conference, 430 papers were presented.
- IEEE SZABIST Student Branch Counsellor, SZABIST
- IEEE TUT Student Branch Founder member and Chairman at Tallinn University of Technology
- Thesis Supervised, Abdul Basit Abdul Qadir, Master's Degree student, 2011, “A Novel Key Generation for FMET” at Institute of Business and Technology.

- e) Complex Project Supervised, Shiva Gowda, Master's Degree student, 2014,,:
"Model based separation of Cardiac and Respiratory Signals" at Tallinn
University of Technology.

**DISSERTATIONS DEFENDED AT
TALLINN UNIVERSITY OF TECHNOLOGY ON
INFORMATICS AND SYSTEM ENGINEERING**

1. **Lea Elmik**. Informational Modelling of a Communication Office. 1992.
2. **Kalle Tammemäe**. Control Intensive Digital System Synthesis. 1997.
3. **Eerik Lossmann**. Complex Signal Classification Algorithms, Based on the Third-Order Statistical Models. 1999.
4. **Kaido Kikkas**. Using the Internet in Rehabilitation of People with Mobility Impairments – Case Studies and Views from Estonia. 1999.
5. **Nazmun Nahar**. Global Electronic Commerce Process: Business-to-Business. 1999.
6. **Jevgeni Riipulk**. Microwave Radiometry for Medical Applications. 2000.
7. **Alar Kuusik**. Compact Smart Home Systems: Design and Verification of Cost Effective Hardware Solutions. 2001.
8. **Jaan Raik**. Hierarchical Test Generation for Digital Circuits Represented by Decision Diagrams. 2001.
9. **Andri Riid**. Transparent Fuzzy Systems: Model and Control. 2002.
10. **Marina Briik**. Investigation and Development of Test Generation Methods for Control Part of Digital Systems. 2002.
11. **Raul Land**. Synchronous Approximation and Processing of Sampled Data Signals. 2002.
12. **Ants Ronk**. An Extended Block-Adaptive Fourier Analyser for Analysis and Reproduction of Periodic Components of Band-Limited Discrete-Time Signals. 2002.
13. **Toivo Paavle**. System Level Modeling of the Phase Locked Loops: Behavioral Analysis and Parameterization. 2003.
14. **Irina Astrova**. On Integration of Object-Oriented Applications with Relational Databases. 2003.
15. **Kuldar Taveter**. A Multi-Perspective Methodology for Agent-Oriented Business Modelling and Simulation. 2004.
16. **Taivo Kangilaski**. Eesti Energia käiduhaldussüsteem. 2004.
17. **Artur Jutman**. Selected Issues of Modeling, Verification and Testing of Digital Systems. 2004.
18. **Ander Tenno**. Simulation and Estimation of Electro-Chemical Processes in Maintenance-Free Batteries with Fixed Electrolyte. 2004.
19. **Oleg Korolkov**. Formation of Diffusion Welded Al Contacts to Semiconductor Silicon. 2004.
20. **Risto Vaarandi**. Tools and Techniques for Event Log Analysis. 2005.

21. **Marko Koort**. Transmitter Power Control in Wireless Communication Systems. 2005.
22. **Raul Savimaa**. Modelling Emergent Behaviour of Organizations. Time-Aware, UML and Agent Based Approach. 2005.
23. **Raido Kurel**. Investigation of Electrical Characteristics of SiC Based Complementary JBS Structures. 2005.
24. **Rainer Taniloo**. Õkonoomsete negatiivse diferentsiaaltakistusega astmete ja elementide disainimine ja optimeerimine. 2005.
25. **Pauli Lallo**. Adaptive Secure Data Transmission Method for OSI Level I. 2005.
26. **Deniss Kumlander**. Some Practical Algorithms to Solve the Maximum Clique Problem. 2005.
27. **Tarmo Vesikioja**. Stable Marriage Problem and College Admission. 2005.
28. **Elena Fomina**. Low Power Finite State Machine Synthesis. 2005.
29. **Eero Ivask**. Digital Test in WEB-Based Environment 2006.
30. **Виктор Войтович**. Разработка технологий выращивания из жидкой фазы эпитаксиальных структур арсенида галлия с высоковольтным p-n переходом и изготовления диодов на их основе. 2006.
31. **Tanel Alumäe**. Methods for Estonian Large Vocabulary Speech Recognition. 2006.
32. **Erki Eessaar**. Relational and Object-Relational Database Management Systems as Platforms for Managing Softwareengineering Artefacts. 2006.
33. **Rauno Gordon**. Modelling of Cardiac Dynamics and Intracardiac Bioimpedance. 2007.
34. **Madis Listak**. A Task-Oriented Design of a Biologically Inspired Underwater Robot. 2007.
35. **Elmet Orasson**. Hybrid Built-in Self-Test. Methods and Tools for Analysis and Optimization of BIST. 2007.
36. **Eduard Petlenkov**. Neural Networks Based Identification and Control of Nonlinear Systems: ANARX Model Based Approach. 2007.
37. **Toomas Kirt**. Concept Formation in Exploratory Data Analysis: Case Studies of Linguistic and Banking Data. 2007.
38. **Juhan-Peep Ernits**. Two State Space Reduction Techniques for Explicit State Model Checking. 2007.
39. **Innar Liiv**. Pattern Discovery Using Seriation and Matrix Reordering: A Unified View, Extensions and an Application to Inventory Management. 2008.

40. **Andrei Pokatilov**. Development of National Standard for Voltage Unit Based on Solid-State References. 2008.
41. **Karin Lindroos**. Mapping Social Structures by Formal Non-Linear Information Processing Methods: Case Studies of Estonian Islands Environments. 2008.
42. **Maksim Jenihhin**. Simulation-Based Hardware Verification with High-Level Decision Diagrams. 2008.
43. **Ando Saabas**. Logics for Low-Level Code and Proof-Preserving Program Transformations. 2008.
44. **Ilja Tšahhiov**. Security Protocols Analysis in the Computational Model – Dependency Flow Graphs-Based Approach. 2008.
45. **Toomas Ruuben**. Wideband Digital Beamforming in Sonar Systems. 2009.
46. **Sergei Devadze**. Fault Simulation of Digital Systems. 2009.
47. **Andrei Krivošei**. Model Based Method for Adaptive Decomposition of the Thoracic Bio-Impedance Variations into Cardiac and Respiratory Components. 2009.
48. **Vineeth Govind**. DfT-Based External Test and Diagnosis of Mesh-like Networks on Chips. 2009.
49. **Andres Kull**. Model-Based Testing of Reactive Systems. 2009.
50. **Ants Torim**. Formal Concepts in the Theory of Monotone Systems. 2009.
51. **Erika Matsak**. Discovering Logical Constructs from Estonian Children Language. 2009.
52. **Paul Annus**. Multichannel Bioimpedance Spectroscopy: Instrumentation Methods and Design Principles. 2009.
53. **Maris Tõnso**. Computer Algebra Tools for Modelling, Analysis and Synthesis for Nonlinear Control Systems. 2010.
54. **Aivo Jürgenson**. Efficient Semantics of Parallel and Serial Models of Attack Trees. 2010.
55. **Erkki Joasoon**. The Tactile Feedback Device for Multi-Touch User Interfaces. 2010.
56. **Jürgo-Sören Preden**. Enhancing Situation – Awareness Cognition and Reasoning of Ad-Hoc Network Agents. 2010.
57. **Pavel Grigorenko**. Higher-Order Attribute Semantics of Flat Languages. 2010.
58. **Anna Rannaste**. Hierarcical Test Pattern Generation and Untestability Identification Techniques for Synchronous Sequential Circuits. 2010.
59. **Sergei Strik**. Battery Charging and Full-Featured Battery Charger Integrated Circuit for Portable Applications. 2011.
60. **Rain Ottis**. A Systematic Approach to Offensive Volunteer Cyber Militia. 2011.

61. **Natalja Sleptšuk.** Investigation of the Intermediate Layer in the Metal-Silicon Carbide Contact Obtained by Diffusion Welding. 2011.
62. **Martin Jaanus.** The Interactive Learning Environment for Mobile Laboratories. 2011.
63. **Argo Kasemaa.** Analog Front End Components for Bio-Impedance Measurement: Current Source Design and Implementation. 2011.
64. **Kenneth Geers.** Strategic Cyber Security: Evaluating Nation-State Cyber Attack Mitigation Strategies. 2011.
65. **Riina Maigre.** Composition of Web Services on Large Service Models. 2011.
66. **Helena Kruus.** Optimization of Built-in Self-Test in Digital Systems. 2011.
67. **Gunnar Piho.** Archetypes Based Techniques for Development of Domains, Requirements and Software. 2011.
68. **Juri Gavšin.** Intrinsic Robot Safety Through Reversibility of Actions. 2011.
69. **Dmitri Mihhailov.** Hardware Implementation of Recursive Sorting Algorithms Using Tree-like Structures and HFSM Models. 2012.
70. **Anton Tšertov.** System Modeling for Processor-Centric Test Automation. 2012.
71. **Sergei Kostin.** Self-Diagnosis in Digital Systems. 2012.
72. **Mihkel Tagel.** System-Level Design of Timing-Sensitive Network-on-Chip Based Dependable Systems. 2012.
73. **Juri Belikov.** Polynomial Methods for Nonlinear Control Systems. 2012.
74. **Kristina Vassiljeva.** Restricted Connectivity Neural Networks based Identification for Control. 2012.
75. **Tarmo Robal.** Towards Adaptive Web – Analysing and Recommending Web Users' Behaviour. 2012.
76. **Anton Karputkin.** Formal Verification and Error Correction on High-Level Decision Diagrams. 2012.
77. **Vadim Kimlaychuk.** Simulations in Multi-Agent Communication System. 2012.
78. **Taavi Viilukas.** Constraints Solving Based Hierarchical Test Generation for Synchronous Sequential Circuits. 2012.
79. **Marko Kääramees.** A Symbolic Approach to Model-based Online Testing. 2012.
80. **Enar Reilent.** Whiteboard Architecture for the Multi-agent Sensor Systems. 2012.
81. **Jaan Ojarand.** Wideband Excitation Signals for Fast Impedance Spectroscopy of Biological Objects. 2012.
82. **Igor Aleksejev.** FPGA-based Embedded Virtual Instrumentation. 2013.

83. **Juri Mihhailov.** Accurate Flexible Current Measurement Method and its Realization in Power and Battery Management Integrated Circuits for Portable Applications. 2013.
84. **Tõnis Saar.** The Piezo-Electric Impedance Spectroscopy: Solutions and Applications. 2013.
85. **Ermo Täks.** An Automated Legal Content Capture and Visualisation Method. 2013.
86. **Uljana Reinsalu.** Fault Simulation and Code Coverage Analysis of RTL Designs Using High-Level Decision Diagrams. 2013.
87. **Anton Tšepurov.** Hardware Modeling for Design Verification and Debug. 2013.
88. **Ivo Määrsepp.** Robust Detectors for Cognitive Radio. 2013.
89. **Jaas Ježov.** Pressure sensitive lateral line for underwater robot. 2013.
90. **Vadim Kaparin.** Transformation of Nonlinear State Equations into Observer Form. 2013.
92. **Reeno Reeder.** Development and Optimisation of Modelling Methods and Algorithms for Terahertz Range Radiation Sources Based on Quantum Well Heterostructures. 2014.
93. **Ants Koel.** GaAs and SiC Semiconductor Materials Based Power Structures: Static and Dynamic Behavior Analysis. 2014.
94. **Jaan Übi.** Methods for Coopetition and Retention Analysis: An Application to University Management. 2014.
95. **Innokenti Sobolev.** Hyperspectral Data Processing and Interpretation in Remote Sensing Based on Laser-Induced Fluorescence Method. 2014.
96. **Jana Toompuu.** Investigation of the Specific Deep Levels in p -, i - and n - Regions of GaAs p^+pin-n^+ Structures. 2014.
97. **Taavi Salumäe.** Flow-Sensitive Robotic Fish: From Concept to Experiments. 2015.